EFFECTS OF GRINDING MEDIA SHAPES ON BALL MILL PERFORMANCE
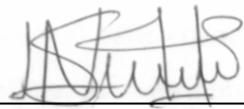
Niyoshaka Nistlaba Stanley Lameck

A dissertation submitted to the Faculty of Engineering and The Built Environment, University of the Witwatersrand, Johannesburg, in fulfilment of the requirements for the degree of Master of Science in Engineering

Johannesburg, October 2005

Declaration

I declare that this dissertation is my own unaided work. It is being submitted for the Degree of Master of Science in Engineering in the University of the Witwatersrand, Johannesburg. It has not been submitted before for any degree or examination in any other University.

Niyoshaka N. S. Lameck

04 Day of November Year 2005.

Abstract

Comminution is an important process in mineral processing, power plants, cement production and pharmaceutical industries. It is costly and an inefficient process in terms of energy requirements and steel consumption related to grinding media and liners.

Spherical grinding media are predominantly used in final stages of ore grinding. The spherical balls change shape through breakage and wear. Though this is universal in milling, its contribution and effect on milling kinetics, load behaviour and mill power is not fully established. One area that is usually ignored is the relationship between media shape and mill power.

The objective of this dissertation was to investigate how media shape affects grinding. Ball size distribution inside an industrial mill was analysed in terms of shapes and sizes. Load behaviour, mill power and breakage as affected by media shapes were studied in a pilot laboratory mill. An inductive proximity probe, light emitting diode, phototransistor and video photographs were used to determine the load orientation in terms of toe and shoulder positions. A load beam was used to measure the torque exerted by the charge.

The variation in load orientation and mill power with speed among different media shapes was observed. Higher shoulder positions were noted with cylpebs than with worn and spherical balls. The power increased to a maximum with increasing mill speed for all media shapes reaching its peak at different mill speeds for the three shapes studied.

Variations of breakage rates with media shapes were found; higher breakage rates were noted with spherical media but the differences narrows with decreasing feed size and increasing material fractional filling U.

Considering that worn balls in an industrial mill charge constitute about 15 to 40 percent and that the highest difference in breakage rate observed being nine percent for purely one shape charge; it is very doubtful whether it is worthwhile in attempting to develop techniques for removing worn balls from the mill.

Dedication

This work is dedicated to special people in my life:

My mother, father, sisters and brothers.

Acknowledgement

Table of Contents

List of Figures

List of Tables

Publications

- Lameck, N.S., Moys, M.H., 2005. Proceedings of The Minerals Processing 2005 Conference, Cape Town, South Africa, pg SP16

- Lameck, N.S., Kiangi, K.K., Moys, M.H., Effects of Grinding Media Shapes on Load Behaviour and Mill Power in a Dry Ball Mill (Mineral Engineering, 2006 DOI: 10.1016/j.mineng.2006.01.005)

- Lameck, N.S., Moys, M.H., Effects of Media Shape on Milling Kinetics (Mineral Engineering, 2006; Article in Press, DOI: 10.1016/j.mineng.2005.12.008)

Chapter 1
Introduction

1.1 Background

Communition is a very important unit operation in mineral processing, power plants, cement and pharmaceutical industries.

In mineral processing, particles containing valuable minerals must be broken sufficiently fine to liberate valuable minerals from waste constituents, so that they can be easily separated by an appropriate beneficiation method. In power plants, coals are ground to increase fineness, which increases particle surface area. This allows for a proportional increase in the burnout rate.

Grinding is generally an inefficient process and there are many factors that can affect grinding performance. Among the ways of assessing mill performance are examining the load behaviour, mill power and the rate of production of fines.

Grinding performance, in terms of material breakage and power consumption, has been studied with a wide range of operating parameters such as mill speed, charge filling, ball size and lifter type (Austin *et al,* 1984; Powell & Smit 1994; Cleary, 2001; Dong & Moys, 2003). It is however very important to explore other available avenues that can lead to an understanding and improvement of the milling process.

One area that is usually ignored is the relationship between media shape and mill power. The presence of worn balls inside the charge is very evident inside the mill, but their contribution and their effects on milling kinetics; load behaviour and mill power is not fully established.

The variation of mill throughput and power draw for fresh ball charge and equilibrium charge (which consists of balls of different properties in terms of size and shape due to breakage and media wear) is not well understood. Indeed there is much we still don't know about the effectiveness of worn balls. The only noted work related to worn balls was the study of effects of scats removal on SAG mill

performance (Powell & Smit, 2001). This work does not give insight into what the effects of these worn balls are on ball mill performance as the environment in a ball mill differs very substantially from that in a SAG mill.

Breakage itself is a well-understood process and models describing the process are well established. Different power models have been developed to describe power relationships with mill design and operating parameters. The deficiency of these models is that the effects of media properties in terms of shape and size are not adequately addressed. In order to address this, it is necessary to have experimental information upon which models can be evaluated.

1.2 Statement of Problem

Rotary milling, as an established process, has been in use for many years. Sometimes two stages of grinding are used: primary and secondary grinding. In primary grinding; autogenous grinding may take place. Ball milling is often used as a final stage of comminution. A product that suits the requirement of the next stage must be produced. The ball media size distribution must be selected to achieve this task effectively. However, size and shape distribution of media change continuously as a result of impact breakage and different wear mechanisms taking place inside the ball mill. The wearing and breakage results in smooth, non-spherical ball shapes, some characterised by exposed cavities or gross porosity holes. The typical mill charge characteristics are illustrated in Figure 1.1.

The movement of these irregularly shaped components through the mass of the charge is believed to differ significantly from the movement of larger, more rounded components, and is believed to constitute a basic factor in the segregation in the mill. Additionally these worn balls have surface and linear contacts with each other, compared to only point contact made among spherical balls. Undoubtedly, the

grinding efficiency of milling is affected and it was therefore decided to conduct a thorough study of the impact of worn balls on grinding.

Figure 1.1 Characteristic shapes of balls inside a ball mill

1.3 Objective

The central aim of this research work was to study the effects of grinding media shapes on ball milling performance and to evaluate the overall impact that the presence of worn balls in a ball mill have on milling. This involves evaluating the

performance of worn balls and comparing it with spherical balls. The criteria for comparison are load behaviour, mill power draw and grinding kinetics.

1.4 Dissertation Layout

This dissertation is organized into seven chapters. The first chapter introduces the work; the importance of milling is discussed and the motivation behind this study is stated. The organization of the dissertation is also covered in this chapter.

The literature review is given in Chapter Two. Breakage modelling using the Population Balance Model (PBM), the load behaviour and mill power is discussed. Although it was not the intention of this work to model mill power, this is included in the literature survey because of its importance in studying mill performance. Theoretical power models are reviewed and their shortcomings in accounting for the effect of media shape are noted. Media wear theories are reviewed as well.

In Chapter Three, equipment and mill instrumentation are discussed. Standard experimental procedures that were repetitively used are given. These included sampling methods and experimental test conditions. Experimental procedures are described under two subtitles; load behaviour and mill power, and milling kinetics.

Chapter Four covers the analysis of ball samples collected from an industrial mill. In order to perform experiments with the laboratory mill, it was necessary that industrial mill ball size and shape distribution be established. The established distribution could then be compared to the theoretical equilibrium charge from which the final distribution for laboratory mill experiments could be reached, being the result of these two.

In chapters Five and Six, the results obtained for load behaviour and mil power, and milling kinetics experiments are respectively discussed.

The load behaviour data obtained enabled toe and shoulder positions defining charge orientation to be obtained. The milling kinetics experiments enabled the estimation of specific rate of breakage and breakage distribution parameters of different single size feed material at different interstitial filling. The final (Seventh) chapter describes the conclusions drawn from this work.

Chapter 2

Literature Review

2.1 Introduction

Grinding is an important process that is used in many industries such as mineral processing, cement production, power plants and pharmaceutical industries. It is an inefficient and costly process in terms of energy and steel requirements. An enormous amount of research has been done in trying to understand and improve the process.

In this Chapter, works that are related to mill performance in terms of breakage, load behaviour and mill power modelling, as well as grinding media distribution, wear and shapes, are reviewed.

A sound background was gained by looking at the evolution of laws governing material breakage and is of great interest in analysing the effect of grinding media shapes in breakage of coarser particles.

It has long been believed that the movements of non spherical-shaped components through the mass of the charge differ significantly from the movements of more rounded components. This is believed to constitute a basic factor in the segregation in the mill (Vermeulen & Howat, 1989). It is obvious that the difference in media movements affects load behaviour in a tumbling mill, thus an understanding of the developments in this area serve as foundation in studying the effects of media shape on load behaviour. Developments in power modelling and parameters affecting it are reviewed. The neglect of incorporating media shape in these models is noted.

Grinding media wear has a great impact on the operation cost and results in huge consumption of liner and grinding media. This also results in a non-spherical media shape, which is of interest in the present research to study as it affects mill performance. Although it was not the intention of this study to investigate media wear; insight into different wearing mechanisms, their effect on mill efficiency and the advancements made in understanding this phenomenon is important.

2.2 Theories of Comminution

Over decades there have been several pseudoscientific attempts to develop fundamental laws governing grinding, in the interest of understanding and improving grinding efficiency.

Numerous investigators (Rittinger, 1867; Kick, 1885; and Bond, 1952) developed grinding hypotheses based on distinct pattern observation. These first attempts related the degree of grinding to the specific energy used in creating new surface areas of particles with a mean size of 80% passing screen sizes. These theories are of limited practical application as size reduction is dependent on several factors that are not considered.

2.2.1 Bond's theory

The Bond law of grinding has been widely used for mill sizing and design. The model is an empirical equation based on analysis of data from laboratory and industrial mills. It is based upon the two-power calculation approaches used in majority of ball and rod mill design processes (Smit, 2000) i.e.;

a. The determination of the power required to grind the ore from the given feed size to a specific product size, and

b. The selection of the grinding circuit with the mill design that will draw the required power.

Bond (1952) mill-sizing procedure, which is the mathematical form of his third comminution theory, estimates mill power per ton of 80 % passing screen size of feed and product and is given as:

$$E = W_i \left(\frac{10}{\sqrt{l_p}} - \frac{10}{\sqrt{l_f}} \right)$$ 2.1

where E is specific grinding energy

l_p= 80% of product passing size

l_f= 80% of feed passing size

W_i= Bond work index

For a desired mill capacity Q, the required shaft mill power P is

$$P = QE \, , kW$$ 2.2

The advantage of the Bond sizing method (Austin *et al,* 1984) is that: (i) it is very simple; (ii) it has been shown to work in many circumstances to a reasonable accuracy, as it is based on plant measurement. There are, however, some disadvantages to this method. Firstly, the specific energy required to take a feed with a certain 80% passing size to a product with a certain 80 %-passing size cannot be the same for a batch test, the standard Bond locked cycle test, or a steady state continuous mill with a real mill residence time distribution. Secondly, the method is purely empirical. Another disadvantage is the neglect of several other important factors such as the influence of lifters, percentage volume filling, ball size distribution, residence time, recycle ratio and material or slurry density.

2.2.2 Modern comminution theory

An alternative approach for modelling the milling process was proposed by Epstein in 1948 (Lynch *et al,* 1986). In this approach it is assumed that comminution is a sum of a repetitive circle of breakage events comprising of two basic mechanisms:

a. $P_n(y)$, probability of breakage of a particle of size y in the nth step of breakage process

b. F (x,y), the distribution by weight of particle of size x less than y arising from breakage of a unit mass of y.

The modelling of the breakage process has developed under the assumption that the grinding process may be adequately represented by size-discretised specific rates of breakage also known as selection function (mechanism **a**) and primary progeny fragments distribution also known as breakage (mechanism **b**). The first relates to the grinding kinetics of each independent particle while the later characterises the size distribution of fractured particles. The concept is useful in analysing test data, and describes the influence of different variables on the grinding process (Austin *et al*, 1984).

Based on the first order concept, numerous authors developed the model describing particle breakage in ball mill (the Size-Mass Balance Model; Austin *et al*, 1984, Population Balance Model; Herbst & Fuerstenau, 1982, and the Multi-segment Model; Kavetsky & Whiten, 1982 and Narayanan, 1987). All the three models use a similar method for expressing the breakage rate and breakage distribution functions and are principally the same. Their differences lie in the manner in which they represent the material transport mechanisms. The Size-mass Balance and Population Balance Models generally use a residence time distribution (RTD) function determined from tracing the flow of water while the Multi-segment Model, models the transport of materials along the mill.

2.2.2.1 Batch grinding

The first order breakage concept leads to a simpler solution and enables one to perform a complete size-mass balance or population balance on the batch grinding

system. In this approach it is assumed that the rate-mass balance on each particle size interval can be represented by the following intermediate equations:

- The rate of disappearance of size j material by breakage to smaller size is

$$\frac{d[w_j(t)]}{dt} = S_j w_j(t) \qquad 2.3$$

where $w_i(t)$ is the mass fraction of the total charge of size i at time t of grinding, and S_i is the proportionality constant known as the specific rate of breakage with per time units.

- The rate of appearance of size i material produced by fracture of size j material

$$= b_{i,j} S_j w_i(t) W \qquad 2.4$$

- The rate of disappearance of size i material by breakage to smaller sizes

$$= S_i w_i(t) W \qquad 2.5$$

- The net rate of production of size i material equals the sum rate appearance from breakage of all larger sizes minus the rate of its disappearance by breakage given by

$$\frac{d[w_i(t)]W}{dt} = -S_i w_i(t) W + \sum_{j=1}^{i-1} b_{i,j} S_j w_j(t) W \qquad 2.6$$

The analytical solution of this system of differential equation assumes that the parameters S and B are invariant with time, giving rise to a particular model, which is expressed in its matrix form as follows;

$$\overline{w(t)} = \underline{\underline{T}} \, \underline{\underline{J}} \, \underline{\underline{T}}^{-1} \, \overline{w(0)} \qquad 2.7$$

where $\overline{w(t)}$ is an nx1 vector matrix of mass fraction of mill product resulting after

grinding time t, $\underline{w}(0)$ is nx1 vector matrix containing the size distribution of the mill feed, $\underset{=}{T}$ is nxn lower triangular matrix of values T_{ij} defined as:

$$T_{i,j} = \begin{cases} 0 & i < j \\ 1 & i = j \\ \displaystyle\sum_{k=j}^{i-1} \frac{b_{i,k} S_k T_{kj}}{S_i - S_j} & i > j \end{cases} \qquad\qquad 2.8$$

and $\underset{=}{\overline{J}}(t)$ is a Diagonal matrix of values J_{ij} defined as:

$$\overline{J}_{i,j}(t) = \begin{cases} o & i \neq j \\ e^{S_i(t)} & i = j \end{cases} \qquad\qquad 2.9$$

Equation 2.8 in its form suggests that the path along which the product size distribution (T_{ij}) evolves during batch grinding is independent of the time but depends on feed size distribution (Austin *et al*, 1984)

The selection and breakage functions need to be established and then used in the Population Balance Model to predict product size distribution in a grinding mill. This is done either experimentally or by back calculation from limited sample data from operation (Austin *et al,* 1984).

2.2.2.1.1 Selection function model

It has been found that for many materials, the normal breakage of a given size fraction (for example, $\sqrt{2}$ size interval) of material in a batch grinding mill can be described by a first-order breakage law (Austin *et al,* 1984) shown in equation 2.3.

The selection function of particles relates very closely to power spent for grinding and provides a measure of the mill performance. Its values have been determined for combinations of mill speed; ball load and particle load with the corresponding measurements of the specific power input to the mill, P/M_p (Herbst & Fuerstaneu, 1973). Over a fairly wide range of conditions, Herbst & Fuerstaneu (1973) showed that the feed size selection function could be approximated by:

$$S_i = S_i^E \left(\frac{P}{m_p} \right)$$ 2.10

where S_i^E is the specific selection function independent of mill operating parameters, P is the industrial mill power drawn and m_p is the industrial mill hold-up.

By scaling up the rate of breakage obtained from a laboratory scale mill, the corresponding rate of breakage for a large mill could be predicted using equation 2.10. Herbst and Fuerstaneu (1973) showed that this approach could be used for sizing or optimising an industrial mill. However it requires the ability to predict the hold-up in industrial scale mills under different operating conditions.

The selection function S_i has been investigated by many researchers using a wide variety of grinding mills and conditions (Austin *et al*, 1984; Kotake *et al*, 2002; and Deniz & Onur, 2002) and even now this item is of great interest when considering the performance of a grinding process in the breakage of coarse particles.

The specific rate of breakage as a simple power of feed size has been amply demonstrated by many experiments (Austin *et al*, 1984; Kotake *et al*, 2002). It has been shown that the specific breakage rate (S_i) increases with l_i as equation 2.11 indicates (Austin *et al*, 1984) and starts to decrease for larger sizes, so that S_i passes through a maximum at a certain l_m. The maximum occurs in the specific rate of breakage because as the particles get larger, they are less likely to be nipped by the balls.

$$S_i = a\left(\frac{l_i}{l_o}\right)^{\alpha} \frac{1}{1+\left(\frac{l_i}{\mu}\right)^{\Lambda}}; \quad l_i << d, \Lambda \geq 0 \qquad\qquad 2.11$$

where α is a positive number, normally in the range 0.5 to 1.5 (Austin *et al*, 1984), being material characteristic and grinding condition in normal operating ranges, a is a constant whose units is the same units as S_i, d is the ball diameter in mm and l_0 is a standard dimension taken as 1mm. μ and Λ are characteristic parameters for material and mill conditions tested.

2.2.2.1.2 Primary breakage distribution function

Grinding of material even of a single size in the mill produces a wide range of product sizes. The set of primary daughter fragments resulting from breakage of size j material represented by b_{ij}, is given by:

$$b_{ij} = \frac{\text{mass of particles broken into size i from class j}}{\text{mass of class j broken}} \qquad\qquad 2.12$$

It is conveniently represented in cumulative form as B_{ij} that is written in the form of:

$$B_{ij} = \sum_{k=n}^{i} b_{kj} \qquad\qquad 2.13$$

where B_{ij} is the sum fraction of material less than the upper size of screen interval i resulting from primary breakage of size j material. Austin *et al*, (1984) showed that B_{ij} values can be estimated from size analysis of the product from grinding of size j materials (single-size fraction BII method) given by:

$$B_{ij} = \frac{\log\left[(1-P_i(0))\right]/\log\left[(1-P_i(t))\right]}{\log\left[(1-P_{j+1}(0))\right]/\log\left[(1-P_{j+1}(t))\right]} \qquad n \geq i \geq j+1 \qquad\qquad 2.14$$

where $P_i(t)$ is the cumulative fraction by mass in the mill charge less than size l_i. B_{ij} can be fitted to an empirical function (Austin *et al*, 1984) for non-normalized B_{ij} values:

$$B_{ij} = \Phi_i \left(\frac{l_{i-1}}{l_j} \right)^{\gamma} + \left(1 - \Phi_j \right) \left(\frac{l_{i-1}}{l_j} \right)^{\beta} \quad , i \geq j \qquad\qquad 2.15$$

where Φ_i, ® and © are model parameters that depend on material properties. It was found that for normalisable B_{ij}, Φ_i and ® do not depend upon the breakage size j (Austin *et al*, 1983).

The variations of *B* parameters with different milling conditions and feed materials have been studied for normal breakage (Austin *et al*, 1984; Herbst & Lo, 1989; Teke *et al*, 2000; and Deniz & Onur, 2002). It has been established that the values of *B* do not change in accordance with the grinding time in the mill.

2.2.2.2 Factors affecting breakage rate

Considering tumbling ball milling; the variation of fraction of mill filled with balls and powder, mill diameter, mill speed, media size and shape, ball density, ore type, and feed particle size distribution, as well as material properties affects the rate of breakage and overall mill performance.

This section considers studies undertaken to determine how some of these variables affect the selection function. The effects of grinding media shape and size on selection function are discussed in Sections 2.3.1 and 2.3.2 respectively.

2.2.2.2.1 Lifter height

Lifters are used to prevent the ball charge from slipping as mass cascades down the mill shell. They also act as keys that project ball charge and keep the layers of balls next to the shell, moving around with the shell.

Increasing lifter height reduces effective mill volume and increases the likelihood of cataracting. Powell and Vermeulen (1994) investigated the effect of lifter design on breakage and found that with correct liner design, it could be possible to minimize the energy consumption while maximizing the milling rate. Fuerstanau and Aboizeid (1985) studied scaling up of lifters in the ball mill. Their finding was that the specific rate of breakage decreased with increase in lifter size, while the breakage distribution function was observed to be independent of the lifter size.

2.2.2.2.2 Fraction of mill filled with balls and powder

Shoji (1982) and Deniz & Onur (2002) studied the effect of powder filling on grinding. A strong correlation between rates of breakage, powder filling (f_c) and ball filling (J) in the mill was found (Shoji 1982). With ball filling (J) of 20% to 50%, and powder filling (U) of 50% to 150, the specific rates of breakage for 0.6m mill internal diameter were found to be well represented by an established empirical correlation:

$$S(f_c, J) = k\left(\frac{1}{1 + 6.6J^{2.3}}\right)\exp(\text{-CU}), \quad 0.2 \leq J \leq 0.5, \quad 0.5 \leq U \leq 1.5 \qquad 2.16$$

where *C* is 1.2 and 1.32 for dry and wet grinding respectively.

Generally, a low powder filling gives a small absolute breakage rate. Increasing powders in the mill fills the collision space between the balls and results in a higher absolute breakage rate. When all the effective spaces in which collision between tumbling balls are occurring are filled with powder, the absolute rate of breakage

reaches a maximum. Further addition of powder increases mill hold-up but does not give increased breakage because the collision zones are already saturated and the additional powder just enters a reservoir of powder. Eventually overfilling leads to deadening of the collisions by the powder cushioning, the ball powder bed expands to give poor ball-ball powder nipping collisions and the breakage rate decreases.

2.3   The Role of Grinding Media in Comminution

Grinding media have a significant impact on the performance of tumbling mills in terms of product size distribution, energy consumption and grinding costs. Figure 2.2 shows main grinding costs for the specified mills (Mineral Processing Handbook, 2002). Considering the contribution of grinding media costs toward overall grinding costs, examining the possibility of minimizing them is worthwhile.

SAG Mill

Grinding media 21%

Liners 21%

Energy 58%

PRIMARY GRINDING MILL

Energy 50%

Grinding media 37%

Liners 13%

SECONDARY GRINDING MILL

Energy 49 %

Ginding media 45%

Liners 6%
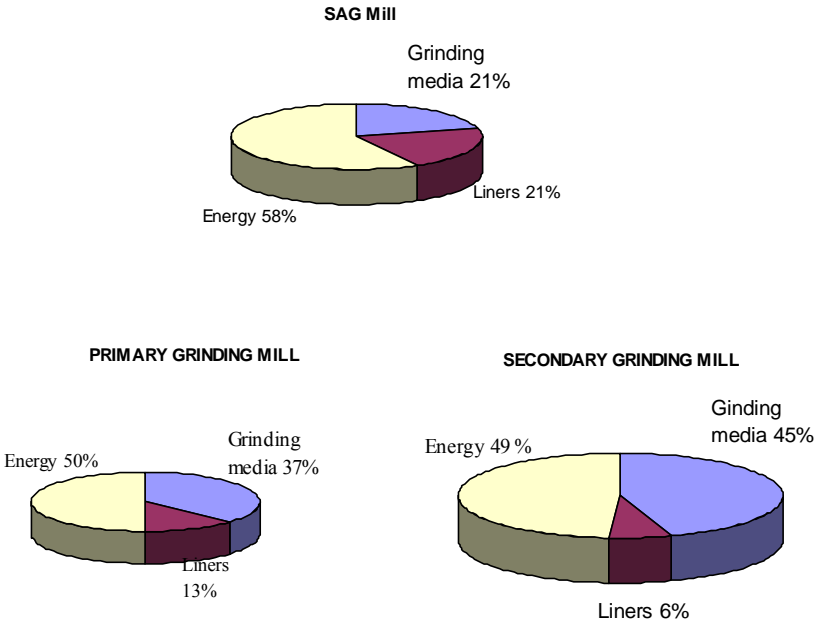
Figure 2.1 Typical grinding costs for grinding mill (Mineral Processing Handbook, 2002)

2.3.1 Media shape

Early work on grinding media focused exclusively on materials and size. However more recently, the role of media shapes on grinding performance is gaining attention.

The acclaimed advantages of non-spherical grinding media are their foundry production costs, which are thought to be lower than those of spheres, and the minimum porosity that can be produced on casting. Cloos (1989) stated that the advantage of a particular grinding media shape depends on the area, linear and point contact of the media with each other. However, ideally grinding media should fulfil the following requirements:

a. They should have the largest possible surface area to provide suitable contact with the material being ground;

b. They should be as heavy as possible to have sufficient energy required for breaking the ore particles.

These requirements must be balanced, since the larger the individual grinding media, the less the specific surface.

In the 1920s, Fairchild made a comparison of cubes against spheres in two full-scale ball mills operated in parallel, and concluded that cubes were more efficient when the assessment was based on iron consumption and power drawn per ton of ore reduced, when similar feed and product size distribution was assumed (Kelsall *et al,* 1973).

In 1953 Norris reported the results of a laboratory scale wet batch-grinding test with uniformly sized spheres, cubes, discs, cylinders and more complex shapes (Kelsall *et al,* 1973). Contrary to Fairchild's findings, it was concluded that for constant batch grinding time, spheres produced the finest products and used the least power, while cubes and discs were the least efficient on the basis of these criteria. However, the cubes used were each approximately 34 percent heavier than the balls used, so it was

not possible to decide unambiguously the precise effect caused by a change in shape alone.

Kelsall *et al,* (1973) studied the influence of different grinding media shapes on the grinding of trace quantities of quartz within a calcite environment in a small continuous wet ball mill using steel spheres, cubes and cylindrical media. The effect of grinding media shapes on first-order breakage rate constant (S) and breakage function was compared. He suggested that grinding media shape had a significant effect on both selection function, S and breakage function *B*.

Cloos (1983) suggested the use of cylpebs as alternative media to balls for fine grinding. Cloos (1983) argued that mill power is determined by the weight of the grinding charge; that for the same total weight of media charge; irrespective of size or shape, the mill power requirement would be the same as such the specific energy consumption could be reduced as shapes and size can increase throughput.

In 1983 the Council of Mineral Technology (MINTEK) launched an investigation to identify the most cost effective ball for the grinding of gold ores (Howat *et al,* 1983). During the investigation, some related questions were raised. If balls were more desirable, what size should they be? Could they be produced as solid castings or is some degree of porosity inevitable?

Howat *et al,* (1988) performed experiments to compare the rate of grinding with balls and conical media. Results reported were derived from experiments carried out in a laboratory mill (0.6m by 0.6m) running at 42 rev/min (77 % of critical speed). The mill was operated with smooth lining and metallic grinding media of mass of 229 Γ 5 kg, which filled the mill to about 45 %. Sixty millimetres high-chromium white iron balls and 60mm cones, with the diameter of the base being equal to the height, were used. He concluded that for equal masses of the grinding charge, conical media produced some coarser grinding of the harmonic mean size and the percentage of fines versus the feed rate.

Herbst & Lo (1989) carried out a study to develop a methodology for comparison of the grinding efficiency of a tumbling mill using balls and truncated cones as grinding media. In all the instances, balls were found to be more efficient than cones with an energy advantage of about 5-20%. The claimed reason for this difference being the probability of capture for different media shapes. They tentatively attributed a higher probability of particle capture with balls. However, the probability of capture is higher for cones, because of their increased surface contact, than for point contact made between balls.

Differently shaped grinding media have been investigated (Norris 1953; Kelsall *et al*, 1973; Cloos, 1983; Howat *et al,* 1983; Howat & Vermeulen, 1988; Herbst & Lo, 1989). However, their evaluation has been only in terms of the rate of breakage of particles, ignoring other parameters defining mill performance such as load behaviour and mill power.

In more effort to understand the relationship between media properties and fundamental aspects defining mill performance, Cleary (2001) studied sensitivity of charge behaviour and power consumption to mill operating conditions, liner geometry and charge composition using DEM (Discrete element method). Among the investigated was the effect of ball shape on mill power per charge mass and load behaviour at different mill speeds.

The author (Cleary, 2001) compared the specific power between circular balls and non-circular balls when the mill was charged with one ball shape. He showed that at N=70%, subtle differences appeared in charge distribution and that below N=75%, there was no change in the mill power draw. The author however lacks proven experimental information upon which the results obtained from DEM can be verified.

2.3.2 Media size

The efficiency of grinding depends on the surface area of the grinding medium. Grinding in a ball mill is effected by contacts between ball and ore particles. The angle of nip is important and ball sizes must be carefully chosen in relation to the largest and hardest particles in the feed.

Various formulae have been proposed for the required ratio of ball size to ore size, however, none of which is entirely satisfactory; the practice of charging balls to a tumbling mill is a matter of experience as well (Concha *et al*, 1992). The capacity of a mill increases with decreasing ball diameter, due to the increase in grinding surface, to the point where the angle of nip between contacting balls and particles is exceeded.

In a representative unit volume of mill, the rate of ball-to-ball contacts per unit time increases as ball diameter decreases because the number of balls in the mill increases as $1/d^3$. Thus the rate of breakage of smaller sizes is higher for smaller ball diameters. Austin *et al,* (1984) studied the variation of *B* values with ball diameter for crystalline quartz. He found that *B* values changed slightly with ball diameter, with larger ball diameters giving proportionally more fines. Thus, the lower specific rate of breakage due to larger balls is partially compensated by the production of a bigger proportion of fines fragments. It is not desirable to feed a mill with particle sizes which are too large, because the S_i values for these sizes will be to the right of the maximum shown with equation 2.11 giving low rates of breakage. Bigger diameter balls will break large particles more efficiently, and can be quantified by equation 2.17.

$$l_m \, \alpha \, d^2 \qquad\qquad\qquad 2.17$$

where l_m is the size at which the maximum value of *S* occurs in mm and *d* is ball diameter. A constant of proportionality varies from soft to hard materials and l_m varies with S_i, as can be seen for equation 2.11. In most cases, a spectrum of ball sizes

can be established in the mill owing to wear of balls and the continual addition of larger ball sizes.

Teke *et al,* (2002) investigated the variation of S_i values for calcite and barite with 46.26 and 12.8mm ball sizes. The S_i values increased when the ball size became smaller. Kotake *et al,* (2002) investigated the effect of feed size and ball diameter on the grinding rate constant of material being ground when the mass of balls, mass of feed and the mill's rotational speed were constant. He found that variation of grinding rate constant with feed size was roughly similar, for all feed materials used.

2.3.3 Grinding media wear

Steel consumption constitutes a significant proportion of grinding cost in industrial ball mills. Approximately 0.23 billion kg of steel (1986) in the US and over 0.45 billion kg in the world were consumed each year in wet grinding alone (Adam *et al,* 1986). This steel consumption is mainly attributed to wear of grinding media and liners. Apart from steel consumption, wear is also thought to affect the grinding performance of ball mills as it results in worn balls

The wear of grinding media in a mill is a contentious subject and many theories exist regarding the laws governing this process.

It is known that the total media wear in the grinding process results from three recognized wear mechanisms: abrasion, impact and corrosion. Corrosive wear is most significant in wet milling and least significant in dry milling, while abrasion and impact wear dominate in dry milling (Rajagopal & Iwasaki, 1992). It is, however, difficult to isolate their relative contributions toward overall wear under the conditions in a mill; the contribution to total media wear of each of these wear mechanisms has not correctly been established.

As mill speed approaches critical speed; ball charge continuously falls from a height of about, or greater than half of the diameter of a mill, and contact is made with ore particles, other balls or mill liners, causing impactive wear of both media and liners. During this impact process, the rate of ball wear, which is the rate of mass lost by the ball, is proportional to the ball mass; the cube of the ball diameter (Davis, 1919). There are ample proofs that balls are projected into flight and collide with the en mass charge, and sometimes with the mill lining. Evidence of impact can be deduced from numerous load behaviour photographs and DEM (Discrete Element Methods) simulations of grinding.

Attrition plays a large part in all fine grinding operations and has been known and acknowledged. However it is associated with abrasive wear, which occurs through penetration and plowing of media materials from the media surfaces by hard ore particles. The rate of ball wear during the abrasive process is proportional to the surface area of the ball or the square of the ball diameter.

Electrochemical interactions between abraded and un-abraded areas of the ball surface, as well as between the grinding media and minerals, occur especially in wet grinding; resulting in media corrosion. In a similar ore-metal/balls-environmental context, the corrosion rate per media surface will be the same, independent of mill size. Increasing mill size increases the energy dissipated in grinding, tumbling and crushing, which in turn would increase metal loss through abrasive and impact wear.

In attempts to reduce balls consumption and the high costs of fine grinding, many studies have focussed on the analysis of factors causing ball wear and theories have been proposed.

2.3.3.1 Theories of media wear

A brief review of the wearing mechanisms and causes of wear are given above. In this section, specific wear theories that have been proposed are discussed. Some work done in trying to establish specific mechanisms dominating wear were also reviewed. Wearing itself is complex and there is no generalised wear theory that adequately describes the wearing phenomenon. However, several authors have made an important contribution to an understanding of the wear process. Among the models and theories put forward are; the Bond Wear Model, Volume Theory and Surface Theory (Vermeulen & Howat, 1983). The Volume and Surface theories relate mainly to the size distribution of balls within the mill. They predict markedly different distributions of balls size.

2.3.3.1.1   Bond wear loss formula

On the basis of data from a large number of experimental tests and from industrial plant experiences, in 1963 Bond developed the following ball wear loss formulae for wet and dry ball milling (Austin *et al,* 1984):

For wet ball milling:

Ball wear (kg /kWh) $=0.16(A_i - 0.015)^{1/3}$ 2.18

And for Dry ball mills (grate discharge)

Ball wear (kg/kWh)$= 0.023A_i^{0.5}$ 2.19

where A_i is the abrasion index of material determined from abrasion test.

The average abrasion indices for various materials were obtained by conducting specific tests using method proposed by Bond in 1963 (Austin *et al*, 1984).

2.3.3.1.2   The volume theory

The volume theory predicts hyperbolic size frequency distribution. According to this theory, the rate at which the weight of any ball decreases is proportional to the mass (volume) of a ball. Its originality is in the idea that most comminution events occur in the toe of the charge, where impactive events predominate (Vermeulen & Howat, 1983).

It was established that during impact, work done by a ball to stress an ore particle is proportional to the kinetic energy of a ball when cataracting and cascading during rotary motion of a mill, and therefore, to the mass or volume of a ball. This can be presented mathematically as;

$$-\frac{dm}{dT} = \mathrm{k_m} m \qquad\qquad 2.20$$

T being the amount of material milled in tons. The constant of proportionality k_m is termed the tonnage constant of balls, measured in the units as per tone.

2.3.3.1.3   The surface theory

According to the surface theory, the size frequency distribution is flat: the same number of balls is found in every interval when the size range is divided into equal widths (Vermeulen & Howat, 1983).

The basic assumption of this theory is that the majority of comminution events are due to abrasive grinding of the particles of ore by the balls, and so suggests that wear rate of balls is proportional to the surface area of a ball. Prentice in 1943 and Norman *et al* in 1949 advanced evidence in support of this theory (Vermeulen & Howat, 1983).

For a ball of mass m, the surface area is proportional to mass to the power of two-thirds; so that the rate of mass loss is:

$$-\frac{dm}{dT} = bm^{2/3}$$
2.21

b is a surface wear constant

$$m(T) = \left(m_0^{1/3} - \frac{1}{3}bT \right)^3$$
2.22

m_o is the original mass of a ball and T carries the same meaning as for the volume theory.

These equations 2.21 and 2.22 are only valid if the sphericity of a ball remains constant, and valid only if

$$T \langle \frac{3m_0^{1/3}}{b}$$
2.23

However, media wear out and deviate from their spherical shape, thus attaining irregular shapes. It is well known that shapes of worn grinding elements can be distinctly non-spherical (Kelsall *et al*, 1973). The constant shape approximation is inadequate to describe worn ball shapes; as such using it independently can introduce an error.

In 1992, Jang & Iwasaki performed an investigation to determine the size distribution and shape of wear debris in a study of wear rates and wear behaviour of grinding balls using hard chromium steel balls and soft, non chromium steel balls. They found that the former generated less and smaller sizes of abraded debris compared to the latter.

In 1983,Vermeulen & Howat performed a marked ball test to verify agreement of both theories. They found that both theories were in good agreement with the data available for actual wear of various size grades of balls and therefore, either theory

could be used in a theoretical discussion of the marked ball test. This is confusing as the wear rate of a ball cannot be proportional to its surface at the same time to its mass. According to both theories ball consumption decreases monotonically with increasing throughput. This is essentially because the wear rates of balls decrease as they become smaller.

The general wear rate law assumes that the wear of a piece of spherical media (mass per unit time) is a power function of its radius, r:

$$f(r) = k(\rho 4\pi r^2) r^{\Delta} \qquad\qquad 2.24$$

where k is a linear wear rate (length per unit time), $\langle$ is the media density and $\cap$ is a constant. When $\cap = 0$, the mass wear rate is proportional to the surface area ($4\lozenge r^2$) (the surface theory) of the piece and the rate of decrease of the radius (-dr/dt) is a constant. When $\cap = 1$, the wear rate is proportional to the volume ($4\lozenge r^3/3$) of the piece (the volume theory).

Yildirim *et al*. (1999) modified the well-known relation for spherical media (equation 2.24) and extended it to a relation for cylindrical media. The modification was based on tests involved sampling the dumped mill charge, micrometering the length and the diameter and weighing a large number of media pieces. They concluded that:

a. Media wore uniformly so that the cylindrical shape was preserved,

b. By plotting the numbers of media with diameters greater than *d* vs *d* they shown that wear of ball diameter followed a Bond wear law; that the diameter decreased linearly with grinding time, and the linear wear rate of the radius of the cylinders of radius r was shown to be represented as follows:

$$-\frac{dr}{dt} = K_1(r) \qquad\qquad 2.25$$

c. The wear of length also followed linear law; the change made to wear law that was required to extend the treatment to non-spherical media was replacement of r with l; length of a cylinder and was represented as:

$$-\frac{dr}{dt} = 2K_2(l) \qquad\qquad 2.26$$

Based on well know Bond wear law, and taking into consideration the radius and length of the cylindrical media, the cumulative mass fraction of the media was represented as (Yildirim & Austin, 1998):

$$M(d) = \frac{\left[\left(\frac{d}{d_0}\right)^4 - \left(\frac{d_{min}}{d_0}\right)^4\right] + \left(\frac{4k_1}{3k_2}\right)\left(\frac{l_0}{d_0} - \frac{k_2}{k_1}\right)\left[\left(\frac{d}{d_0}\right)^3 - \left(\frac{d_{min}}{d_0}\right)^3\right]}{\left[1 - \left(\frac{d_{min}}{d_0}\right)^4\right] + \left(\frac{4k_1}{3k_2}\right)\left(\frac{l_0}{d_0} - \frac{k_2}{k_1}\right)\left[1 - \left(\frac{d_{min}}{d_0}\right)^3\right]} \qquad 2.27$$

k_1 being the wear rate of diameter d, k_2 is the wear rate of length l, d_{min} is the dimension of the opening of the retaining discharge grate and d_0 is the diameter of make-up media. For a special case of $l_o = d_o$ and $k_1 = k_2$, equation 2.27 reduces to the same expression as for spheres.

Radziszewski (2002) explored further and developed the total media wear model by incorporating all the three wear mechanisms. The model is based on the assumption that the effect of each wear mechanism can be independently determined, and thus allows for a total media wear model to be defined as the summation of the result of each mechanism. The difficulty in applying the equation lies in the impossibility of isolating the contribution of each mechanism.

2.4   Load Behaviour

Davis in 1919, and Rose *et al,* in 1958, realized the importance of describing the behaviour of grinding mills in order to predict how various parameters affect the performance of a grinding circuit in terms of load behaviour and power consumption (Dong & Moys, 2003). Mathematical models have been developed that can be used to simulate the behaviour of a real system by changing suitably chosen parameters to predict the response of various changes in the operating conditions. With such a system it is easy to draw a conclusion from the observation of a simulated process, instead of performing experiments on the real process.

2.4.1   Load orientation

The general orientation assumed by the load in a rotary grinding mill is accepted to be a quarter-moon shape profile similar to that illustrated in Figure 2.2. The key parameters describing this orientation are the surface of the pool, $\neg_{pool}$, the position of the toe, $\neg_{toe}$ and the shoulder position of the load, $\neg_{shoulder}$. The toe position is a point where lifters/liner come into contact with the load after being in flight and the shoulder position is a point where the load leaves the liners/lifters in a circular path along the mill shell. These two; toe and shoulder positions, give an approximate indication of load profile.

Davis in 1919 was among the first people to attempt to study charge motion and its profile inside a mill. He used a description of the charge motion in which balls move in a circular path up to a point at which centrifugal and gravitational forces are in balance. At this point, balls fall into a parabolic path until they impact the mill shell and come into circular path once again. Using this approach, Davis related charge motion to observed power drawn by the mill. It is from the basis of this work that most research exploring load behaviour and mill power modelling has advanced.
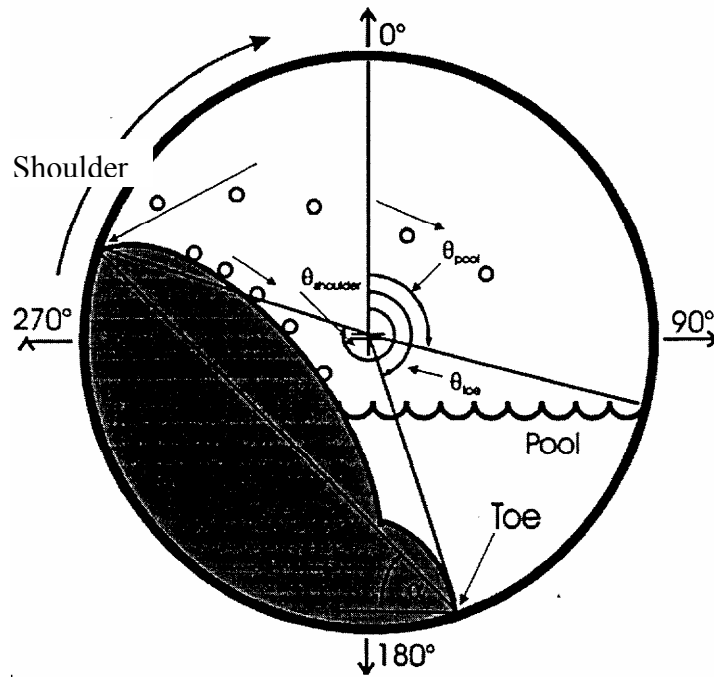
Figure 2.2 Profile assumed by the charge in tumbling mill (van Nieriop & Moys, 1999)

In further attempts to describe the behaviour of the charge in the mill, Vermeulen *et al*, (1984) used a piezo-electric device built into a liner bolt to sense mechanical impact and disturbance within the mill. With such an installation, he was able to collect information on the angular distribution of direct impacts, the average number of impacts with the shell liner in a unit time, the power requirement in promoting impacts, impact velocity and the amount of material in flight.

The use of conductivity measurement in the control of a grinding mill was implemented to indicate the point when the probe comes into the charge (toe) and leaves the charge (shoulder) referenced at a fixed point in a circle of rotation (Moys & Montini, 1987). They showed that the use of conductivity could provide information relating to slurry rheology in wet milling. Its application is, however, limited to wet grinding in which the slurry acts as the conducting medium.

More work has been done to predict load behaviour in tumbling mills. Among other efforts to characterize the charge motion and load behaviour are measurement of radial and tangential forces exerted by the load in a rotary mill as a function of load volume and mill speed (Moys & Skorupa, 1993), measurement of load behaviour in an industrial grinding mill (van Nierop & Moys, 1997), use of digital virtual images (Dong & Moys, 2003) and a study of charge motion in a rotary mill using a bi-planar angioscope (Powell & Nurick, 1996 parts 1, 2 & 3). Moys and Skorupa (1993) found that measurement could provide detailed and quantitative information about forces exerted on the liner and about load behaviour in the mill.

Liddell and Moys (1988) studied factors that affect load behaviour in terms of toe and shoulder positions. Among the factors investigated were mill speed and charge filling levels. The authors observed that the toe positions were affected by changes in mill speed beyond 80%, while the shoulder position was found to be dependent on mill speed and mill filling levels.

2.4.2 Mill power models

It is acceptable that power is an essential requirement for meaningful evaluation of grinding mill performance. Because milling is energy intensive and relatively inefficient in energy use, earlier investigations of mill performance were devoted to understanding and developing energy-size relationships (Kick, 1885; Bond, 1961). However, mill power draw is a strong function of mill size (L and D), loading (J) and operating conditions such as mill speed N, slurry/void ratio, and slurry density (Sullivan *et al*, 1958)

Taggart, in 1939 realized that the power prediction problem lies in incapability to determinate net power analytically because of ignorance of the internal dynamics of the tumbling mill. Thus a clear understanding of the motion mechanics of mill charge is crucial for accurate power prediction. Many have tried, and because of the many

variables involved, major variables have been treated differently leading to various power models.
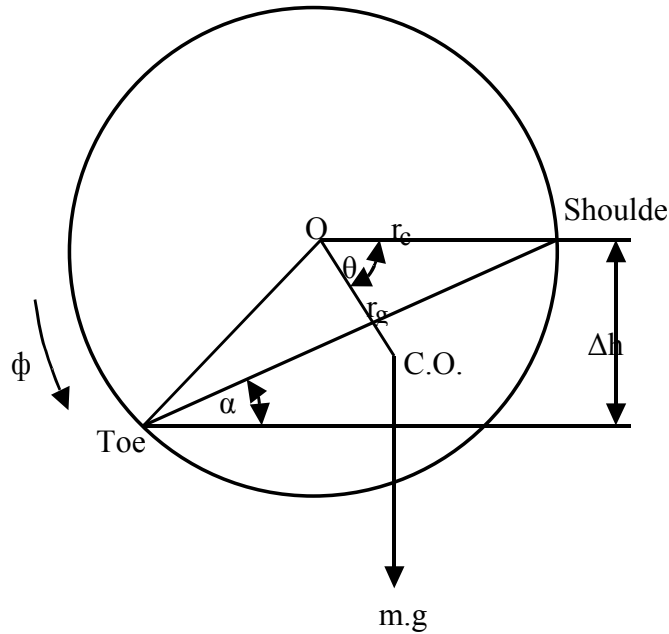
Figure 2.3 Load orientation used for development of mill power equation based on torque arm-model (Liddell & Moys, 1988)

Power model developments have been based either on industrial and laboratory data (Bond, 1961) or on derivation of equations describing the power requirement by calculating the paths of balls tumbling in the mill and integrating the energy required to raise the balls over all possible paths (Guerrero & Arbiter, 1960). Another approach treats the ball powder bed as a single mass, assuming that the turning moment of the friction force balances the turning moment of the centre of gravity of the bed around the mill centre. The latter approach assumes a torque-arm model, which includes major power related parameters (Hogg & Fuerstaneu, 1972). This is based on the concept that the profile of the load can be approximated by a chord (Figure 2.3) drawn between the toe and the shoulder, at an angle to the horizontal, termed the dynamic angle of repose of the load. The method assumes that the mass of

the load lies below the cord and the centre of gravity of the load through which the load act could easily be established. The basic power equation is equation 2.28.

$$P = \frac{2\pi N \tau}{60}$$

<div align="right">2.28</div>

where

$$\tau = m_g r_g \sin \theta_R (Nm)$$

<div align="right">2.29</div>

With higher rotational speed, some media tend to cataract and centrifuge. The shape of the load deviates from that of a chord approximation. In this situation, portions of the load are out of shell contact and some materials are in flight. The torque-arm model is less valid, as the chord can no longer define and represent the load profile and the centre of gravity becomes difficult to establish. This makes models developed based on this assumption of limited application in estimating power drawn by the mill.

Liddell and Moys (1988) was among the first to establish the variations in positions and shape of the mill charge under wide ranges of operating conditions, including mill speed, charge filling level and slurry rheological conditions. From observations, they made three conclusions:

a. The maximum power drawn by the mill is a function of complex operating variables;

b. The previous models (Bond, 1961; Hogg & Fuerstaneu, 1972; Harris *et al*, 1985) did not match well his observed power draw over a full range of speed and filling conditions;

c. Until the motion of a mill can be characterised mathematically, the power drawn by the mill cannot be calculated realistically.

In developing a more accurate power predictive model, Moys (1993) derived a model which combined the conventional torque arm model with a tendency of a load to centrifuge at high speed describing the effect of lifter bar design, mill speed and its filling ratio. The model was based upon the semi-phenomenological understanding of mill behaviour and reflected the non-linear dependence of mill power on the load volume J, and mill speed N, as a percentage of critical speed and also the effect of slurry viscosity and liner design were related to model parameters. The model assumes that the load is divided into two portions: one which is centrifuging at high speed, thus drawing no power and the other an active non- centrifuging portion of the load, drawing power according to Bond's model.

The author modified Bond's 1961 power model (by introducing the effect of centrifuging, which reduces the effective load volume) as follows:

$$P = K_2 D_{eff}^{2.3} \rho_L J_{eff} L \left(1 - \beta J_{eff}\right) N_{eff} \sin \alpha \qquad\qquad 2.30$$

The effective fractional volume of a mill filled with a charge that is not centrifuging was given as:

$$J_{eff} = \frac{4 V_{eff=}}{\pi D_{eff}^2 L_{eff}} = \frac{J - 4\delta_c (1 - \delta_c)}{1 - 2\delta_c^2} \qquad\qquad 2.31$$

The reduced volume is given as:

$$V_{eff} = \frac{J \pi D^2}{4} L - V_c ; \quad V_c = \frac{\pi}{4}\left(D^2 - D_{eff}^2\right) L \qquad\qquad 2.32$$

and

$$D_{eff} = \left(1 - 2\delta_c\right) D \qquad\qquad 2.33$$

where $\delta_c D$ is the assumed thickness of the centrifuged layer which also depends on J and liner profile.

The centrifuging layer thickness (δ_c) was represented by the following empirical formula:

$$\delta_c = J^{\Delta J} e^{-\frac{N_{100} - N}{\Delta N}}$$
2.34

At low speed; δ_c=0, and the model reduces to Bond's model without the empirical term.

Morell in 1993 developed the theoretical power draw equation by considering three different approaches describing the manner by which a mill draws power: torque exerted by the load, potential and kinetic energy balance and frictional force balance.

These approaches assumed that once in free flight, the energy of particles was not recovered by the mill. The author supported this argument on the basis of photographs taken, which showed that, at the point of impact at the toe, the particle trajectories were approximately radial and hence little tangential component was present.

The developed equations for the torque and frictional force approaches were identical. However, the author showed that these two approaches oversimplified the milling conditions by failing to account for kinetic energy.

To provide a basis for the development of an industrial grinding mill power model, Morell used the more comprehensive energy balance based equation with grate and overflow discharge taken into account. The author extrapolated the power equation for a simple tumbling vessel to account for the machine design related effects of grate discharge mechanisms and conical end section. The difficulty associated with the model lies in applying it in the real world.

All models developed describing mill power use the "lumped parameter" approach; as such empirical approximations are inevitable. Considerable numbers of parameters have to be determined empirically for best use of these models. For this reason these

models are still incapable of adequately addressing the effect of several important parameters such as liner design, media size and shape, liner and grinding media properties like coefficient of friction and restitution and grate design.

In this context, Mishra and Rajaman (1992) advocated the use of DEM (Discrete Element Method) in the field of mineral processing. This takes advantage of technological advancements, modern computers and suitable numerical methods to estimate and simulate the path and dynamic equilibrium of each individual ball in the charge. It allows computation of the position of individual balls at discrete times as the mill rotates. The methodology was first pioneered by Cundall and Strack in 1979 in the field of soil mechanics; it was however realized that the method could be applied to any particulate system.

The dynamic equilibrium equation for each individual ball can be written in a general form as:

$$M\frac{d^2x}{dt^2} + C\frac{dx}{dt} + Kx = p \qquad\qquad 2.35$$

where M=mass

      C- damping

      K- Stiffness matrix

      P- force vector

      x- Position vector.

Equation 2.35 describes the motion of a system of balls, where the internal restoring forces are due to a pair springs acting on contact in both normal and shear directions. The model also incorporates the aspects of charge motion and energy loss due to friction and damping. The net power loss over a period, t in the model, is given as:

$$E = \sum_t \sum_n \left(\mathbf{F}_d + \mathbf{F}_f \right) dr \qquad\qquad 2.36$$

n- all contacts

t-time

F_d-Work done by dissipative forces

F_f- frictional force.

With the DEM, the effects of liner profile, media size distribution, load volume, mill speed, contacts among grinding media and mill liners are easily incorporated. Thus their effects on load behaviour and mill power can be explored.

The early simulation work involved a two-dimensional mill approximation to reduce computational time and memory constrains, however the method has advanced to three dimensional as a result of availability of very fast and large memory personal computers.

2.5   Conclusion

This chapter has covered a wide range of researches in parameters defining mill performance in terms of breakage, load behaviour and mill power and in grinding media properties. A sound background was provided.

Comminution theories were reviewed and a well-developed modern comminution theory was considered in the study of the effect of grinding media shapes on the removal of coarser particles in the product.

Media wear not only has a significant impact on grinding cost but also results in non-spherical shapes of originally spherical balls. The mechanisms and theories behind

the wearing process were reviewed. While wearing itself is known to be a product of different wearing mechanisms, the need for establishing a model that includes all wearing mechanisms was realized (Radzwiesk 2002). This is very important in establishing and studying ball size and shape distribution and their effects toward ball mill performance.

Studies that were done to investigate media shapes have also been reviewed. In studying media shapes, it has been revealed that previous efforts were exclusively devoted to breakage, ignoring other parameters defining mill performance; such as load behaviour and mill power. Understanding the effect that media shape has on power draw is a possible avenue for understanding and improving grinding costs.

Developments in understanding load behaviour and wide ranges of power predictive models have been reviewed. Despite the enormous amount of work done, the effect of media shape on mill power and load behaviour was not addressed in these models.

With confidence gained from use of DEM (Hlungwani *et al*, 2003) as a tool for modelling the milling process, different media shapes can now be incorporated in studying load behaviour and power prediction. However, the lack of relevant experimental data limits the successful evaluation of DEM for this matter. The only reported work involving worn media was about the effect of scat removal of worn balls in a SAG mill (Powell & Smit, 2002). However, this does not give insight into what is happening, as the environment differs substantially from wet SAG mills to dry ball mills.

From this review it is clear that there is no published experimental information on the effects that shapes have on load behaviour, mill power and milling kinetics. The aim of this study is to establish information that may help in incorporating the effect of the shape of grinding media in describing the milling process.

Chapter 3

Experimental Equipment and Programme

3.1 Introduction

This chapter describes all the experiments that were conducted to generate the experimental data analysed and discussed in chapters that follow. Equipment is described in detail and methods used in obtaining experimental data are discussed.

3.2 Laboratory Grinding Mill

Experiments were performed using a pilot mill shown in Figure 3.1. The mill was mounted on a milling rig as shown in Figure 3.2. The mill can be fitted with different liner profiles and allows a wide range of mill speeds to be used.

Figure 3.1 Mill lifters configuration

The mill is 0.54m-internal diameter and 0.4m internal length fitted with twelve (12) trapezoidal lifters. Figure 3.3 illustrates the lifter dimensions, while Table 3.1 summarises the specifications of the lifters and mill dimensions. The mill is driven by 2.5kW variable speed motor mounted in a mill rig (Moys 1984). The rig consists of

three components: the supporting frame, the main shaft and the motor cage. The cage is suspended from the main axle by a set of bearings and the entire assembly is suspended from the two load cells, which are connected to a support frame. Figure 3.2 shows the assembly of the mill rig used. The motor cage is connected to a third load cell via a torque arm, which enables measurement of the force on the cage in the horizontal plane (i.e. a measure of the torque produced by the motor). The mill is designed to accommodate various modes of operation at various speeds. Using a movable diaphragm, the mill length can be changed to suit experimental need.
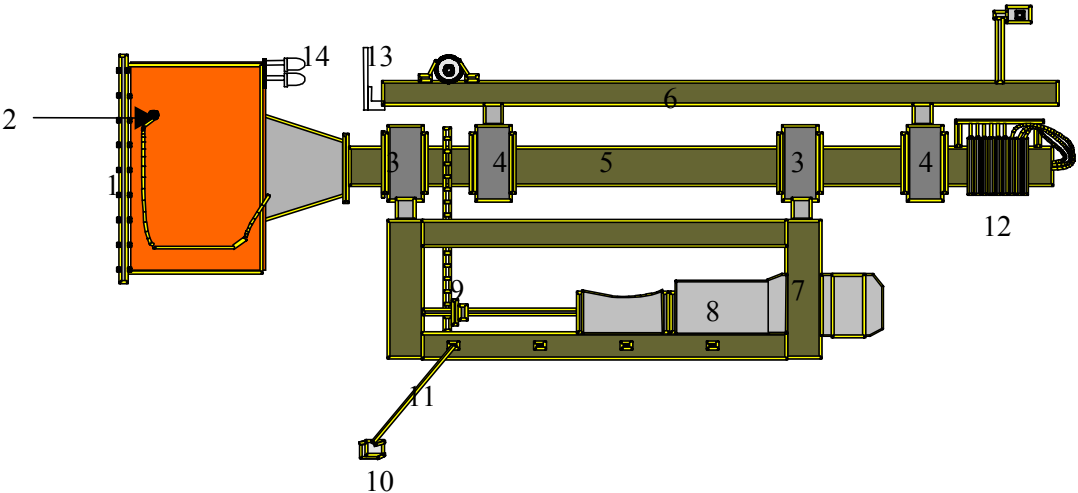
1: Front plate   8: 2.5 kW motor

2: Inductive proximity probe 9: Driving chain

3: Motor cage-bearing   10: Torque load beam

4: Axle bearing   11: Torque arm

5: Axle   12: Slip ring assembly

6: Supporting frame   13: Mirror

7: Motor and gear box cage   14 Infra-red LED and phototransistor

Figure 3.2 Mill rig assembly
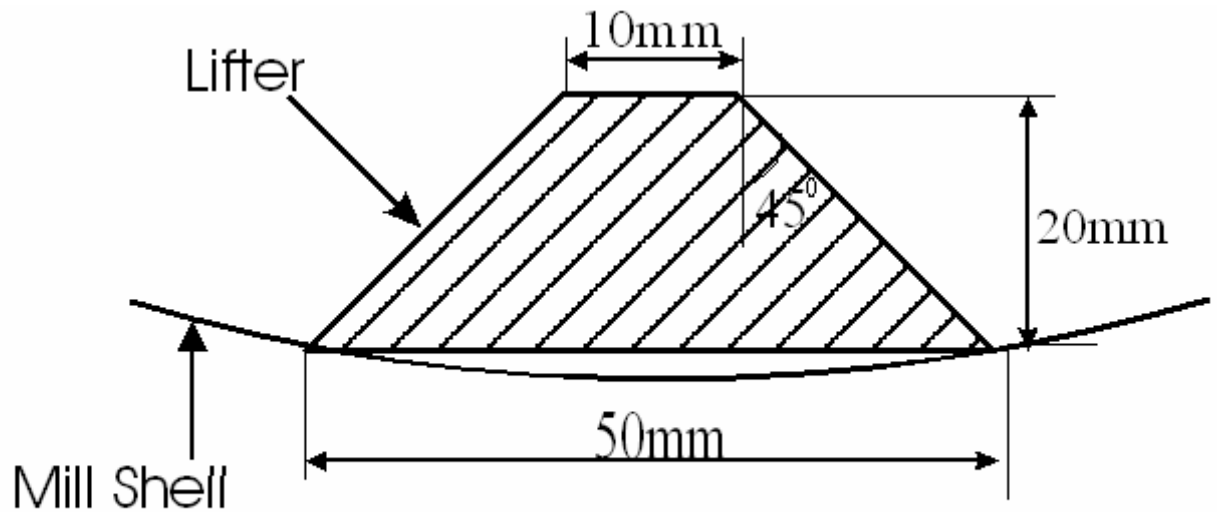
Figure 3.3 Lifter geometry

The mill is connected to the torque arm to enable measurement of forces exerted on the beam, making it possible for mill power to be obtained. An inductive proximity probe (Kiangi & Moys, 2005) designed by fellow student; inserted through the mill shell was used to obtain charge positions in reference to a 12 o'clock position that is determined using a signal produced by a light emitting diode (LED). The circuit is connected to a computer data collection system through an interface.

The mill was loaded and unloaded through a 250mm diameter opening on a removable front plate. The opening is covered during experiments to prevent material from escaping from the mill.

Table 3.1 Pilot mill specifications

Wits Mill	Internal diameter (D), mm	540
	Length, mm	400
	Volume, cm^3	88765.7
	Critical speed	59.50
Feed end-plate	Feed –end opening diameter (mm)	250
	Material	Grey PVC
Lifters	Materials	Mild steel
	Number	12
	Profile	Trapezoidal
	Height, mm	20
	Top width, mm	10
	Angles	45^0
	Spacing (mm)	143

3.3 Mill Instrumentation

3.3.1 Inductive proximity probe

A metal sheet was inserted inside the mill onto which trapezoidal lifters were bolted from outside. The inductive probe was inserted at 50 mm from the mill front end between two lifters. This was inserted from the outer shell, right through the lining metal sheet. The sensing face was covered by a 3mm PVC plate to protect it from being damaged by media tumbling inside the mill. The probe was able to detect any metal present within the range of 3mm to 8mm from the probe face or 0-5mm from the PVC plate face. Figure 3.4 illustrates the mounting of the probe on the mill.
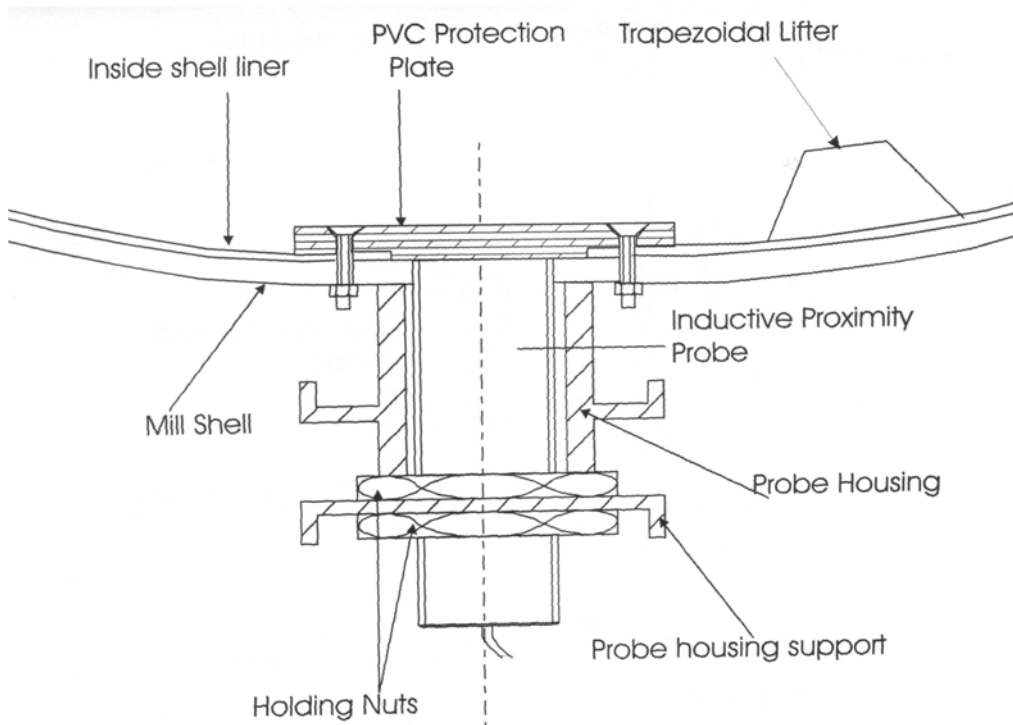
Figure 3.4 Inductive probe installation onto the pilot mill.

3.3.1.1 Probe features and mode of operation

The features of the inductive probe are shown in Figure 3.5. The probe mainly consists of an oscillator, a trigger circuit and solid state switching (storage) device components. The oscillator creates a high frequency field that is emitted on the sensing face. When a metal enters the field, it induces eddy currents; energy is required from the oscillator to counter the eddy currents induced by the approaching metal. As the metal enters the sensing range of the sensor, the induced eddy current magnetically pushes back and dampens the probe's low energy oscillating magnetic field. The detection circuit senses this dampening effect and signals the switch to change state. After the metal target leaves the sensing range, the oscillator resumes its normal functioning, and the switch returns to its normal state.

Active Face   Oscillator   Trigger Circuit   Output Stage
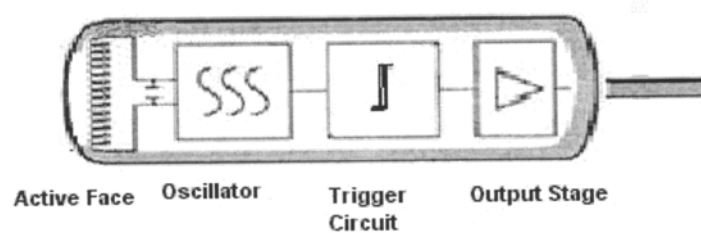
Figure 3.5 Inductive probe features.

3.3.2 12 o'clock marker probe

The 12 o'clock probe was used to indicate the time when the mill reached a specific point in a revolution. It consisted of a reflecting mirror, an infrared light emitting diode (LED) and a phototransistor. The infrared emitting diode and phototransistor were mounted and rotated with the mill while a mirror was fixed at a 12 0'clock position on a supporting frame opposite to infrared emitting diode and phototransistor. The LED emitted light, which was reflected by the mirror and

detected by the phototransistor, was then transmitted into a personal computer as a voltage signal.

Information obtained from the inductive probe and 12 o'clock marker signal enabled the charge orientation to be defined. Figure 3.6 shows the typical data profile obtained from the inductive probe and the 12 o'clock marker probe plotted against time for three complete revolutions.
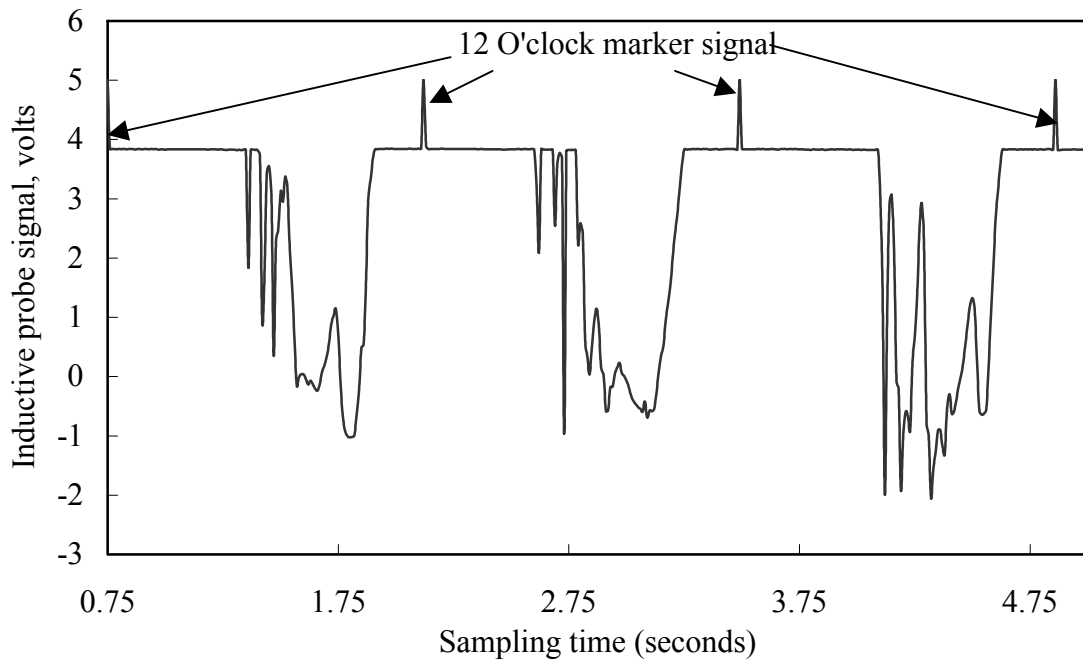
Figure 3.6 Typical signal produced by inductive and marker probes

3.4 Experimental Programme

In fulfilling the objectives of this research work, the experimental programme was divided into two parts.

The first part involved characterization of ball mill media distribution in terms of size and shape in an industrial mill. The details of the sampling procedure used and results are discussed in Chapter Four.

The second part involved laboratory tests to determine the effects of media shape on load behaviour, mill power draw and milling kinetics. This part was sub-divided into two sub-programmes. The first sub-programme aimed at measuring load behaviour and mill power draw with three media shapes. The second involved comparing the milling kinetics of non-spherical worn balls with un-worn, spherical media. The worn balls used in these experiments were collected from the industrial ball mill described in Chapter Four.

Laboratory experiments that were conducted are discussed in the following sections: 3.4.1, for the study of load behaviour and mill power, and 3.4.2, for the study of milling kinetics. The results of these experiments are discussed in Chapters Five and Six respectively.

3.4.1 Load behaviour and mill power experimental programme

3.4.1.1 Experimental design

The effect of media shape on load behaviour and mill power was investigated using three different media shapes: unworn spherical balls, cylpebs media with a diameter equal to the height and non-spherical worn balls (shape of originally spherical media changed due to different wearing mechanisms inside ball mill). Worn ball samples were collected from an industrial mill as described in Chapter Four. A 3x3x9 factorial design approach was used for three dependent and three independent variables. It was, however, possible for the three dependent variables to be obtained from a single experiment. The dependent variables were mill power draw, toe positions and shoulder positions while independent variables were: three media shapes (spheres, worn and cylpeb media), three mill charge filling levels (15, 20 and 25 percents) and nine (9) mill speeds as a percentage of critical speed (20, 30, 40, 50, 60, 70, 75, 80 and 90 percent) at mill length of 100mm. Table 3.2 summarizes the experimental parameters used. The charge filling levels were chosen such that, they included the

operating ranges for industrial mills in coal pulverisation. Mill speed was varied over a wide range.

Testing of all possible combinations of 3x3x9 independent variables translates into eighty-one experiments. For practical reasons it was not possible to replicate every experiment. However, the limited number of replicated experiments done (Table 3.4), showed no significant difference. Thus only one test was done for each of the remaining experiments

Table 3.2 Media characteristics and test condition for load behaviour experiments

	Cylpebs	**Spherical**	**Worn balls**
Mill length (mm)	100	100	100
Media diameter range (LXd),	24X24	22.4-26.5	22.4-26.5
Specific gravity	7.74	7.74	7.67
Voidage	-	0.4	-
Charge Mass, kg	20.64	20.64	20.62
Speed (% **N_c)	20-90	20-90	20-90
J	0.15 & 0.25	0.15 & 0.25	0.15& 0.25

$$^{**}N_c = \frac{42.3}{\sqrt{D-d}}, \ rpm \ (D, d \ in \ meters)$$

$$Charge \ mass \ (kg) = \frac{0.6 J\pi D_{inside}^2 L\rho_{Ball}}{4} \hspace{3cm} 3.1$$

Material properties such as coefficient of friction, size and shape affect media packing (Zhou *et al*, 2002). With this fact in consideration equation 3.1 was used to calculate the spherical ball charge mass at the desired charge filling level. The charge mass involving cylpebs and worn balls were equivalent to that of spherical balls. This

implies that media shapes were compared based on the same mass criterion. The voidage of 0.4 was assumed in calculating spherical balls mass.

3.4.1.2 Data sampling method and analysis

Measurement of load behaviour was accomplished using the inductive proximity probe described in Section 3.3 above and video photographs were taken for visual observation of the actual load orientation. Mill torque was recorded using the torque beam attached to the mill rig while an infrared light-emitting diode (LED), a phototransistor and a mirror were used for position marking.

Signals from the torque beam, inductive proximity probe and marker probe were transmitted into a computer through an interface. The interface ensured that these signals were within –5 to +5 volts range, suitably filtered to reduce noise.

Probe data determining charge position inside the mill and torque data for power measurement were collected at a pre-set sampling frequency and time. A total of six thousand readings of data points were sampled for each of the two channels.

A sampling frequency of 100Hz was used for gathering data for all speeds for a period of one minute each. The mill was always allowed to run for about ten seconds, in order to reach a steady state, before sampling was commenced. The number of mill revolutions sampled depended on mill speed. Consequently, more data were generated per revolution for slower mill speeds and less data were available per revolution for higher speeds. However, the sampling frequency was adequate for all the speeds and a clear indication of the trend for each experiment was observed. Table 3.3 shows angular distance in degrees between two adjacent points introduced by sampling frequency for speeds listed.

Table 3.3 Data point recording interval for 100Hz sampling frequency as a function of mill speed

Mill speed (% Critical)	Time/Rev (Sec.)	Data point interval (Degrees)
20	5.08	0.71
30	3.45	1.04
40	2.55	1.43
50	2.06	1.76
60	1.7	2.12
70	1.47	2.45
75	1.36	2.63
80	1.29	2.81
90	1.15	3.13

3.4.1.2.1   Probe data characteristics

Figure 3.7 shows a typical signal obtained when using an inductive proximity probe for one revolution and the nomenclature used to define the toe and shoulder positions. The toe position was taken as a point when the inductive probe showed a persistent signal of the presence of balls around its sensing face, while the shoulder position was obtained when the signal ceased due to media departure from the mill liners.

Data sampled using the inductive probe from two replicates done with the spherical media shape, at 20 percent charge-filling level and 75% critical speed were analysed for reproducibility.

Table 3.4 Replicate toe and shoulder position ranges (J20, N75%)

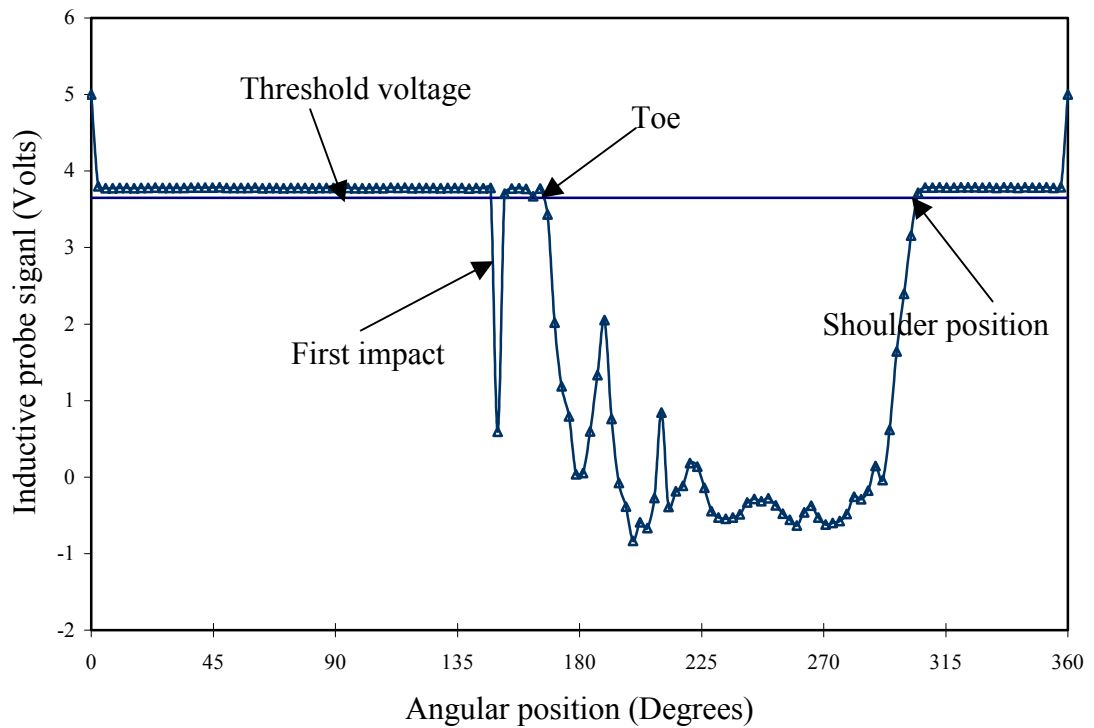|	Toe		Shoulder	
	Position	Standard Deviation	Position	Standard Deviation
Run1	169	10.6	291	6.1
Run2	167	9.9	289	8.1

Figure 3.7: Typical signal produced by inductive and marker probes (spheres, one rev., N50% & J=20%).

Table 3.4 shows the mean toe and shoulder positions with their respective standard deviations for 43 full revolutions over a period of one minute. The analysis of individual revolutions data obtained for a single experiment showed that, even within

the same experiment, load positions were not reproducible for different revolutions. However, for the two replicates, the significance test, using a t- test at a 95 % confidence limit for the averages of all revolutions for toe and shoulder positions indicated that the differences were insignificant. The calculated t- values were 0.88 for toe and 1.27 for shoulder positions. At the 95% confidence limit; two-sided test, $t_{0.95}$ for 43+43-2=84 degrees of freedom is in the range of -1.66 to 1.66; therefore the differences were not significant between the two experiments.

The average load positions (Table 3.4) for all revolutions within the period of one minute for the two replicates analysed fell within the same range. Thus it was assumed that the load positions over the sampled speed could be represented by the mean position of all individual revolutions within the whole sampling time with their associated standard deviations. This assumption was adopted and used for presentation of toe and shoulder positions.

3.4.1.3 Power calibration

Mill power was obtained from data produced by the torque beam. The beam was calibrated to ensure that information obtained was the actual representation of torque exerted by the charge in the mill. It was calibrated using a known weight suspended on a rod at a known distance from the centre of the mill.

Torque produced as a result of suspended masses was obtained by multiplying the weight and distance between the mill centre and the point of application. The masses were suspended at 295mm from the centre of the mill. The net torque was obtained as a difference between torques obtained with a charge (gross torque) and zero load torque at the particular speed.

$Net\ Torque = Gross\ Torque - Zero\ load\ Torque$

$$P_{Net} = \frac{2\pi N T_{Net}}{60}$$ 3.2

where N is mill speed in rpm

Because of variations in the room temperature due to changes in weather and other disturbances, the mill had to be recalibrated before commencement of milling kinetics experiments, conducted about a month after load behaviour and power experiments. Figure B.1 in Appendix shows the calibration chart used to obtain charge power for load behaviour and power experiments.

3.4.2 Milling kinetics experimental programme

3.4.2.1 Feed material characteristics and preparation

Quartz feed material graded into –300, 400-850 and 800-1800μm particle sizes were delivered in separate 40kg bags. The supplier's typical chemical analysis information is shown in Table 3.5. The material was screened to prepare mill feed samples each predominantly of a single size of 300x425, 600x850 and 1180x1700 microns.

Mill feed content was calculated using equation 3.3. The f_c value was calculated from equation 3.4 by first setting the interstitial filling U.

$$M_{feed} = V_{mill} * \rho_{bulk} f_c$$ 3.3

where

$$U = \frac{f_c}{0.4J}$$ 3.4

and

$$\rho_{bulk} = (1 - \varepsilon)\rho_{quartz} \qquad\qquad 3.5$$

Table 3.5 Typical quartz chemical composition

Component	% Composition
SiO$_2$	98.01
Al$_2$O$_2$	0.3
Fe$_2$O$_2$	0.2
ZnO$_2$	0.001
Cao	<0.01
mgO	<0.001

3.4.2.2 Experimental method

Experiments were done using the laboratory mill described in Section 3.1. The tests were done according to the conditions specified in Table 3.6 using ball size distributions shown in Table 3.7.

The experiments were designed after completion of the industrial mill ball size and shape characterization that provided initial data required for selecting the ball size distribution to be used in the laboratory-grinding mill. Owing to the size of the laboratory mill, the top size of the balls used was 30mm, instead of the typical industrial size of 50mm for coal pulverization. Chapter Four describes the observation of industrial ball size and shape distribution and characteristics, while Table 3.7 shows the size distribution used in experiments. From Figure 4.6 it is clearly

observable that below 31mm, balls start to deviate from being spherical. It is on this basis that the ball size of 30mm was used as the top size.

Table 3.6 Test condition for milling kinetics experiments

Parameter	Experiment conditions
Ball filling % (J)	20
Ball shapes	Spheres and worn ball
Ball size, mm	10.0-30.0
Mill speed (% Critical)	75
Feed material	Quartz
Interstitial filling %, U	20,50 and 80
Feed size (Single size)	300X425, 600X860 and 1180X1700μm

All milling experiments were done with 75% speed of critical (N_{Cr}=59.23Rpm) at a ball charge filling level of 20%. The disappearance of size j feed material was monitored for grinding time series of 0.5, 1, 2 & 4 minutes. Grinding time was recorded at each grinding step.

After grinding times, t_i (i=1,2,3 & 4) the whole charge was taken from the mill. Samples were obtained by tipping the charge through a screen big enough to retain all the balls, and were split to obtain about 50gram samples for particle size analysis. After obtaining a sample for analysis, the content was loaded back into the mill for the next test. The mill sampling method adopted is explained in appendix D

For every single size feed, eight $\sqrt{2}$ geometric series screens were used to analyse particle size distribution. This was because the shaker could only accommodate a

maximum of eight screens and also the effectiveness of a shaker decreases with an increase in the number of screens stacked. The top screen used allowed all the material to pass through.

Table 3.7 Media size distribution used for milling experiments

Size Interval	Weight fraction	Spherical Balls		Worn Balls	
		Mass (kg)	Number of balls	Mass (kg)	Number of balls
26.5-30.00	0.42	34.640	338	34.645	333
22.4-26.5	0.27	22.190	383	22.29	329
19.00-22.4	0.19	15.56	440	15.365	352
9.500-	0.12	9.850	597	9.910	475
Total	**1.00**	**82.240**	**1758**	**82.21**	**1489**

Size analysis was done, first by wet screening to remove material smaller than the bottom screen. Samples were then dried in the oven, and dry screening was done for 20minutes. The sieving time was established as described in Section 3.4.2.3

3.4.2.3 Sieving time

Ideally batch sieving for a long time should remove all the near size material. This is because the near size particles are continually abraded to a size that will pass the screen. Thus a suitable sieving time must be established which is sufficient to permit small size materials to fall through, yet not long enough to give much abrasion.

In order to establish an optimum sieving time, a sieving rate study was carried out as per standard procedure (Austin *et al*, 1984). Fine quartz material passing 600microns from a supplier was used to establish sieving time. Eight samples of about 50grams each, obtained by splitting a half-kilogram, were screened for 10, 15, 20 and 25 sieving minutes for two replicates.

Materials passing through the smallest screen size were monitored for all sieving times until there were no more significant changes. A suitable sieving time of 20 minutes was established and adopted.

Chapter 4

Industrial Ball Mill Media Characterisation

4.1 Introduction

The study of milling kinetics related to media shape and size distribution required the preparation of a consistent ball charge. The grinding experiments had to be conducted using a well-defined media size and shape distribution allowing the assessment of milling performance to be linked to media characteristics. Theoretical methods for estimating size distribution proposed (Bond, 1958) have been based on theoretical principles. It is, however, important that the actual industrial ball size and shape distribution be obtained. Thus, grinding media from an industrial mill were obtained and their ball size and shape distribution studied. Determination of ball mill composition in terms of ball size and shape was undertaken at two points inside the mill: the mill centre and the mill feed end, deep to the centre of the mill charge.

4.2 Experiment

4.2.1 Experimental mill

Grinding media for subsequent experiments were obtained from the Kendal power plant ball mill at specific sections shown in Figure 4.1 and the ball distribution was studied. The plant is an indirect dry-cooled power plant consisting of six 686Mw turbo-generator units. Coal of 35 mm nominal top size is fed into the mills to obtain pulverised fuel (PF) with about 99% passing 300 microns. The mill is 6.56m long and 4.6m inner diameters from the liner, each. The mill is air swept mill, designed to be fed from both ends. The mill is fitted with wave type liners and the media charge is 83 tons with 50mm steel balls used to top up.

4.2.2 Experimental procedures

The grinding media were collected from a crash-stopped mill, from the positions indicated in Figure 4.1. The mill was crash-stopped to maintain the normal operation charge mix. Five ball samples were drawn from each of the two axial mill positions: at the centre, and at the feed end, as shown in Figure 4.1. The sampling points are indicated as C1, C2, C3, C4, C5 and F1, F2, F3, F4, F5 for the mill centre and feed end respectively. The notation F indicates the mill feed end and C the mill centre sampled points, the numerals show the depth, starting with 1 at the charge surface. Each sample was drawn at a depth of 10cm by digging from the surface to the centre of the charge rotation. The collected samples were transported to The University of Witwatersrand for analysis.
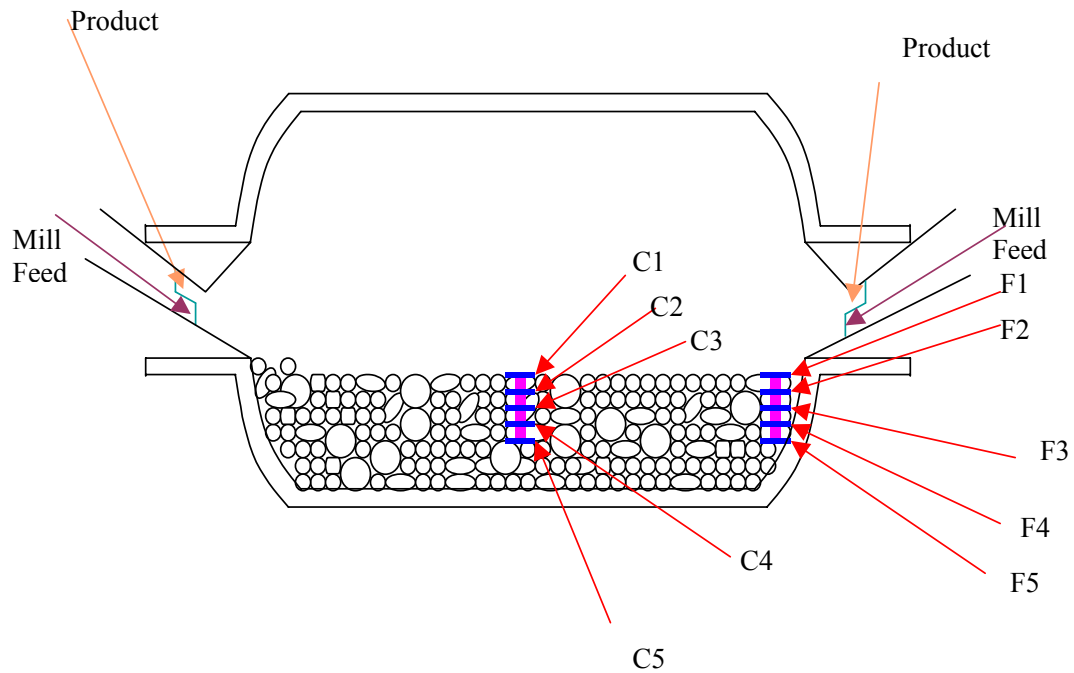

Figure 4.1 Mill sampled points

Size analysis was conducted on each sample and the number of balls and the mass in each size class were obtained. 16, 19, 22.4, 26.5, 31.5, 37.5 and 44mm screens were used for ball size analysis and OPTIMAS image analysing software was used to analyse photographic images of the balls for media shape.

The software enabled extraction of information about the area, size, shape and position of the balls. The function of area morphometry was used. The circularity measurement was the main focus in this analysis for the determination of the extent of media deviation/shift from the spherical shape.

Initial calibration was carried out to correct any distortion on the photographic image. This was a crucial step in ensuring that the information obtained was a true representation of the real world, as accuracy of measurements in the samples could be affected by image distortion

4.2.3 Results and discussion

4.2.3.1 Ball size distribution

The results of the ball size analysis of samples taken from the positions indicated in Figure 4.1 are shown in Figures 4.2 and 4.3 for radial distribution in which cumulative mass fractions passing the top size are plotted against ball size.

A trend in ball size distribution with charge depth was found. It was observed that the fraction of small balls increased with increase in charge depth for samples removed from both the centre and the feed end. The axial variation in average ball size distribution inside the mill is shown in Figure 4.4. Proportions of larger balls increased toward the centre of the mill as shown in Figure 4.5 where d_{50} size of samples from both the mill centre and the feed end are plotted against mill depth.

It is clear from these observations that ball segregation occurs along the length and depth of the mill. This segregation is likely to cause variation in the grinding rates within different regions of a mill.
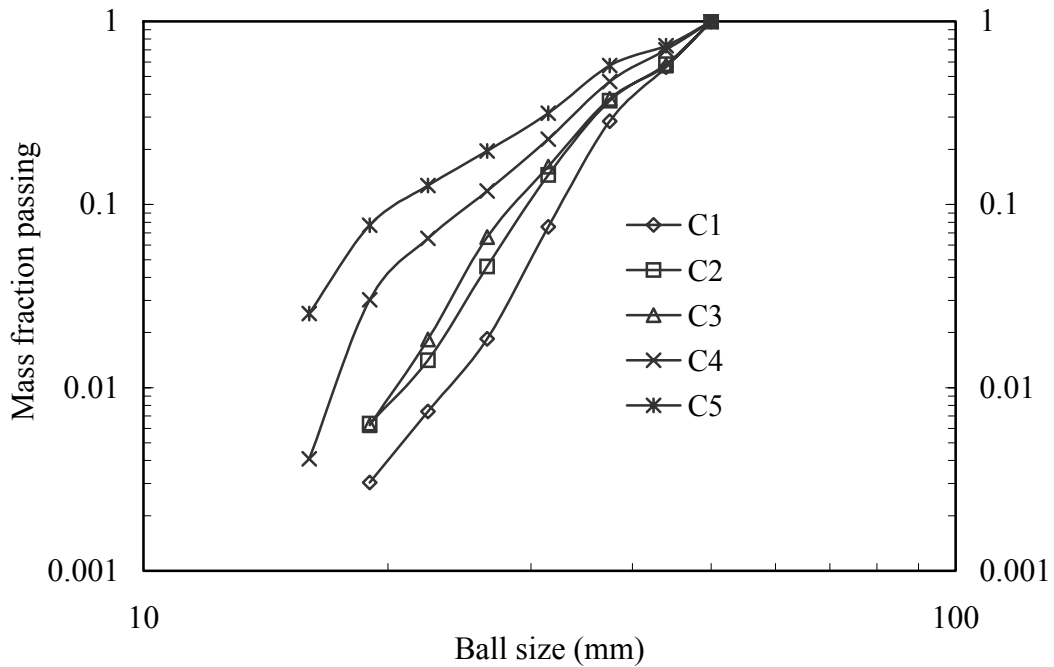

Figure 4.2 Ball size distributions at different charge depth for mill central sample

There are possible explanations for this axial non-uniform ball distribution. For air swept mills, where material enters the mill on one side and exits on the other side, the discharge side is under-filled with material, which results in excessive wear of grinding media at this point. However, this does not apply to a mill that is fed from both ends. It is thought that there exists a dead zone at the centre of the mill, where an equilibrium position is reached by material and air coming from the two mill ends. This results in accumulation of material, which then acts as a cushion that reduces ball impact and wear at the centre of the mill.
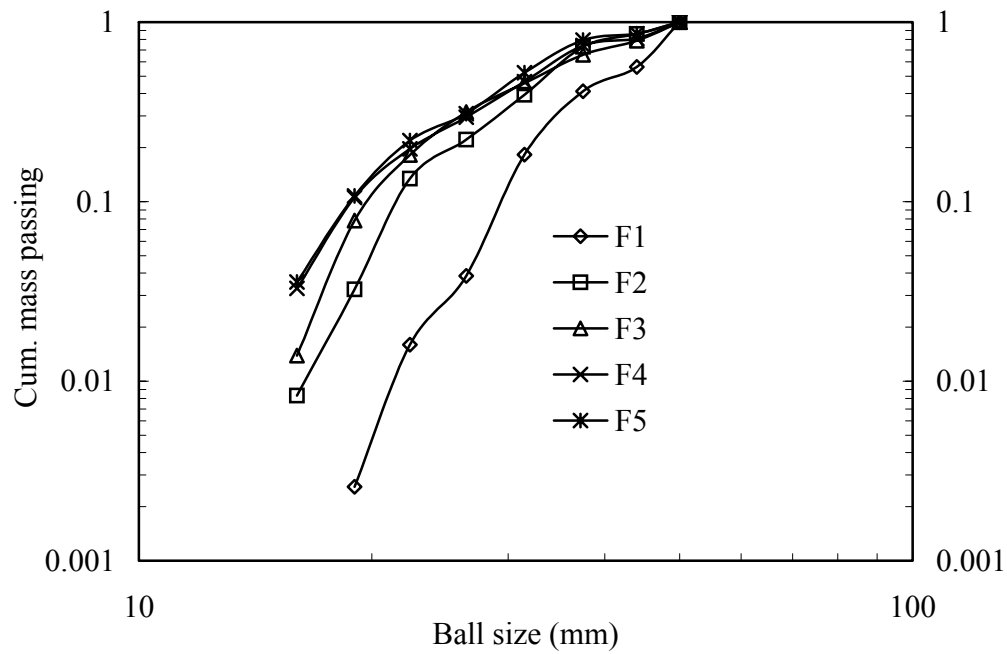
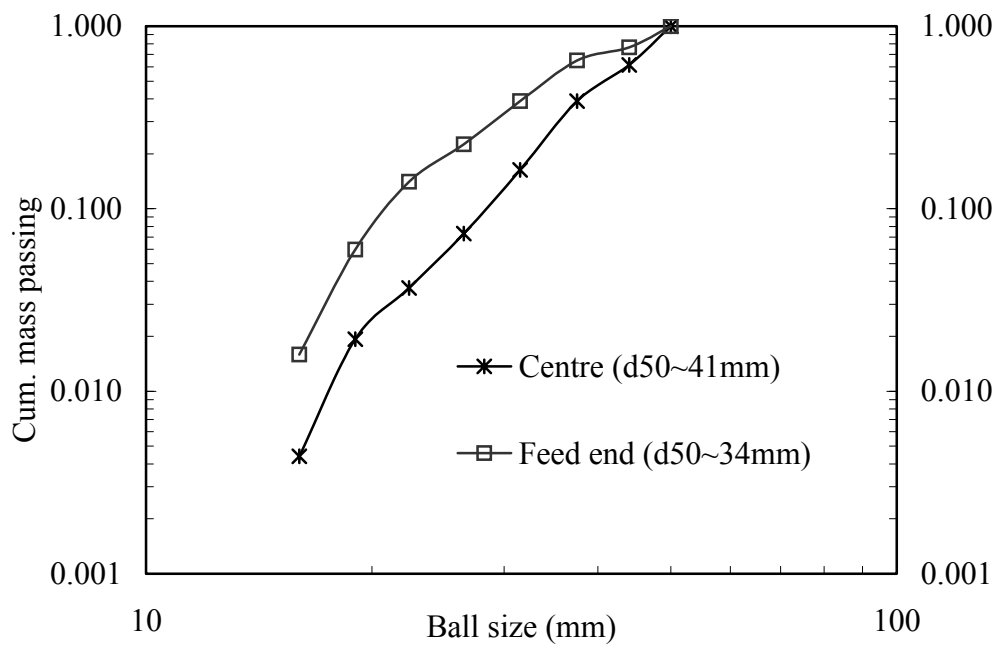**Figure 4.3** Ball size distributions at different charge depth for mill feed end sample.

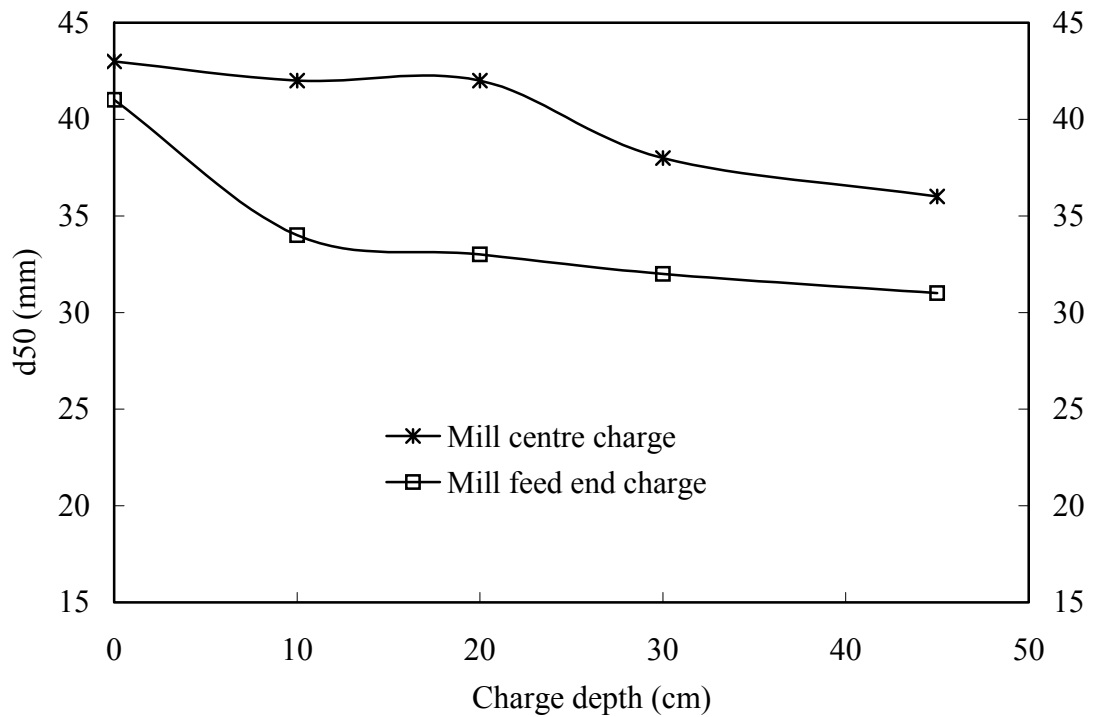**Figure 4.4** Ball size distributions along the mill length

Figure 4.5 Ball size (d_{50}) distribution to the depth of the centre of the charge.

4.2.3.2 Ball shape

The grinding media obtained from the industrial ball mill were sized and visually examined for deviation from the initial spherical shape. The 2D plane ball shapes photographed using a camera, were used to represent the shape of the media. Figure 4.6 shows ball shapes projected area in different ball size classes.

Figure 4.6 shows that almost all grinding media less than 31.5mm in diameter no longer maintain a spherical shape; with the tendency increasing with decreasing media size. This is a result of continuous breakage and wear occurring in the mill environment for a substantial length of milling time. For a sample drawn from the centre of a mill, this makes of about 15 percent of the charge (Figure 4.4). While it may seem not very significant at this point, considering the composition of the mill feed end, balls smaller than 31.5mm constitute about 40 per cent of the charge; this

explains why it was necessary to study the effect of the presence of worn balls inside the mill.

| +44mm | +37.5-44mm | +31.5-37.5mm | +26.5-31.5mm |
| +22.4-26.5mm | +19.0-22.4mm | +16.0-19.0mm | -16.0mm |

Figure 4.6 Characteristic features of balls inside ball mill

Figures 4.7 and 4.8 plot the non-spherical factors, which are the percentage of deviation from being spherical, against media size (upper sizes of the screen interval), for the mill centre and feed end positions respectively. The non-spherical factor was calculated from circularity, estimated using OPTIMUS software, and is defined as given in equation 4.1. Only a true circle achieves a minimum value of 4л, while for a square it has a value of 15.

$$\text{Circularity} = \frac{(\text{Perimeter of a projected area})^2}{\text{Projected Area}} \qquad 4.1$$

A relative scale that uses sphere as the base index can thus be written as follows:

$$\text{Non-Spherical factor} = \frac{\text{Circularity of Media} - \text{Circularity of a sphere}}{\text{Circularity of a sphere}} X100\% \qquad 4.2$$

Based on equation 4.2; a perfect sphere will thus have a non-spherical factor of 0 (zero) while a square will have a value of 27.32. From Figure 4.7, it is clearly seen that as media wear down to a small size, their morphological shape changes to non-spherical.
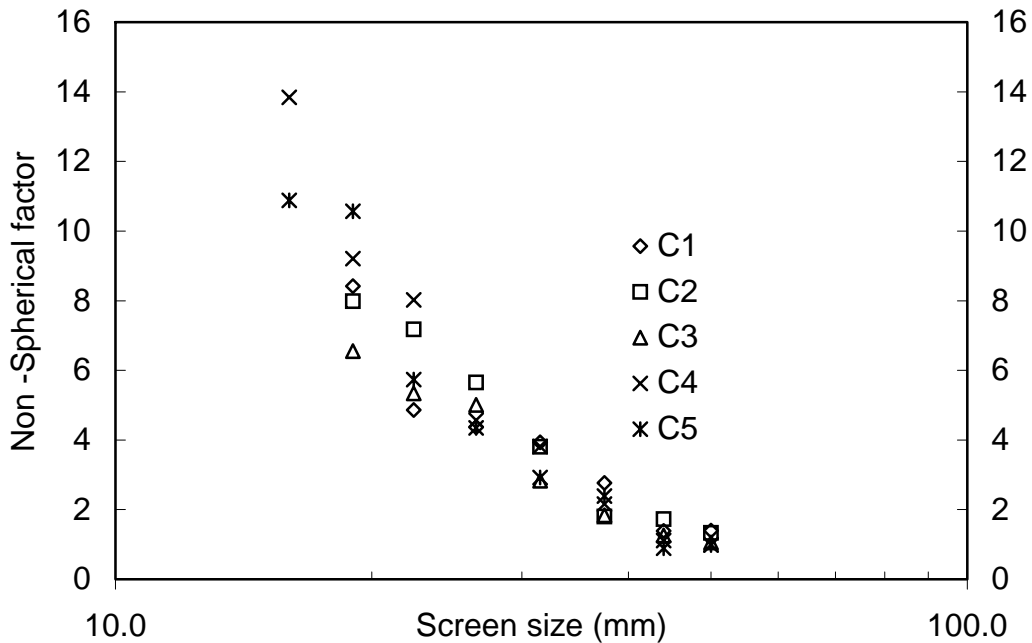

Figure 4.7 Change in media sphericity with media size at different charge depth (mill centre)

The variations of non-spherical factor with media size are shown in Figures 4.7 and 4.8, for the variation with depth in the mill charge; and Figure 4.9 for overall non-spherical factors variation along the mill length. It was observed that non-spherical factors increased systematically with decreasing media sizes.

While the proportion of small balls increases in accordance with depth and along the mill length to the feed end and the larger ball proportion decreases, deviation of media from spherical does not occur in a well-defined manner according to depth at which the sample was taken.
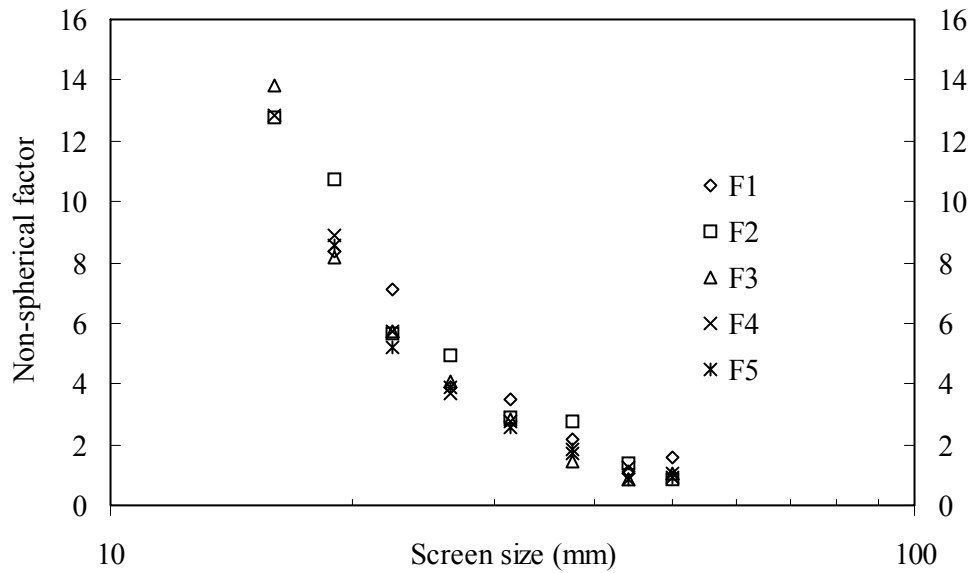
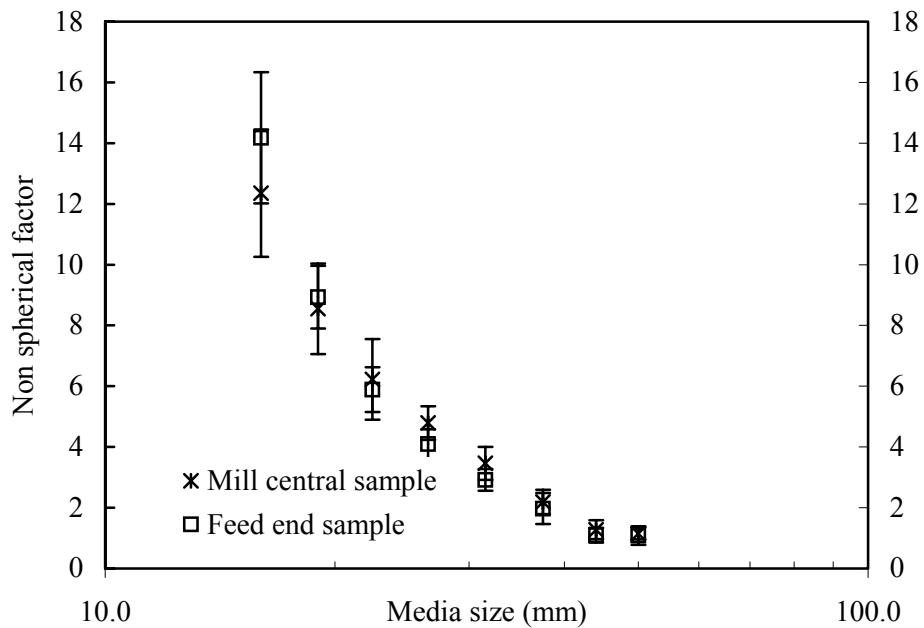**Figure 4.8** Change in media sphericity with media size at different charge depth (feed end)

Figure 4.9 Overall change in media sphericity with media size along the length of the mill

4.2.4 Source of error in data correction

The software allows manual data correction by drawing an area on the image using a mouse. It involves anchoring the beginning point of the area boundary, moving around the area and then exiting the area-marking mode. This manual data generating technique introduces an error into measurement due to the inaccuracy of tracing around the image. While change in non-spherical factors of up to 2.5 percent could be assumed to be a result of moulding and casting effects, as well as the circularity data generating technique; increased deviation from spherical is, to a great extent, attributable to media wear as a result of breakage, abrasion and impact inside the mill.

4.3 Mathematical Description of Non-spherical Factors with Media Size

The observed non-spherical factors for the sample drawn from the mill were correlated against the size of the balls. The variation of non-spherical factors with ball size suggested an exponential increase as balls wear down to a small size. Equation 4.3 was found to represent well the dependence of the non-spherical factor on ball size in mm.

$$\text{Non} - \text{spherical Factor} = X_i^{\varepsilon} * e^{\left(\omega - \lambda X_i\right)} \qquad\qquad 4.3$$

where ε, ω and λ are constant model parameters. The value of ε, ω and λ depends on the axial positions of the mill sampled and x_i is the top screen size in the interval. The values of ε are -1.70 and -3.07 that of ω are 7.42 and 10.73, while those of λ are 0.01 and -0.03 for the samples drawn from the centre and feed end of the mill respectively. Figures 4.10 and 4.11 compare experimental data with that computed using equation 4.3 using ε, ω and λ values stated above for the two mill sections.
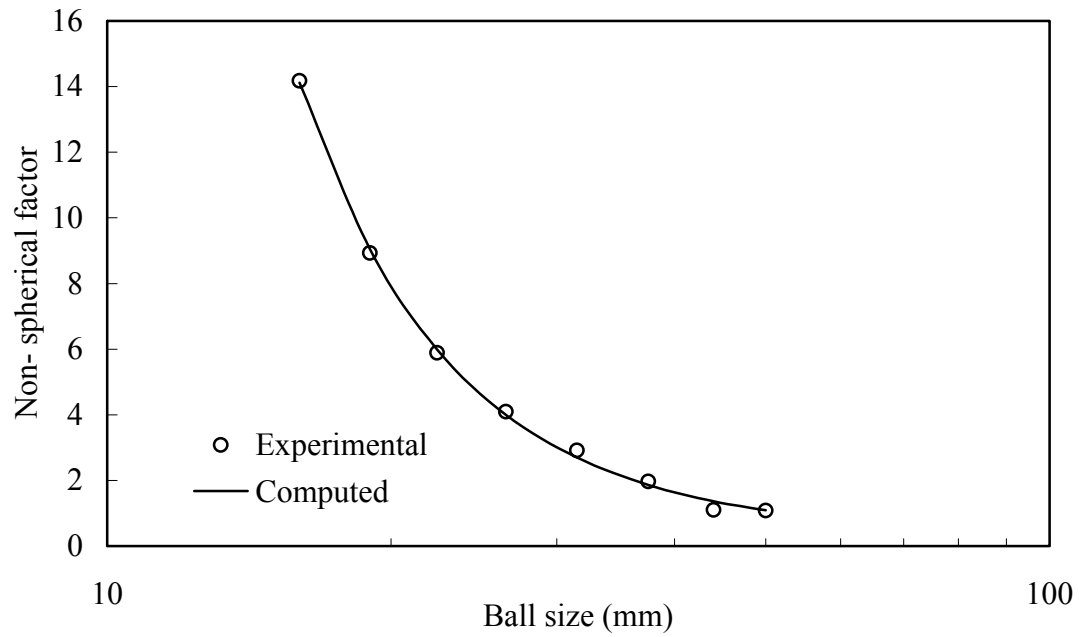
Figure 4.10 Comparison of experimental and computed non-spherical factors, feed end
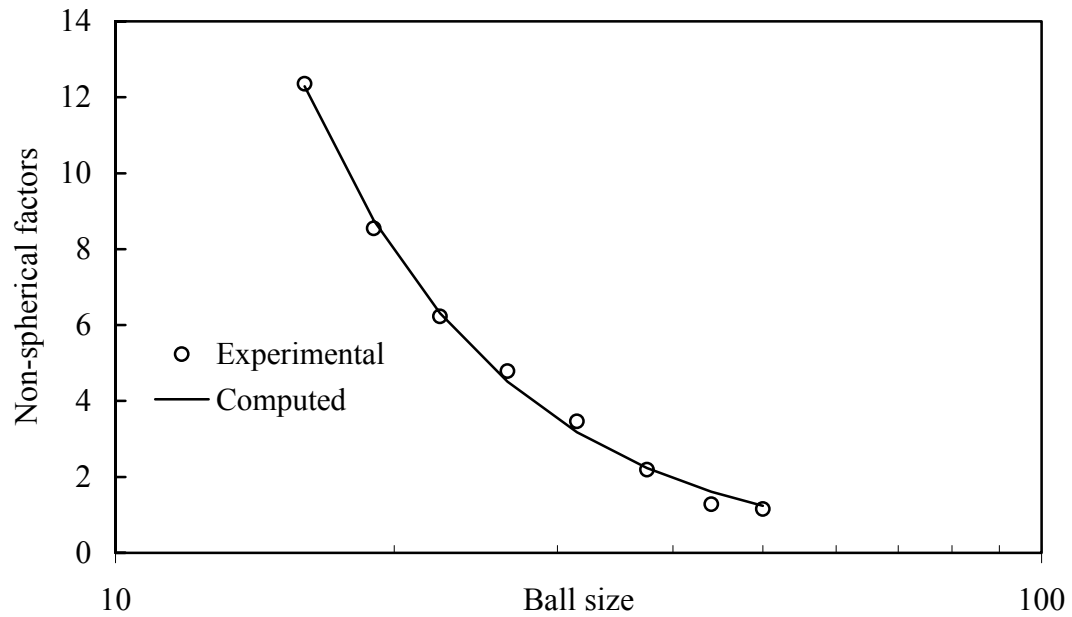

Figure 4.11 Comparison of experimental and computed non-spherical factors, mill centre

The equation developed fits the experimental data trend well. While the non-spherical factors for larger balls can be attributed to casting and the technique used to develop circularity data, it can be accepted that the equation represents well the relationship between ball size and expected deviation from sphericity for smaller balls.

4.4 Wear Mechanisms Inside Industrial Ball Mill

Grinding media wear is a contentious subject and many theories exist regarding the laws governing the process. Measurement of ball size distribution within a ball mill can provide data on ball wearing mechanisms and indicates the relative intensities of abrasion and impactive forces within the mill.

The general wear model is expressed as:

$$\frac{dM}{dT} \alpha X^{q} \hspace{5cm} 4.4$$

M is a cumulative mass of balls smaller than size X, T is an amount of materials milled in tons and q is a constant governing milling situation, a value close to 2 indicating that the balls are predominantly wearing down due to abrasion whereas a value close to 3 indicates that the balls are predominantly wearing through impact. Bond (1958) suggested that the equilibrium charge can be represented by a straight line with a slope m=3.84 when the percent weight passing the diameter is plotted against the diameter. The intersection of vertical lines drawn representing mid-points between ball size with the equilibrium line determine the percent of each size to be used in the initial charge. This was based on the rule that an equal film thickness is removed from all ball sizes in a mill during milling for a given time.

Ball size distributions obtained from industry were compared to that predicted by the proposed wearing theories; impactive (Volume theory), abrasive (surface theory) and

the initial charge calculated based on equal film wear (Bond's) and are plotted in Figure 4.12
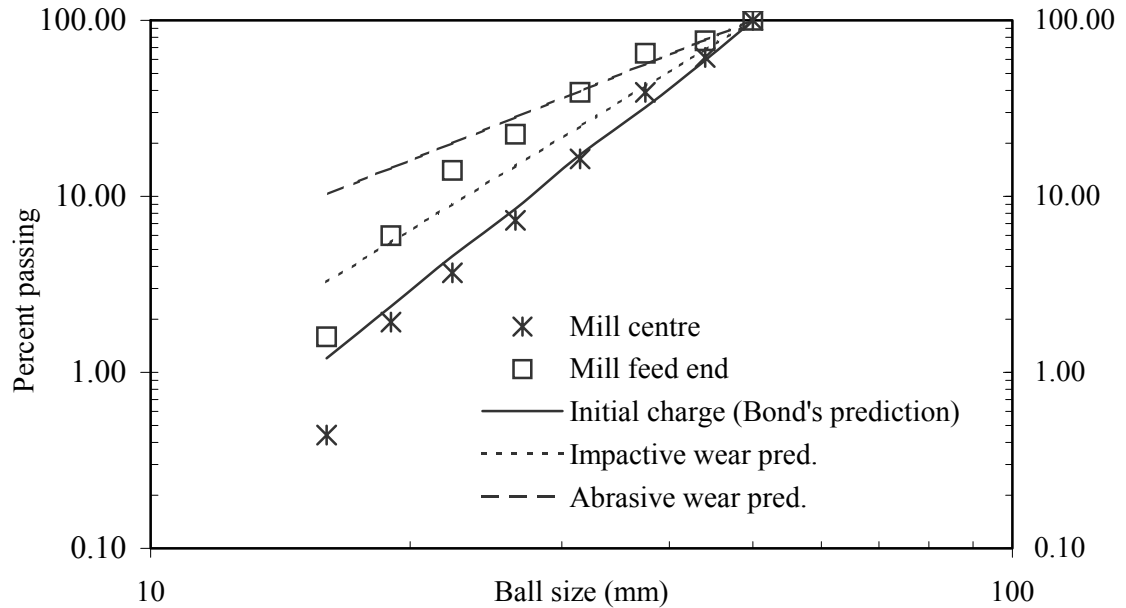

Figure 4.12 Comparison of experimental ball size distribution with that predicted by different wear theories

It is clear that the results deviate from those of the three proposed models. However, the charge composition of balls passing 16mm constitutes about 0.4 and 1.5 percent for mill centre and feed end respectively. If it is assumed that this composition is negligible; then the ball size distribution obtained from the mill feed end tends to approach the abrasive wear mechanism prediction, while that at the mill centre is very close to the equilibrium distribution predicted by Bond's equal film wear theory.

Equation 4.4 was fitted to experimental ball size distributions with balls smaller than 16mm ignored, and the q values estimated as a slope of the line of cumulative percent passing screen size plotted against ball size. The q values obtained were 2.20 for the mill feed end and 3.71 for the mill centre, which suggested that ball wear at the feed end is predominantly caused by abrasion, while that at the mill centre approaches the mill initial charge proposed by Bond's prediction based on equilibrium distribution.

However balls move from the feed end toward the centre of the mill as such does not exhibit characteristic of feed or centre wear. These observations necessitate the need to study and establish an optimal particle filling level high enough to reduce wear and sufficiently low to not affect the mill grinding rate.

4.5   Conclusions

Information has been gained in terms of media shapes and size distribution inside the mill.

Data obtained clearly indicate the presence of ball segregation from the feed end to the centre, with the centre relatively coarser than the feed end, as well as segregation with the charge depth. The proportion of finer balls increases with depth in the mill.

This non-uniform distribution of media suggests possible variation of breakage rates and breakage distribution inside the mill.

A clear trend in ball shape in relation to ball size is observed.

The experiment serves as a guide in deciding the actual media size and shape distribution to be used for further milling kinetics experiments

Chapter 5

Load Behaviour and Mill Power
as Affected by Media Shape

5.1 Introduction

Load orientation affects the amount of power drawn by the mill, and is thus an important aspect when considering mill performance. Load orientation and mill power have been studied as a function of mill filling, mill speed and lifter type. In exploring alternatives for improving milling, it is important to look at other available avenues that can lead to an understanding and improvement of the milling process.

The impact of media shape on the milling process has only been investigated to a limited extent, though; it has a significant effect on the tumbling process

This chapter describes experiments done to study the effect of media shape on load orientation and mill power. The effects of media shape on both load behaviour and power were evaluated for cases where the mill was filled with only one type of media, without ore. Variations of the toe and shoulder positions with media shape, under conditions stated in Table 5.1, were compared. The experimental programme and conditions have already been discussed in Section 3.4.1. In this chapter experimental results are discussed.

5.2 Description of Load Position

The patterns of the signals obtained over one mill revolution from the inductive probe are shown in Figure 5.1 for the three media shapes. The approach utilised in marking the toe and shoulder positions is described in Section 3.4.1.2.1. Generally, the first momentary contacts were considered to be the result of balls bouncing around due to the turbulent nature of the charge. The actual toe position was taken as a point when the probe was in persistent detection of media, while the shoulder positions were obtained when detection of media around the sensing face ceased due to media departure from the mill liners (Figure 5.2).
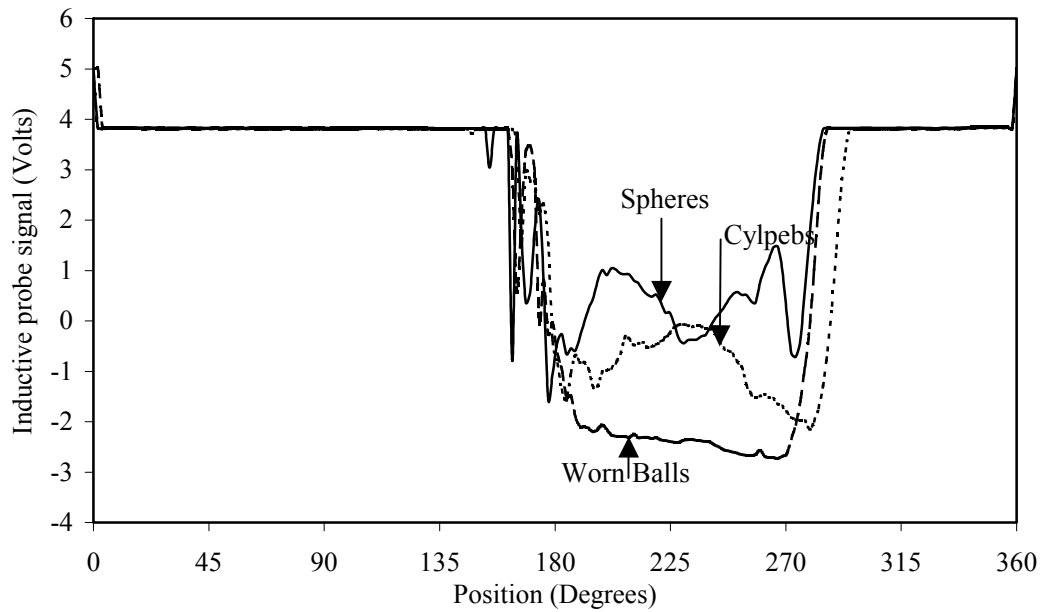
Figure 5.1 Variation of inductive probe signal magnitude with media shape.

It is observed from Figure 5.1 that the shape of media affects packing. When a probe is completely under the load, the magnitude of the signal detected for the worn ball was greater than that of cylpebs and spherical media. Spherical media have the lowest signal magnitude. This suggested closer packing for worn balls around the probe sensing face. This however does not seem to affect much the shoulder position as cylpebs retain higher shoulder positions than worn balls. The load orientation shown in Figure 5.2 was used to illustrate the charge positions inside a tumbling mill.

Figure 5.2 Load orientation profile description

5.2.1 Variation of toe and shoulder positions with media shape

Results presented in Figures 5.3, 5.4 and 5.5, show the variation of toe and shoulder positions with mill filling at 15, 20 and 25 percent charge filling levels respectively.

One can generally note that, at lower speed, $\leq 60\%$ of critical, the toe positions are similar for all the media types. However, at higher mill speeds, lower toe positions were obtained for cylpebs than for the other two media shapes.

Toe position data were analysed using the t-test at 95% confidence limit for hypothesis testing for significant differences among the shapes. Spherical and worn, spherical and cylpebs, as well as worn and cylpebs differences were tested. From the t-test analysis results it was found that at all mill speeds studied, toe positions varied among media shapes. However at mill speeds ≤ 60 percent of critical, variations in

toe positions with media shape were less than that at speeds greater than 60 percent of critical.
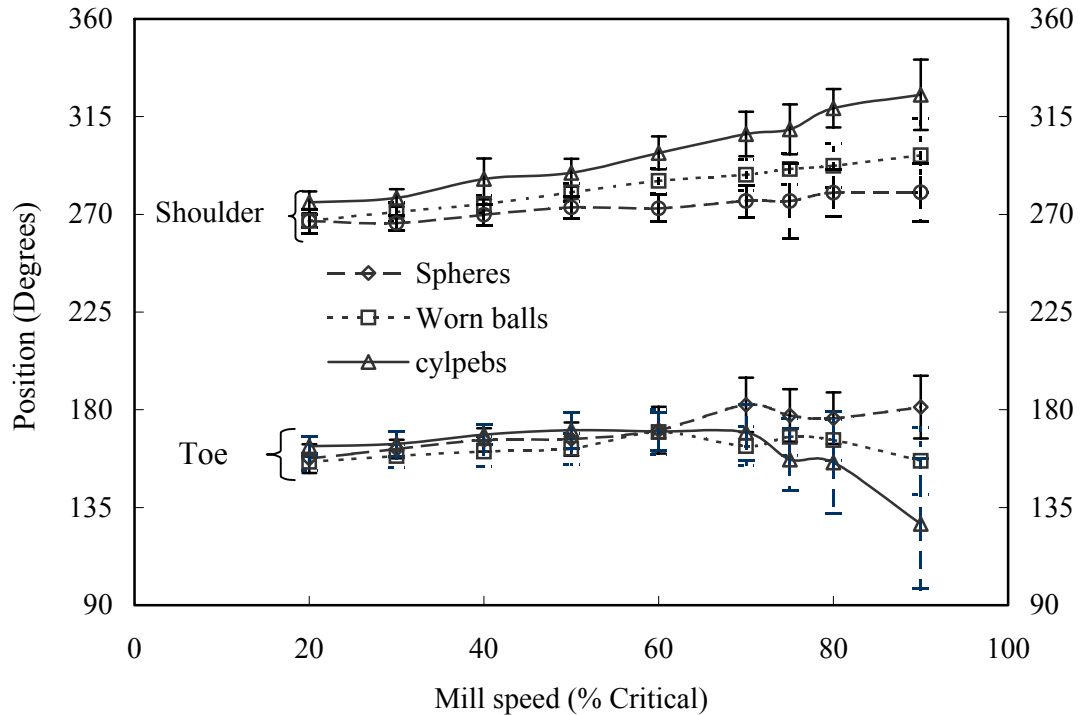

Figure 5.3 Variation of toe and shoulder positions with mill speed (J=15%)

The lower toe positions for the cylpebs can be attributed to close packing and locking of the media such that their cascading speed is relatively less compared to mill speed, and is also hindered by their shape. However, with increasing speed, they are thrown a greater distance and impact on the mill at lower angular displacement than spherical and worn media.

The error bars in Figures 5.3, 5.4 and 5.5, show that there is wide variation in the toe positions at higher mill speeds. This is due to the turbulent nature of the charge at the toe as media are falling and the aggressiveness of lifters used.
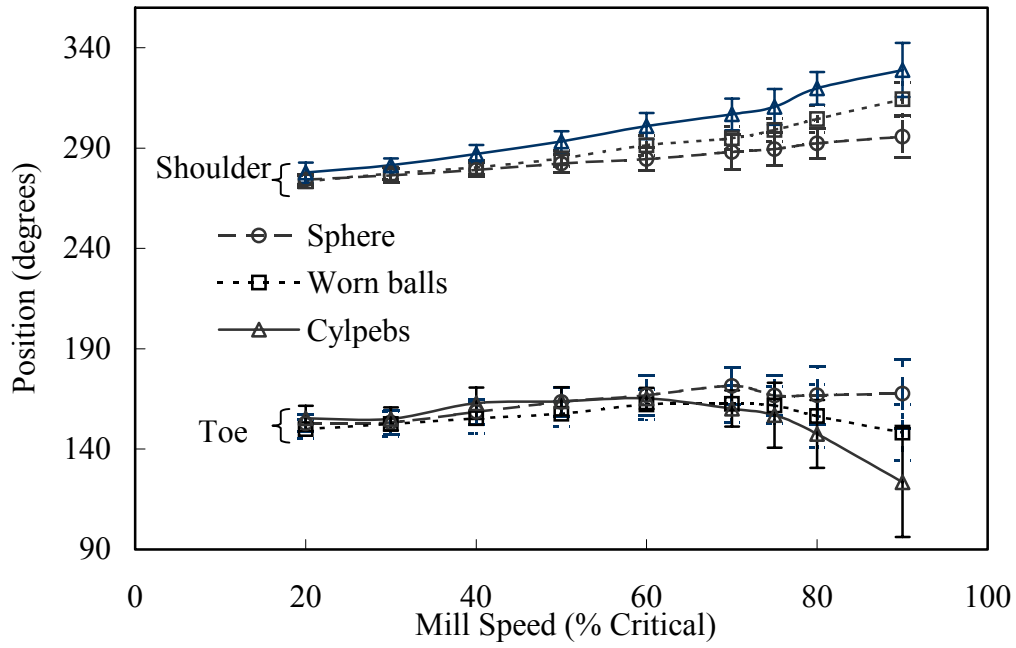
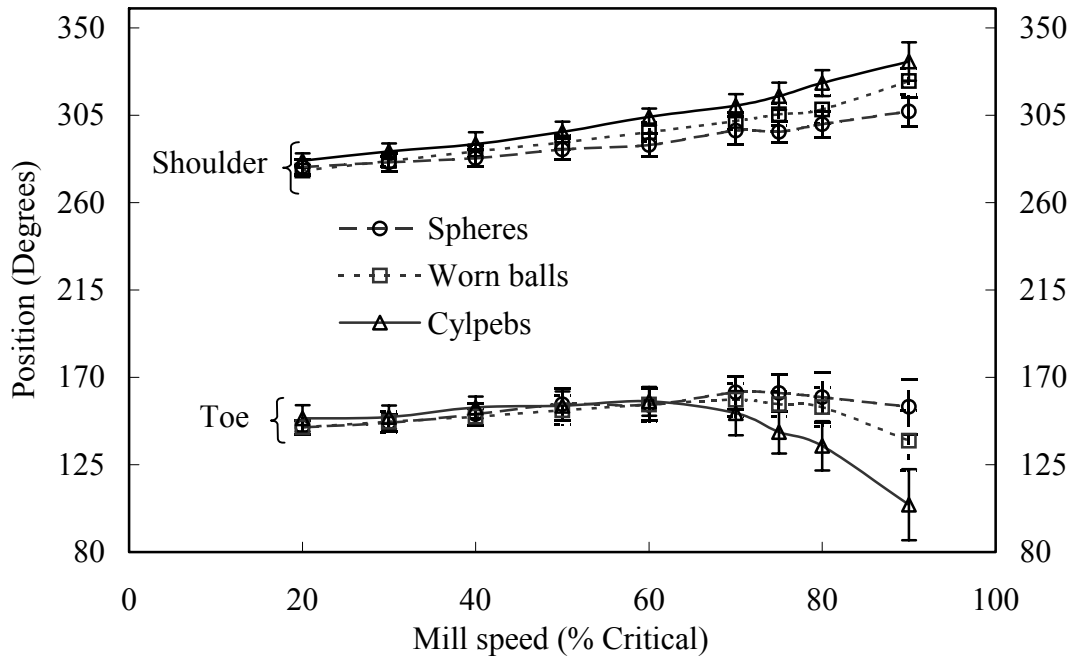**Figure 5.4** Variation of toe and shoulder positions with mill speed (J=20%).

Figure 5.5 Variation of toe and shoulder positions with mill speed (J=25%)

Observation of charge shoulder positions showed that the cylpebs are raised higher as compared to worn and spherical media. This is clearly shown in Figures 5.3, 5.4 and 5.5. The higher shoulder positions of cylpebs than other media also suggested early cataracting and premature centrifuging for cylpebs as compared to the other two shapes.

It was further observed that the difference in shoulder positions between media shapes decreases with increasing mill charge filling. While the differences between cylpebs and spheres were 16, 33 and 45 degrees at 50, 75 and 90 percent mill speeds for J15; at J20, their differences were 11, 21 and 33 degrees and 9, 18 and 26 degrees for J25 at the above mill speeds. The same trend was observed between spheres and worn balls and between worn balls and cylpebs at all speeds. The decrease in the difference occurred because the shoulder positions for spheres increased with mill filling levels while those of worn and cylpebs showed little variation in shoulder positions with mill filling. This can be seen in Figures 5.3, 5.4 and 5.5 showing comparison of variation of shoulder positions according to media shape, and Figures 5.6, 5.70 and 5.8, in which variation of toe and shoulder positions are compared for various filling levels.

5.2.2 Variation of toe and shoulder positions with load filling levels (J)

The variations in toe and shoulder positions with load filling levels were studied. It was observed that the shoulder positions increased with increasing mill speed and charge filling, in conformity with previous findings (Lidell & Moys 1988, Moys, 1993). The angular toe positions were steady with mill speed up to about 70% critical. Beyond this speed, the three shapes exhibited different patterns: sphere toe positions remained almost constant; worn balls shown a decrease and cylpebs, a marked decrease; with increase in mill speed.

Another important observation was that between different charge filling levels for a particular media shape for the three shapes studied. It was observed that, for the spherical shape, shoulder positions were affected by charge filling, while the difference for cylpebs between different charge filling levels at a particular mill speed were not as significant.
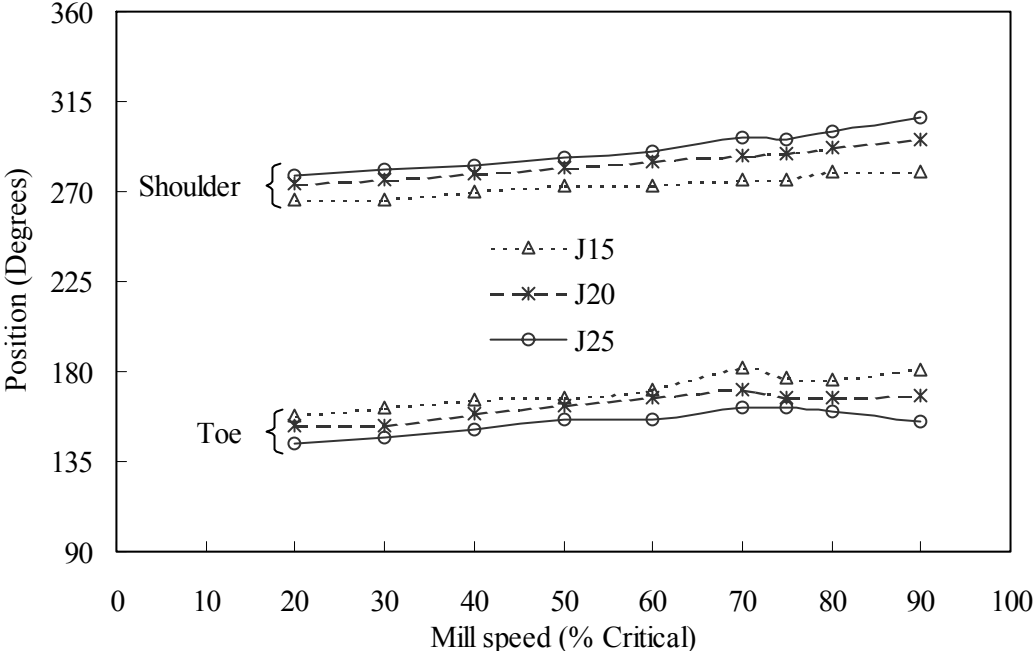

Figure 5.6 Variation of toe and shoulder position with mill speed at different charge filling levels (spherical media)
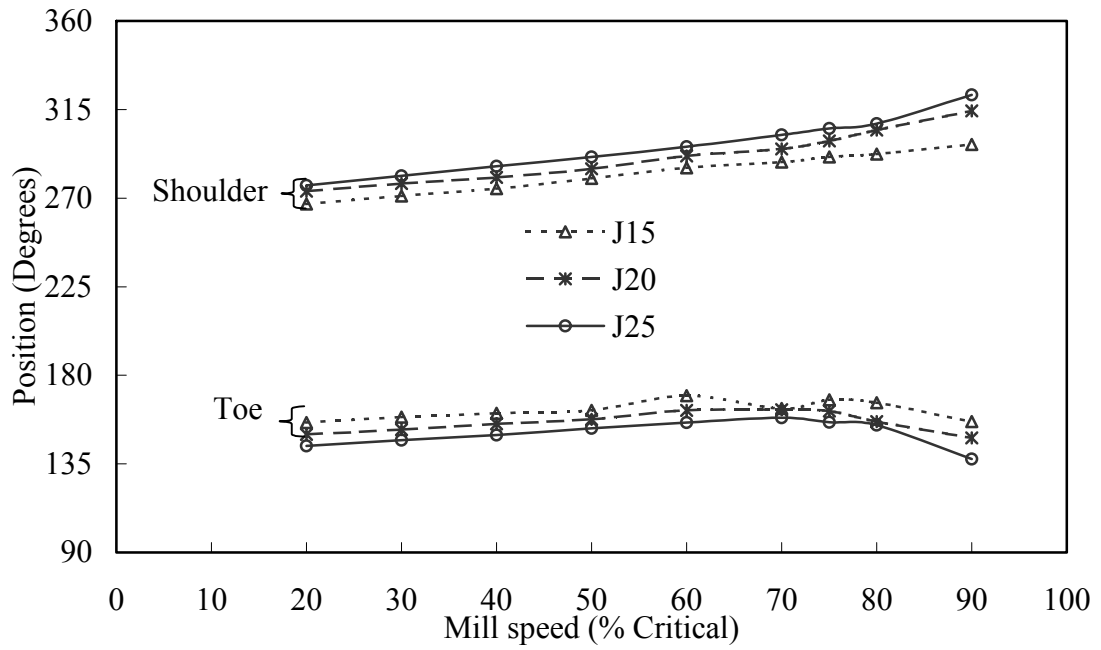
Figure 5.7 Variation of toe and shoulder positions with mill speed at different charge filling levels (worn balls)
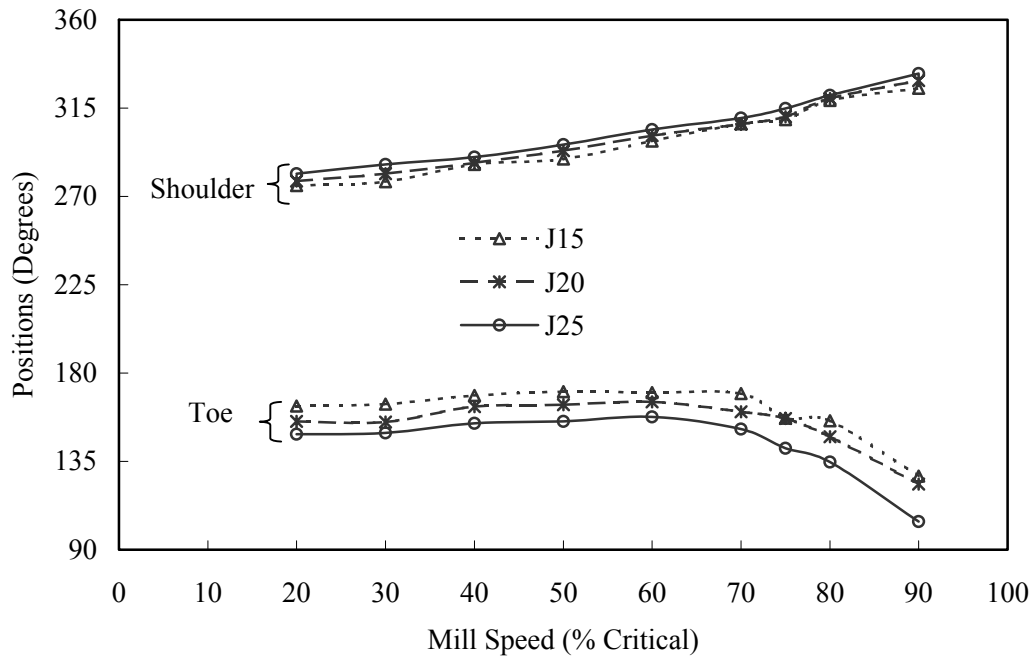

Figure 5.8 Variation of toe and shoulder positions with mill speed at different charge filling levels (cylpebs)

5.3   Media Motion

The motion of the charge inside the mill was examined by looking at videos taken at 75% mill speed for the three media shapes at three charge filling levels. The aim of this observation was to determine whether different media shapes exhibited different tumbling behaviours and motion inside the mill and to assess the usefulness of an inductive probe in relation to data directly obtained from the video.

Figure 5.9 illustrates trajectories followed by different media shapes at a 20 percent mill filling level. The trajectories were obtained by tracing the outer layer of the charge from the video pictures filmed during experimentation. The video analysing software was used for this task. The videos were taken through a transparent mill front-end cover. Results showed that charges were cataracting with cylpebs showing more cataracting than worn and spherical media. The video confirmed that cylpebs were lifted to higher shoulder positions and impacted on the charge at a lower angular position.
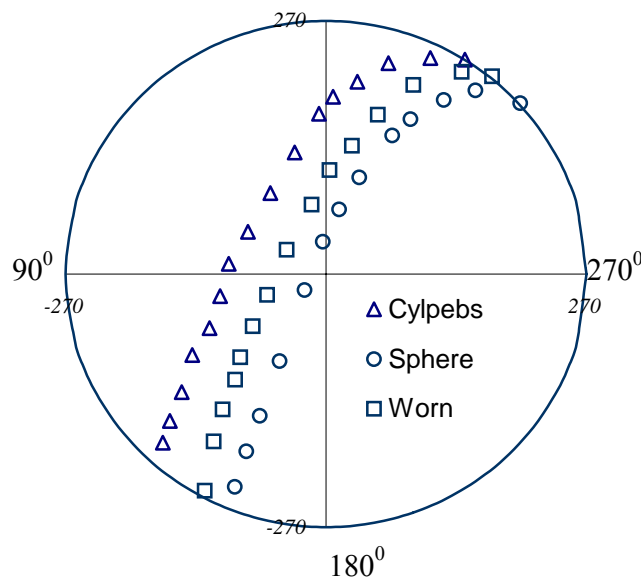

Figure 5.9 Media trajectory observed from video pictures at J=20%, N=75% N_{Cr}

The media shapes shoulder positions were similar to those measured using the inductive probe, which validated the use of the inductive probe to determine the orientation of the charge.

The angle of repose of the charge can be used to estimate the charge volume at lower mill speeds; this assumes that, a simple chord joining the toe and shoulder position can be used to represent the charge profile. At higher speeds, the chord approximation in not valid as such it cannot give the actual load volume or used in predicting mill power for general cases. This was clear on examination of the charge outer layer trajectories observed in Figure 5.9 which was obtained from the photograph of the mill charge tumbling inside the mill taken during experiments and has been discussed by Vermeulen *et al*, (1986).

Table 5.1 Summary of dynamic angle of repose at 20 percent mill speed

Mill filling	Spheres		Worn balls		Cylpebs	
	Angle of repose	Standard deviation	Angle of repose	Standard deviation	Angle of repose	Standard deviation
J15	31.72	3.23	31.71	1.86	39.36	3.36
J20	33.65	2.47	31.68	1.86	36.60	4.22
J25	31.23	2.60	30.35	1.75	35.25	3.50

The angle of repose can also be used in estimating the dynamic coefficient of friction of the charge cascading down the toe position.

The experimental results obtained at mill speeds ≤ 60 were used to estimate the dynamic angle of repose of the charge for the three media shapes. Table 5.1 summarizes the angle of repose with their standard deviations estimated from

experimental data for 20 percent mill speed and Figure 5.10 compares the angle of repose at various speeds for 20 percent mill filling. It was found that angles of repose of the charge increased with mill speeds for the studied mill speeds. It was further established that cylpebs have higher dynamic angles of repose compared to the other two media shapes.
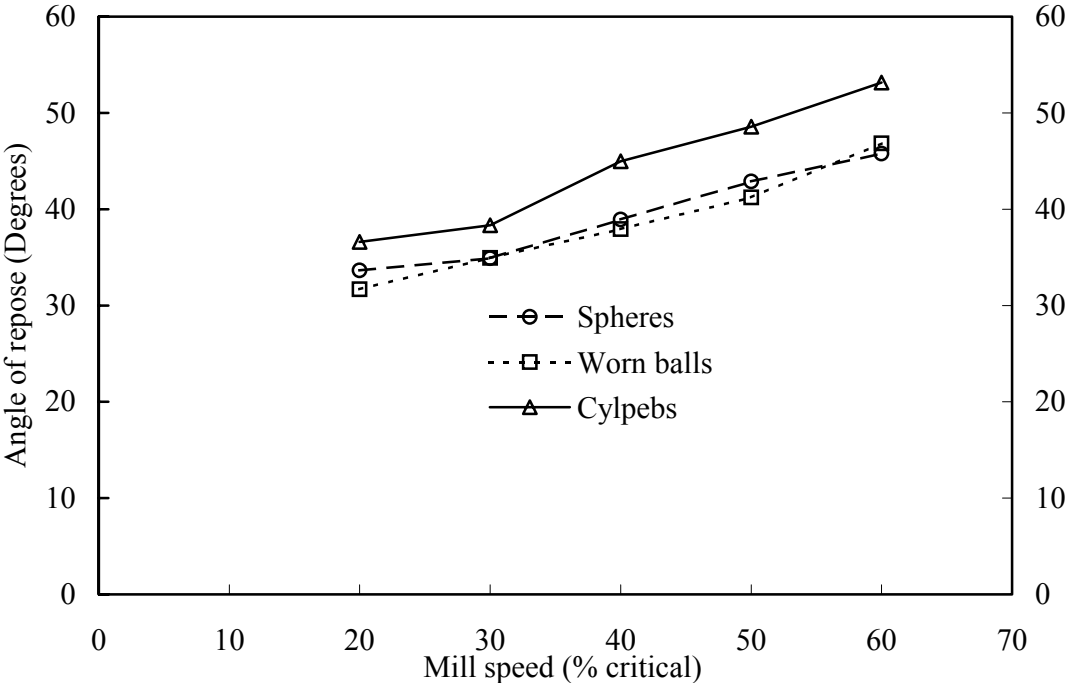

Figure 5.10: Comparison of dynamic angle of repose at various mill speeds

5.4 Mill Power Draw

Sensitivity of power draw to media shape and operating parameters in terms of speed and charge filling level was analysed. The power drawn was found to be sensitive to media shape at all charge filling levels studied. Figures 5.11, 5.12 and 5.13 show mill power drawn for the three studied media shapes as a function of mill speed for three

charge filling levels. Variations in mill power draw with different media shapes were clearly observed.

Charge power draw was in descending order of: cylpebs, worn balls and spheres, at mill speeds lower than 72% of critical. At a speed of about 72%, which is in the speed range most mills are operated, cylpebs and spherical media drew the same amount of power at all charge levels studied. However, beyond this speed, power drawn by cylpebs started to decrease while that drawn by spheres was still increasing. Likewise at a speed about 65%, cylpebs and worn balls drew the same power while at about 82%, the power drawn by spheres and worn balls were the same. It was also observed that the maximum power drawn was reached at different mill speeds for different media shapes.

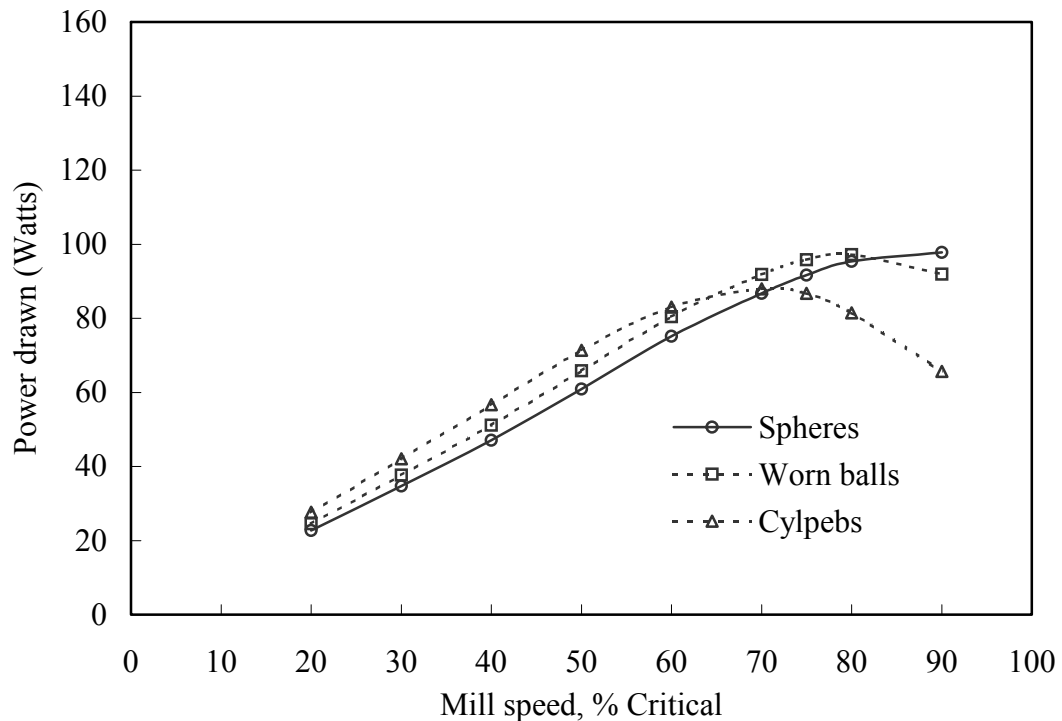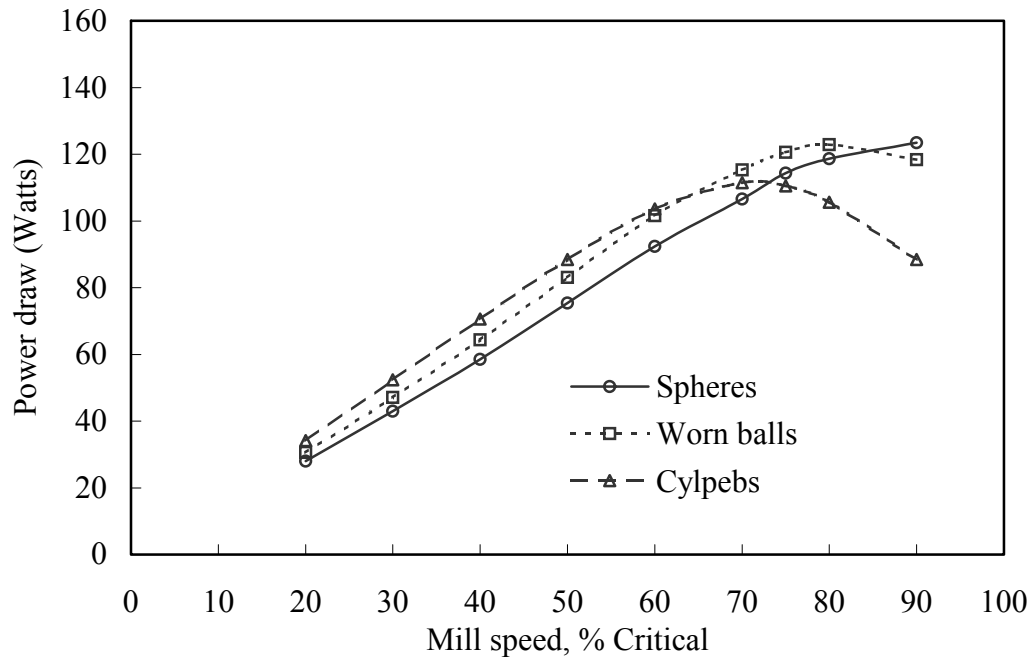**Figure 5.11** Power variation with mill speed for different media shapes (J=15%)

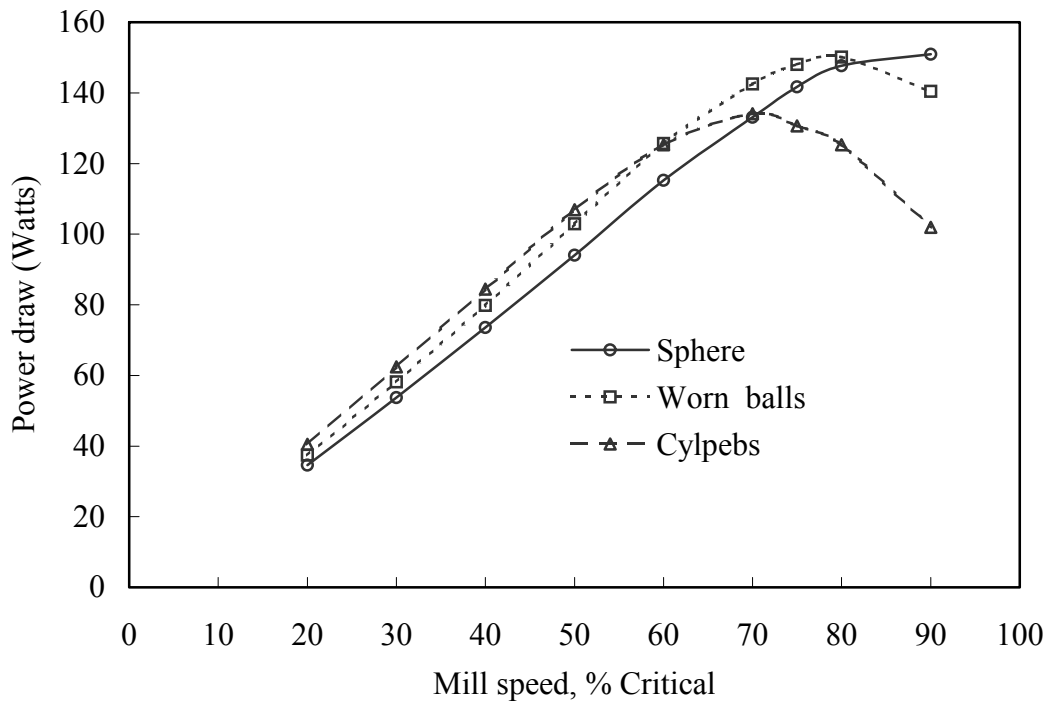**Figure 5.12** Power variation with mill speed for different media shapes (J=20%)

Figure 5.13 Power variation with mill speed for different media shapes (J=25%)

The power and shoulder data were analysed for direct correlation, to determine whether the peak power was reached at one point of shoulder position. However, no correlation was found as the peak power draw was found to have occurred at different shoulder positions for different media shapes and mill filling charge levels.

Variation of mill power draw with mill filling was studied. The observations made from experimental data conform to the previously established theories. It was found that mill power draw increased with increasing mill-filling levels for all the three shapes. It was further observed that for one media shape, the power draw reached a maximum at a particular mill speed. This can be clearly seen by looking at Figure 5.14 below.
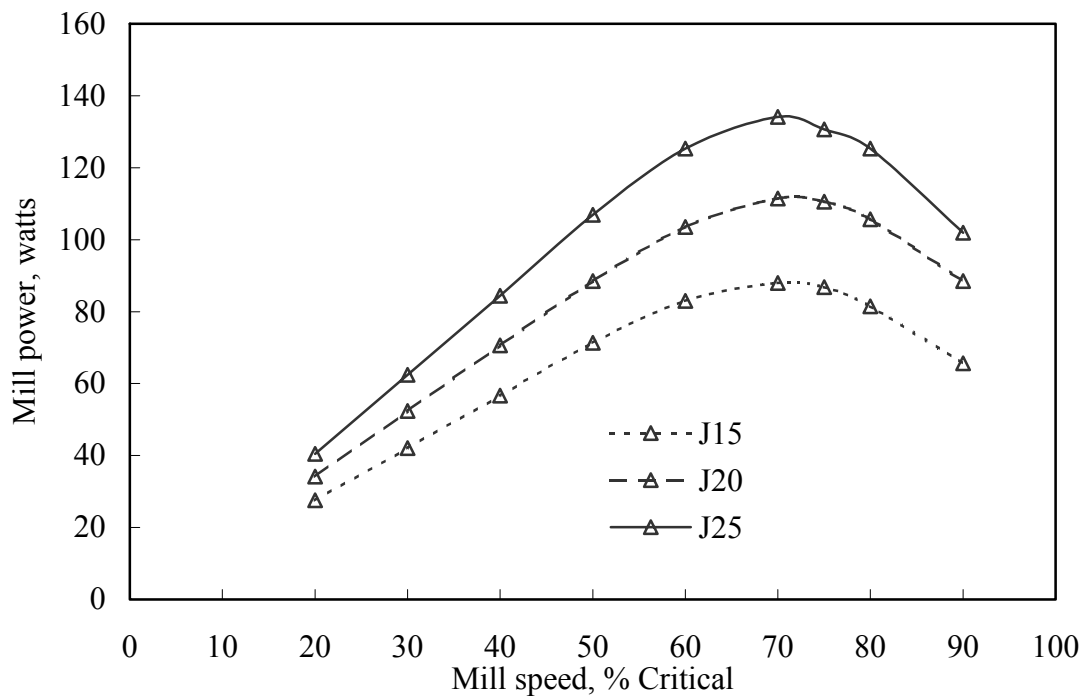

Figure 5.14 Variation of mill power draw with mill filling, J (cylpebs media)

5.5 Discussion

The load behaviour inside the tumbling mills depends on collective interaction and interlocking between individual media and between media and lifters. This interaction and interlocking is greatly influenced by point or surface contact among media to each other, and/or with lifters. For the media in contact with liner elements, the nature of contact is characterised by three types of motion: vibration, rolling and sliding on the slanting faces of the lifter. Of the three, rolling and sliding are significantly affected by media shape, depending on the contact made between the media and lifters. Generally, spherical media are likely to be subjected to all three motions, while irregular and cylindrical shapes experience restricted rolling motion due to surface contact. This may result in delayed departure from the mill surface or lifter and hence, may be raised to a higher shoulder position than that of spherical media.

All power predicting models developed (Bond 1961, Guerrero *et al*, 1960; Hogg & Fuerstanae, 1972; Harris *et al*, 1985; Moys, 1993; and Morell, 1993) had lumped the effect of grinding media into a constant. This suggests that, for any media shape used, the maximum power draw would occur at the one fixed speed. This is not the case as the experimental results show. Cylpebs power draw reached its maximum at lower speed, while spherical media power draw had not reached a peak up to 90 percent of mill speed. The worn ball's maximum power draw occurred at about 80 percent of mill critical speed.

This observation is supported by shoulder position data observed in Figures 5.9, 5.10 and 5.11. This may possibly be explained by looking at shoulder positions among media shapes. As load shoulder position increases, power also increases. However, continuous increases in shoulder results in more cataracting, increasing the number of balls in flight as well as impacting at the toe of the mill. Energy is imparted back to the mill by the impacting balls at the toe, leading to a loss in power as the amount of centrifuging increases.

5.6 Conclusion

The study was carried out to provide an understanding of the effect that media shape has on load behaviour in terms of toe and shoulder positions, as well as mill power.

Results indicate that media shape has an effect on toe and shoulder positions and on power drawn by the mill.

Cylpebs media had higher shoulder positions, compared to worn and spherical media. Spheres had the lowest shoulder positions of the three shapes. The trends were such that for all the three media shapes, shoulder positions increased with mill speed. While the shoulder position for spheres increased with mill charge filling, there was little variation in the shoulder positions with mill speed for cylindrical media.

It was found that at speeds less than 70 percent, the toe positions varied little with mill speed but above this speed, cylpebs media had the lower angular toe positions of the three, decreasing with mill speed increase. The toe positions for the sphere were inherently constant above 70 percent and higher than for worn and cylpebs media.

Cataracting is normally achieved by increased mill speed and/or changing the liner/lifter profile. This could, however, result in an increase in media impact onto mill shell/liners.

Opting for different media may change charge motion from cascading to more cataracting and vice versa, depending to what media shape is used. This in turns results in variation of the pulverised fuel being presented to air while also changing the impact onto the mill liners.

Power draw sensitivity to media shape was observed. Power draw increased to the maximum with increasing mill speed, for all media shapes. The maximum power draw for cylpebs media occurred at a lower speed than for the other media shapes

studied. At lower speeds, cylpebs media drew more power, followed by worn balls and lastly, spherical balls.

This study has given insight into the effects of media shape on mill power draw and might be useful when considering media shape for specific milling objectives and conditions of operation.

Chapter 6
Effects of Media Shape on Milling Kinetics

6.1   Introduction

Grindability is an important aspect when considering the breakage of coarser particles in fines production. In ball milling, breakage is described using specific rates of breakage (Selection Function) and breakage distribution (Breakage Function) and may be affected by various factors. The selection function is used in evaluating the effectiveness of a milling process. The Size reduction involves, mainly, two breakage mechanisms; impact and attrition. These mainly depend on grinding media and feed material characteristics such as size, shape, weight and composition. For breakage to occur, the media must provide sufficient force to the particles to effect breakage; thus a charge composed of smaller balls will not effectively break large particles in the feed. On the other hand, larger media minimise the surface area available for contact with particles. With smaller size feed material and less mass, grinding efficiency decreases because particles become difficult to break, and abrasion becomes the dominating mode of breakage while, for larger particle sizes, particles can be easily broken down because of high impactive forces imparted by falling balls.

In ball milling, spherical balls are the dominant media shape used in the tumbling mills, however spherical balls wear into non-spherical fragments as a result of breakage due to impact and different wearing mechanisms inside the mill. Thus at any one time a mill charge is a mixture ranging from larger spherical balls to worn irregular fragments. To date, not much has been done to assess the impact of worn balls on mill performance. Powell and Smit (2001) investigated the effect of removing scats from a SAG mill, however the SAG mill environment differs from that of ball mill, so it is worth assessing the impact of worn balls on ball mill performance.

It would be expected that increased surface contact by polygonal balls and flat chips (compared to only point contact that is made by spherical media) should promote increased grinding by attrition. On the other hand, worn balls may pack closely thus reducing the void space available for material to be ground. The larger surface area

per unit mass of polygonal (worn) media may also result in more effective support of the media by the ore, leading to reduced media-media forces in the grinding zones.

This chapter discusses work done to investigate the impact of worn balls on milling kinetics and assesses whether the effect of worn balls on mill performance requires any action to maintain maximum mill productivity. Experimental findings of tests done to study particle breakage with spherical and worn balls are discussed.

6.2   Experimental Results

Feed material characteristics and procedures followed in conducting these experiments have been discussed in Section 3.4.2. The experimental conditions applying to each experiment are described in Tables 3.6 and 3.7.

6.2.1   Determination of specific rate of breakage

The specific rate of breakage was obtained from a first order plot of the form of equation 6.1, in which log w_1 (t) was plotted against time.

$$\log w_1(t) = \log w_1(0) - \frac{S}{2.3}t$$
<div align="right">6.1</div>

where w_1 is the weight fraction of the starting size 1 after grinding time t and S is the specific rate of breakage assumed invariant with time.

The results presented in Figures 6.1, 6.2 and 6.3 compare the first order plot for quartz material feed of sizes 1180x1700μm, 600x850μm and 300x425μm, using spherical and worn grinding media shapes. The single size feed class was obtained by sieving material from the supplier. With decreasing size, the process became more

difficult in obtaining pure single size material to make a charge necessary for experiment at the desired material filling level. It is because of this fact that the initial filling mass fraction of the feed for Figure 6.3 in which $w_1(t)$ is plotted against time for 300x425μm is about 75%.

The results suggest that, for the two media shapes studied, breakage followed a first order law. Higher specific rates of breakage were obtained with spherical balls for the feed sizes studied.

The variations in specific rates of breakage with feed sizes, shown in Figure 6.4, indicated that spherical media have a higher breakage rate for the coarsest fraction (1180x1700μm) but the difference narrows as the feed becomes finer.

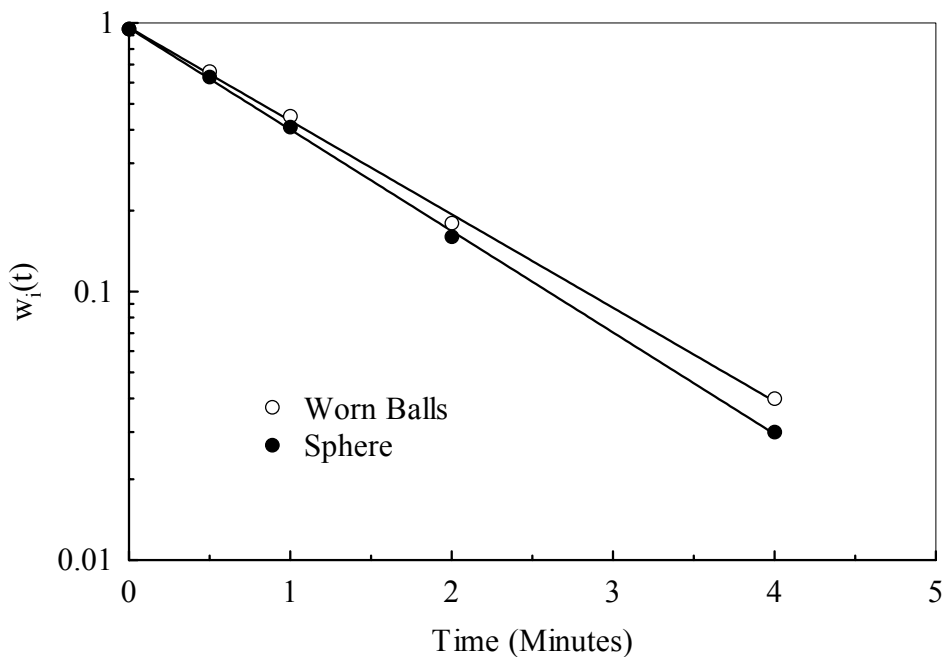**Figure 6.1** First order plot of batch ball milling of quartz (1180X1700μm).
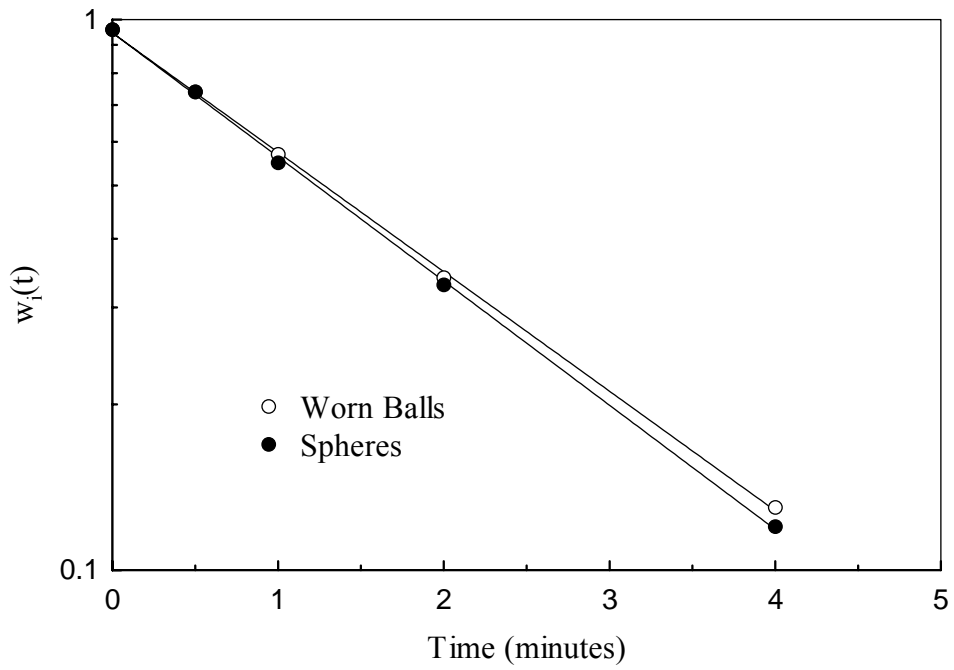
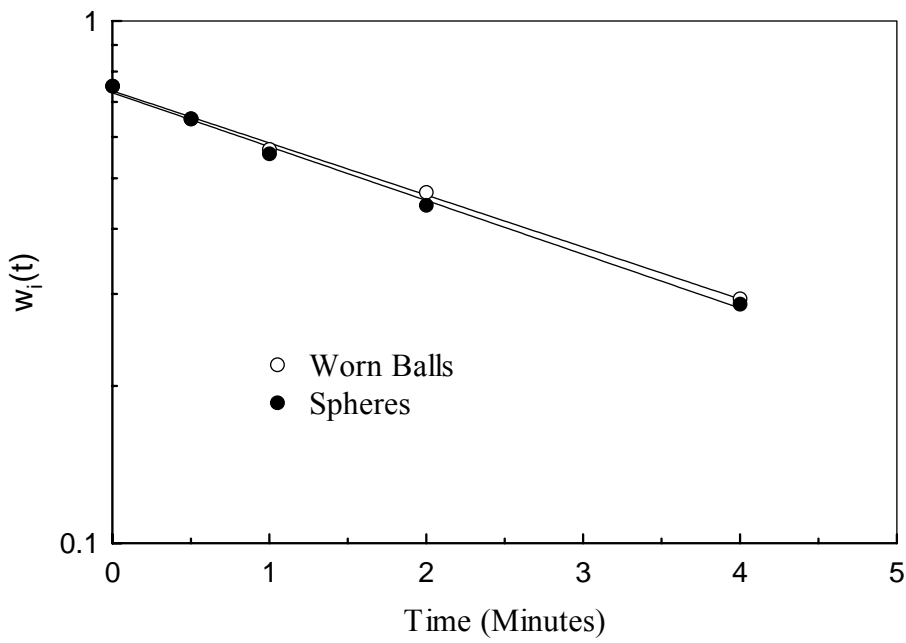**Figure 6.2** First order plot of batch ball milling of quartz (600X850μm).

Figure 6.3 First order plot of batch ball milling of quartz (300x425μm).

It is understood that larger particles undergo impact breakage when impacted by balls with sufficient kinetic energy. As particles get smaller they become difficult to break by impact hence breakage rates decreases with decreasing particle size and attrition becomes the dominant mode of breakage for finer particle sizes. Considering the two media charges: worn balls have linear and point contacts, while spheres have only point contact. This implies an increase in breakage by abrasion for worn balls, which suggests the reason why differences in breakage rate between the two media shapes decrease with decreasing feed size. On the other hand, the use of test screens in sizing the media might be the factor accounting for higher breakage rate for spherical media with coarse feed. For the same screen size class, the non-spherical (worn) media constituted heavier balls as relatively bigger balls pass through the screen aperture. Thus to maintain an equal total mass and same screen mass fraction, 1489 worn balls were used compared to 1758 spherical balls. The increased ball number results in more ball-to-ball and ball to liner collision for spherical balls than worn balls, which result in higher catastrophic breakage by impact in favour of larger particle sizes.
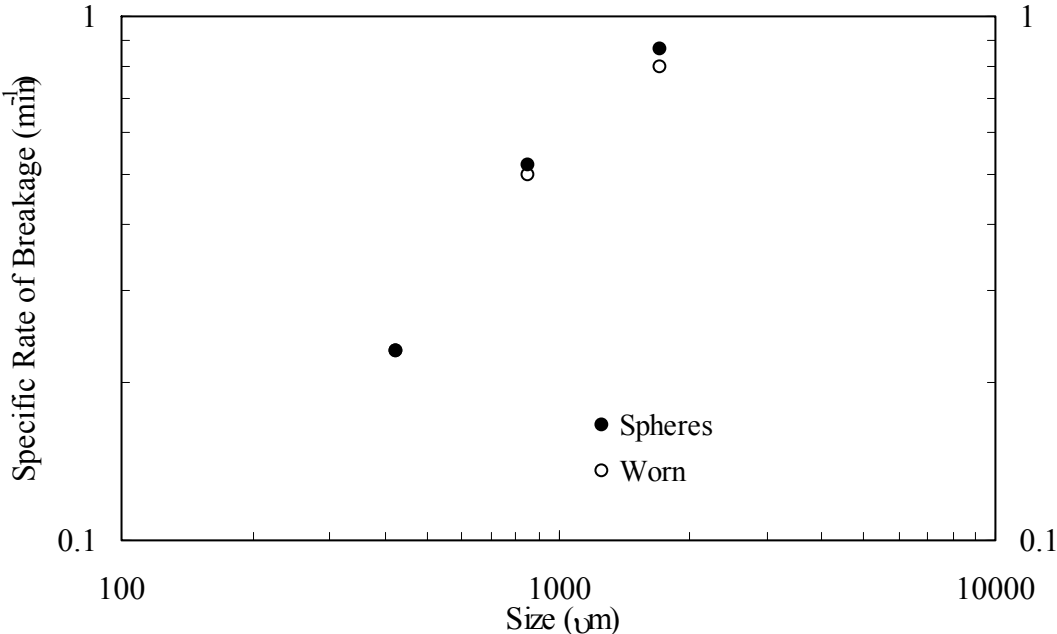

Figure 6.4 Variation of specific rate of breakage with particle size (U=0.8)

6.2.2 Variation of breakage rate with interstitial filling, U

The variations in specific rates of breakage, S_i with interstitial filling U, were studied using 600x850μm feed material. It was observed that the specific rate of breakage, S_i, decreased with increasing interstitial filling. It was also observed that the differences in the breakage rates between the two media shapes decreased as U approached unity. This suggested that under normal operation (0.8 < U ≤ 1.0) there would be no difference in the grinding rates of the two media type. At lower U value, the amount of ball-to-ball contacts is higher; increasing powder filling reduces the number of contacts while increasing the cushioning effect. This results in a faster decrease in the rate of breakage by impact for spherical balls but has less effect on breakage by abrasion.
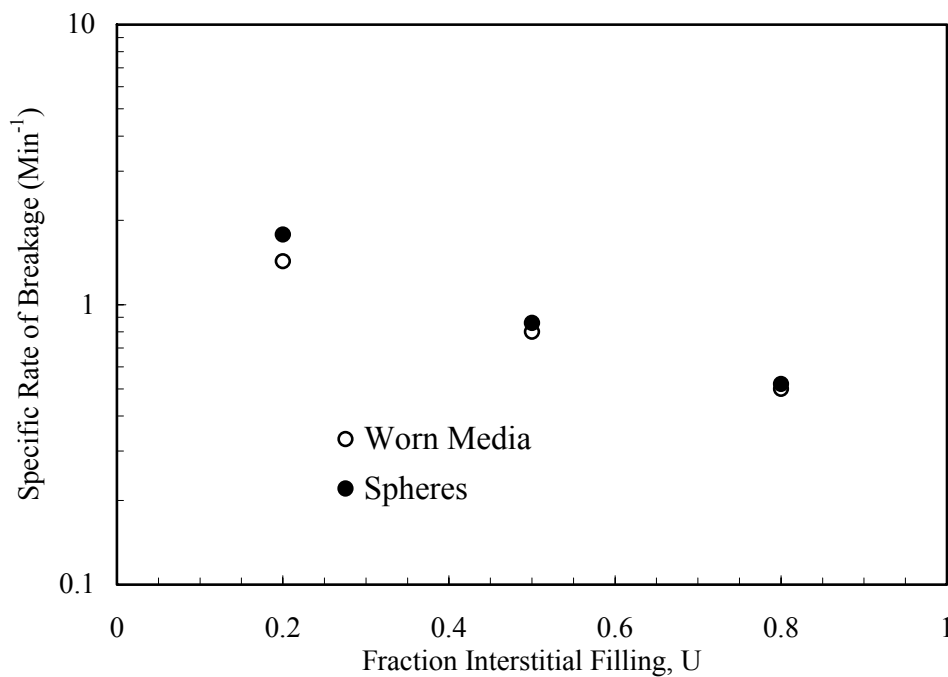

Figure 6.5 Variation of specific rate of breakage with interstitial filling, U (600x850μm)

A relationship between specific rate of breakage, interstitial filling and material feed size x_i was developed (equation 6.5) The general form of the relationship, relating specific rate of breakage and interstitial filling when J and x_i are kept constant could be represented as equation 6.2 which is in agreement of Austin *et al,* (1984) law (equation 6.2) when J is kept constant.

$$S \, \alpha \, Exp\,(-\lambda U) \qquad\qquad 6.2$$

The fitting of equation 6.2 to experimental data for one feed size class of 600x850μm gave a good fit with coefficient of multiple determinations (R^2) of 0.997 and 0.994 for worn and spherical media respectively. The values of λ were 1.894 and 2.241 for worn and spherical media respectively while the constant of proportionality were 2.05 and 2.75 for worn and spherical media

Austin (1984) developed an equation that relates the specific rate of breakage S_i, with feed size x_i at a constant interstitial filling U, of the form:

$$S_i = a \, x_i^{\,\alpha} \, Q_i \qquad\qquad 6.3$$

where a and α are model parameters and x_i is screen size, top of the interval.

When Q_i is assumed to be 1, which is valid at $x_i \ll d$; equation 6.3 simplifies to equation 6.4.

$$S_i = a \, x_i^{\,\alpha} \qquad\qquad 6.4$$

Equation 6.4 was extended to include the effect of interstitial filling U and equation 6.5 was obtained as a representative of the effect of feed size and interstitial filling, U

$$S_i = a' \, x_i^{\,\alpha} \, Exp\!\left(-\lambda U\right) \qquad\qquad 6.5$$

where a' is a proportionality constant resulting from equation 6.2 and 6.4.

The equation was fitted to experimental data in which x_i and U were varied and a good fit was obtained.

While spherical balls showed a higher breakage rate than worn balls, it was observed that the difference in breakage rate was marginal. Looking at industrial charge compositions discussed in chapter four for two points sampled would be helpful in assessing the effects of worn balls among the charge. From Figure 4.4, it was found that balls smaller than 31.5mm, which observation revealed were no longer spherical, constituted 15 and 40 percent for samples drawn from the centre and mill feed end respectively. The observed variation in breakage rate for worn balls from that of spherical balls occurs when the charge is a hundred percent of one media shape. If a linear relationship between breakage and ball shape distribution were assumed to exist, then the presence of worn balls in the mill charge would result in negligible decreases in breakage rate.

6.2.3 Material breakage distribution

The size distributions of mill products were established as described in Section 3.4.2. Results from short grinding times that gave about 30 percent of material broken out of the feed size were used to obtain breakage parameters by plotting *Bij* values against x_{i-1}/x_j, as shown in equation 6.6

$$B_{i,j} = \Phi_i \left(\frac{x_{i-1}}{x_j} \right)^{\gamma} + \left(1 - \Phi_j \right) \left(\frac{x_{i-1}}{x_j} \right)^{\beta} \quad , i \geq j \qquad\qquad 6.6$$

The $B_{i,j}$ values were obtained using equation 6.7 suggested by Austin *et al*, (1984).

$$B_{i,j} = \frac{\log\left[(1 - P_i(0))\right] / \log\left[(1 - P_i(t))\right]}{\log\left[(1 - P_{j+1}(0))\right] / \log\left[(1 - P_{j+1}(t))\right]} \quad n \geq i \geq j+1 \qquad\qquad 6.7$$
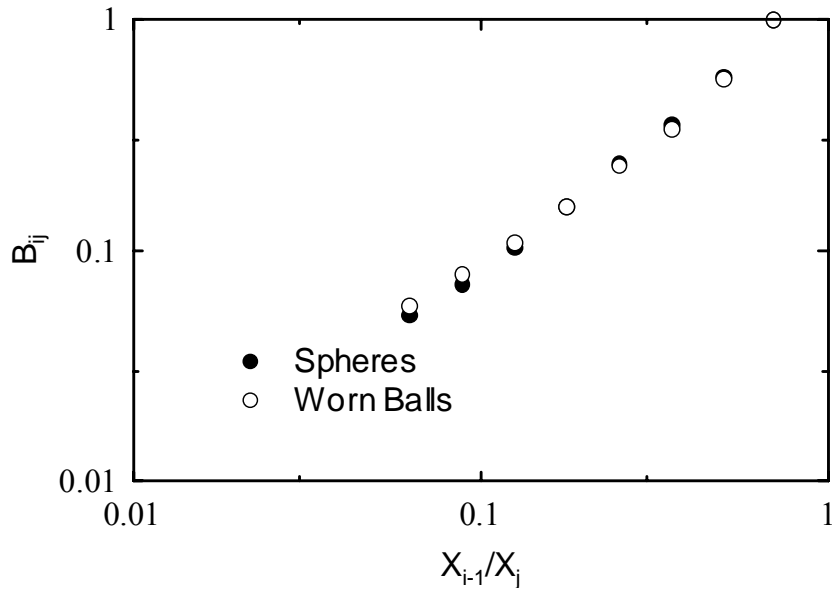
Figure 6.6 Comparison of experimental breakage distribution (spherical Vs worn balls, 1180x1700μm, J=0.2 and N75%)
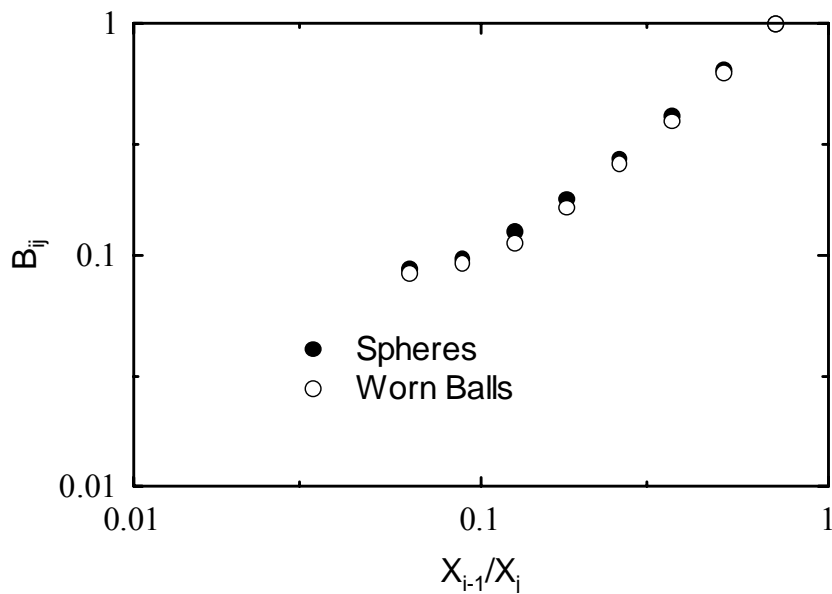

Figure 6.7 Comparison of experimental breakage distribution (spherical Vs worn balls, 600x850μm, J=0.2 and N75%)

Product size distributions obtained for the two media shapes are shown in Figures 6.6 and 6.7 for 1180x1700μm and 600x8500μm single size feed. From Figures 6.6 and 6.7, it was observed that the breakage distribution characteristics for spherical and worn balls were essentially similar.

6.3 Prediction of Breakage and Selection Parameters

Based on batch grinding data obtained from the pilot ball mill, the breakage and selection function parameters were predicted, using an Excel solver program adapted from MOLY COP tools. The program calculated the selection and breakage functions parameters using equation and 6.5 and 6.6 by the least square method. The parameters that minimised the difference were obtained by searching equation 6.8 as a summation of the square of the weighted percentage error over all grinding times.

$$
Objective\ function = \sum_{T=1}^{4}\sum_{i=1}^{n}\left(\frac{w_i}{W} X \left(\frac{p_{iExpt} - p_{iModel}}{p_{iModel}} X100 \right)^2 \right) \qquad 6.8
$$

where n is the total number of size intervals, p_{iExpt} represents the experimental size distribution of the mill product (as percentage retained on a screen i), p_{iModel} represents the model response for each corresponding p_{iExpt} for a given set of model parameters and w_i represents weighting factors that quantify the relative quality and reliability of each particular mesh value with respect to the other screens' data. W is the sum total of w_i's. The relatively high value of w_i indicates more reliable measurements.

Given that for the same material, values of γ, β and Φ are independent of milling conditions such as ball filling, ball diameter or mill diameter and do not vary with

grinding time, that the value of α is constant for a given material for all mill conditions, the variation in mill performance occurs with changes in $a^{'}$.
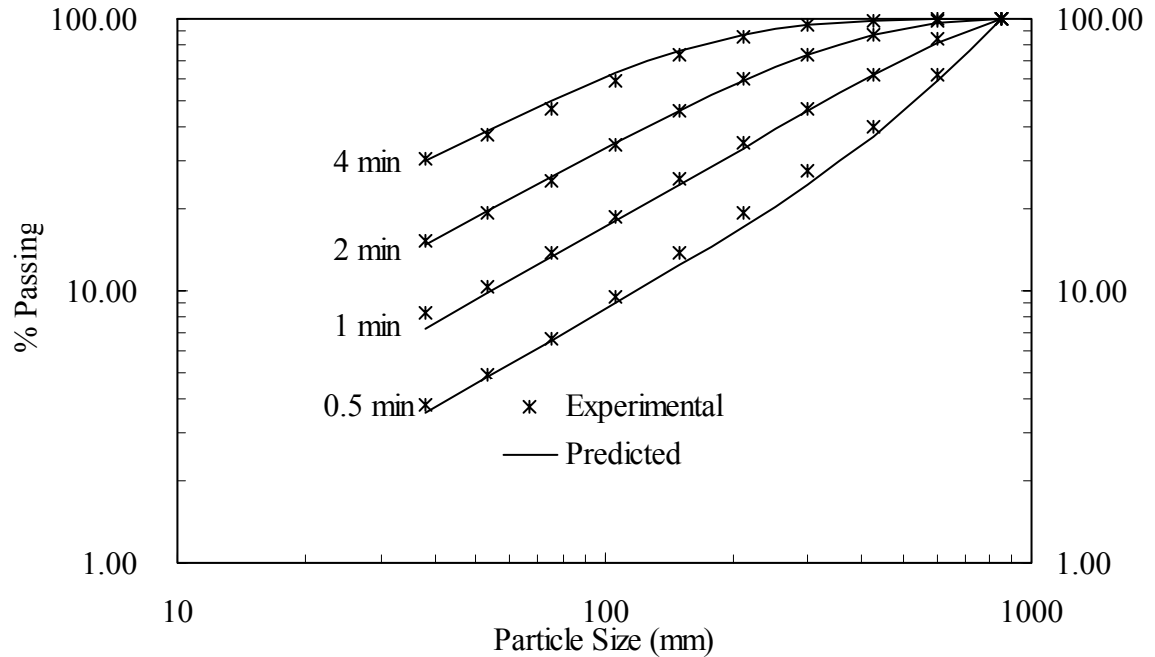

Figure 6.8 Comparison of particle size distribution (experimental and predicted, spherical balls, 600x850μm, U=0.2).

The experimental observations and model predictions obtained for 600x850μm and 1180x1700μm particle feed sizes for twenty and eighty percent particle filling respectively using parameters described in Tables 6.1 and 6.2 and their corresponding goodness of fit for spherical and worn balls respectively are shown in Figures 6.8, 6.9, 6.10 and 6.11 The root mean squares of residuals (RMS_R's) of less than 0.01 was found; the established RMS_R for good estimate on the basis of typical error associated with laboratory sieving (Rajamani & Herbst, 1984).
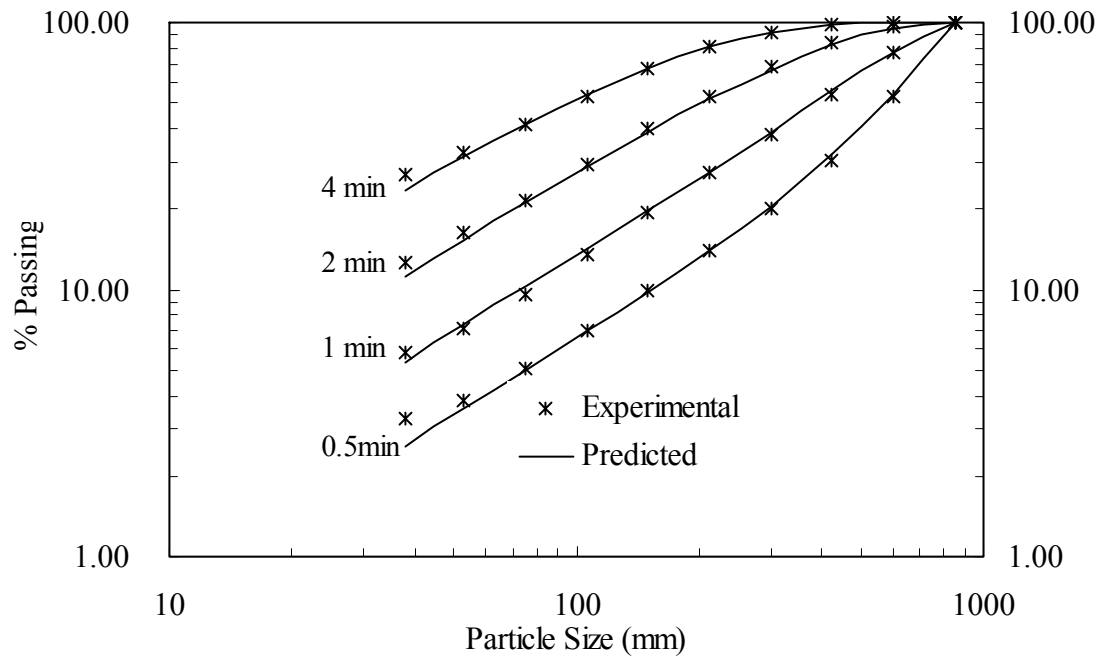
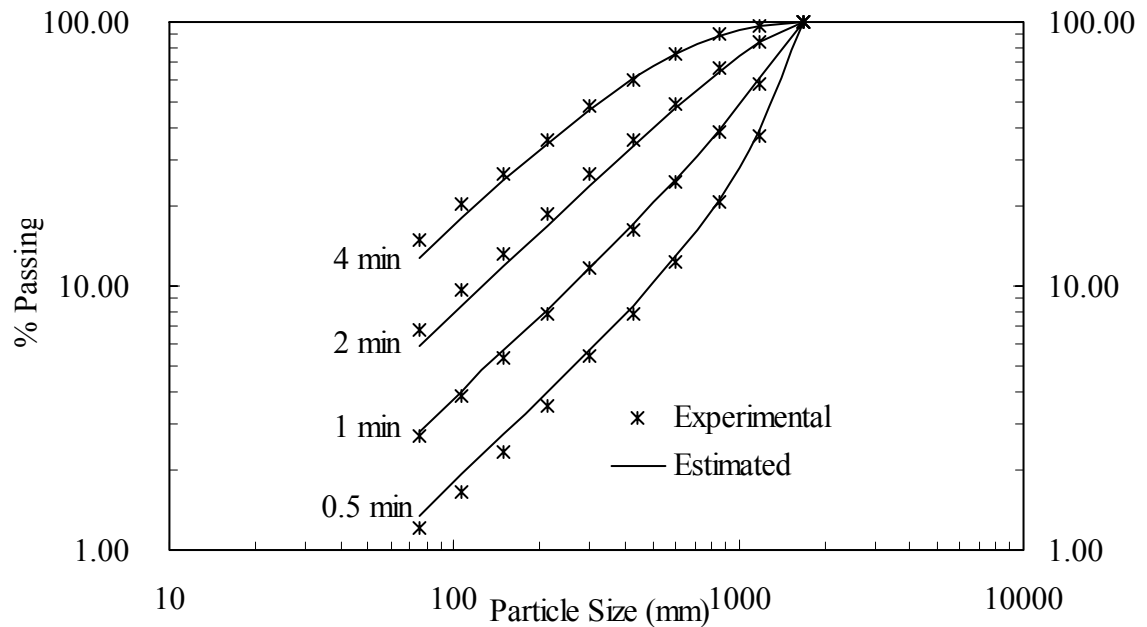**Figure 6.9** Comparison of particle size distribution (experimental and predicted, worn balls, 600x850μm, U=0.2).

Figure 6.10 Comparison of particle size distribution (experimental and predicted, spherical balls, 1180x1700μm, U=0.8).
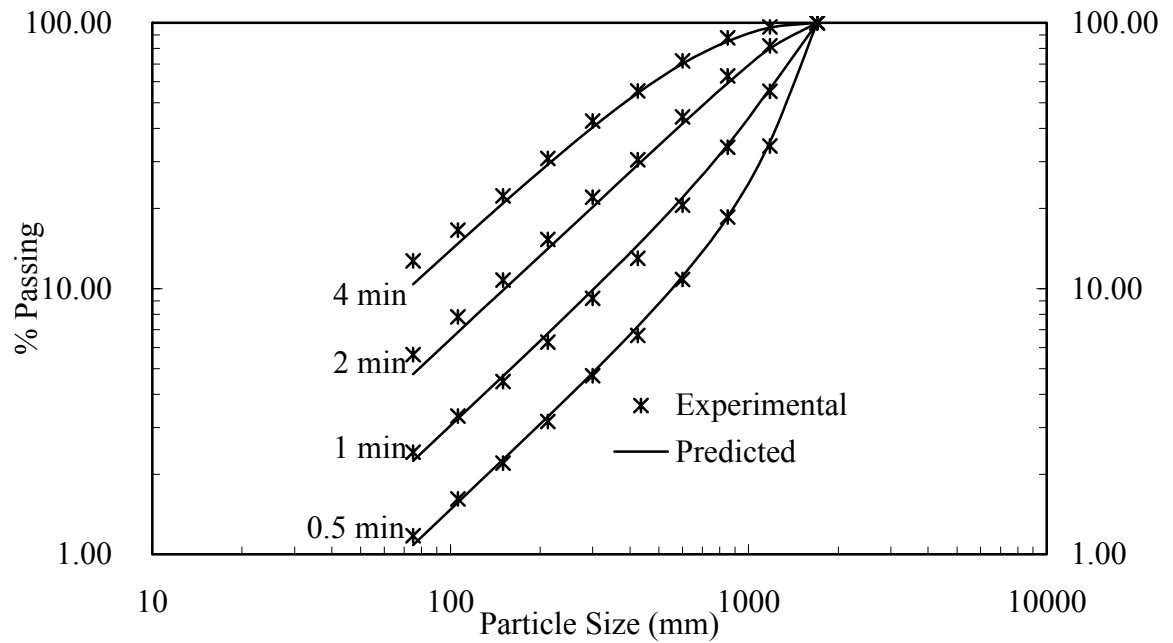
Figure 6.11 Comparison of particle size distribution (experimental and predicted, worn balls, 1180x1700µm, U=0.8).

Table 6.1 Breakage descriptive parameters for spherical balls

Parameter	1180x1700µm	600x850µm		
	U=0.8	U=0.8	U=0.5	U=0.2
a'	3.509	3.717	2.884	2.957
α	0.8	0.8	0.8	0.8
λ	2.241	2.241	2.241	2.241
Φ	0.505	0.505	0.505	0.505
γ	1.036	1.012	0.893	0.902
β	3.9	3.9	3.9	3.9
*RMS	0.0039	0.0035	0.0040	0.0043

105

Table 6.2 Breakage descriptive parameters for worn balls

Parameter	1180x1700µm	600x850µm		
	U=0.8	U=0.8	U=0.5	U=0.2
α'	2.318	2.611	2.167	2.344
α	0.8	0.8	0.8	0.8
λ	1.894	1.894	1.894	1.894
Φ	0.505	0.505	0.505	0.505
γ	1.068	1.051	1.035	0.964
β	3.9	3.9	3.9	3.9
*RMS	0.0040	0.0052	0.0034	0.0023

$$*\,RMS_R = \frac{\sqrt{\sum_{j=1}^{J}\sum_{i=1}^{n}\left(\dfrac{P_{ijexpt}-P_{ijpred}}{P_{ijpred}}\right)^2}}{(n-1)J-2}$$

where p_{ijexpt} and p_{ijpred} are the experimental and predicted cumulative fraction finer than size x_i for the jth grinding time.

6.4   Conclusion

Variation of breakage rates with media shape was noted. The differences were higher with coarser feed; decreasing for finer feed.

From cumulative primary progeny fragment distribution, it was established that the breakage characteristics were similar for the two media shapes. However, spheres produced some finer materials than worn balls.

Considering steel costs and costs due to down time for removing and replacing worn balls, the effect on the overall performance does not justify such excises.

While spherical media are the dominantly used grinding media, the variation of specific rate of breakage with feed size for the two media shapes suggests that other non-spherical shapes might perform better than spheres in terms of cost for finer grinding, since the rates of breakage are the same for finer feed.

Chapter 7

Conclusion

7.1 Introduction

Experiments were undertaken to obtain information on the effect media shape have on ball mill performance.

Measurement of charge toe and shoulder positions was achieved using inductive proximity and marker probes. The power measurements were accomplished using a torque beam that measured accurately the torque exerted by the charge mass. Inductive proximity probe data combined with marker probe data and torque beam data were analysed for load orientation and mill power draw respectively.

Comparison of milling kinetics used feed materials predominantly of a single size. The experiments were designed to investigate variation of breakage rates with feed sizes and interstitial filling for both worn and spherical balls.

Breakage parameters characterizing material grindability were estimated using an excel spreadsheet with a solver program. The spreadsheet estimated the solution of the population balance model equation expressed in a matrix form, by minimizing the sum of the square of percentage residual error of experimental and predicted mill products.

7.2 Summary of Findings

7.2.1 Industrial mill media distribution

The distribution of balls, in terms of size and shape, were studied along the length of the mill and depth of the mill charge. Results indicated that ball size distribution varies both along the length and depth the mill. The ball samples showed that larger balls tend to reside near the surface, with the finer ball proportion becoming progressively higher deep towards the centre of the charge. The results also showed an increase in finer balls from the mill centre to the mill feed end.

Another trend observed from the industrial sampling exercise is that the finer the ball; the less it maintains its spherical shape. This is linked to the ball age in the mill, as small balls will have been subjected to wearing and breakage processes much longer than larger ones; hence shape alteration is more severe.

7.2.2 Load behaviour and mill power as affected by media shape

Load orientation and mill power vary with media shape. The shoulder positions were found to be in ascending order, of spheres, worn balls and cylpebs. The shoulder positions increase with mill speed and mill filling, however the magnitude of increase in shoulder position with filling is minimum for cylpebs.

At mill speed lower than 60 percent of critical, there is little variation of toe positions with mill speed. Beyond this speed, there is marked difference in toe positions among media shapes. Those of spheres seem to remain constant with mill speed while that of cylpebs shows marked decrease with increase in speed. The variation of mill power draw among the media shapes is observed. The cylpebs draw more power at lower speed compared to worn and spherical balls. The maximum power draw is reached at different mill speeds for the three media shapes with cylpebs reaching the maximum at lower speed. For the same media shape, the maximum power is reached at a particular one constant speed for all charge filling levels.

The higher shoulder positions of cylpeb media observed are associated with more cataracting and premature centrifuging. The increased cataracting and premature centrifuging result in more charge in flight, reducing the active mass that contributes toward power draw. At this point, spherical media shoulder positions are lowest and the charge is still cascading down the mill thus drawing more power. The spherical balls power draw continues to increase with mill speed until sufficient charge mass comes into flight which occurs at higher speed compared to worn and cylpeb media. This explains why maximum power draw occurred at different mill speeds.

7.2.3 Effect of media shape on breakage functions

The variation of breakage rates with media shape is observed. Spheres have higher rate of breakage compared to worn balls. The differences in breakage rate decrease with decreasing material feed size and with increasing interstitial filling U. The model relating specific rate of breakage S and feed size x_i (Austin, 1984) was extended to include the effect of interstitial filling based on experimental data and is shown in Section 6.2.2, equation 6.5.

The breakage distribution characteristics for the two media shapes are similar. The breakage model parameters $a^{'}$ and γ, which are measure of breakage rates and fineness respectively, conforms to experimental findings and the trend follows established theories.

Despite spheres having higher breakage rates than worn balls, considering that worn balls make only about 15 and 40 percent by composition for mill centre and mill feed end respectively; that the highest difference in breakage rate is less than 10 percent when the charge is 100 percent one media shape. The presence of worn balls inside a ball mill has a negligible effect on fines production.

7.3 Overall Conclusion

An understanding of the milling process and factors affecting it is being improved. Data from an industrial mill and a pilot laboratory mill were collected and analysed. Information was gained on the effect that media shape has on load behaviour, mill power and specific rate of breakage, as well as breakage distribution.

The results indicated that the presence of worn balls has little impact on the grinding process and removal of the worn media would not result in justifiable gains. On the other hand, the load behaviour and mill power draw results indicated that these two are strong functions of media shapes.

While the effect of media shape has been ignored in various ball mill power models; which are useful tools in evaluating different control strategies in the light of impact that load behaviour has on milling; the information can be of much usefulness in improving these models. The DEM having an opportunity to incorporate this effect, this information obtained in this work has added to current knowledge and should prove useful in further studies involving media shapes in mill modelling.

References

Adam, K., Natarajan, K.A., Riemer, S.C. & Iwasaki, I., 1985. Electrochemical aspect of grinding media –mineral interaction in sulphide ore grinding. *Corrosion,* **104,** 49-64.

Austin, L. G. & Brame, K. 1983. A Comparison of the Bond method for sizing wet tumbling ball mills with a size-mass balance simulation model. *Powder Technology,* **34**, 261-274.

Austin, L. G., Klimpel, R.R. & Luckie, P.T, 1984. Process Engineering of Size Reduction: Ball Milling. *AIME-SME, New York, USA*

Banisi, S., Langari-Zadeh, G., Pourkan, M. & Kargar, M., 2000. Measurement of ball size distribution and wear kinetics in 8m by 5m primary mill of Sarcheshmeh copper mine. *CIM Bulletin* 93, (1041) 145-149.

Berube, M.A. & Berube, Y., 1978. A semi-empirical relationship between selection function and particle load in batch ball milling. *Powder Technology*, **19**, 89-92

Bond, F.C. 1952. The third theory of comminution. Mining Engineering. *Trans. AIME* 484-492

Bond, F.C. 1958. Ball size selection. Mining Engineering. *Trans. AIME* 592-595

Bond, F.C. 1961. Crushing and grinding calculations. Part II. *Mining Engineering. Trans. AIME* 543-548

Cleary, P.W., 2001. Charge behaviour and power consumption in ball mills: sensitivity to mill operating conditions, liner geometry and charge composition. *International Journal of Mineral Processing*, **63**, 79-114.

Cloos, U., 1989. (Doering GmbH, West Germany). Cylpebs: An alternative to balls as grinding media. *World Mining,* **36**, (10) 59.

Concha, F., Magne, L. & Austin, L. G. Optimisation of the make-up ball charge in a grinding mill. *International Journal of Mineral Processing*, **34**, 231-241.

Davis, E. W., 1919. Fine Crushing in ball mills" *AIME Trans*. **61**, 250-297

Deniz, V. & Onur, T., 2002. Investigation of the breakage kinetics of pumice samples as dependent on powder filling in a ball mill. *International Journal of Mineral Processing*, **67**, 71-78.

Dong, H. & Moys, M.H., 2003. Load behaviour and mill power. *International Journal of Mineral Processing*, **69**, 11-28

Guerrero, P.K. & Arbiter, N., 1960. Tumbling mill power at cataracting speeds. *Trans. SME/AIME* **217**, 73-75

Harris, C.C., Schnock, E.M. & Arbiter, N., 1985. Grinding mill power consumption. *Mineral Processing and Technology Review*, **1**, 297-345

Herbst, J.A. & Fuerstenau, D.W. 1972. Influence of mill speed and ball load on the parameters of the batch grinding equation. *Trans. AIME & Met. Pet. Eng.* **252** 169-176

Herbst, J.A. & Fuerstenau, D.W., 1973. Mathematical simulation of dry ball milling using specific power information. *S ME/ AIME* **254**, 343-348.

Herbst, J.A. & Lo, Y.C., 1989. Grinding efficiency with balls or cones as media. *International Journal of Mineral Processing*, 26, 141-151.

Hlungwani, O., Rikhotso, J., Dong, H & Moys, M.H., 2003. Further validation of DEM modelling of milling: Effects of liner profile and mill speed. *Minerals Engineering*, **16**, (10), 993-998

Hogg, R. & Fuerstenau, D.W., 1972. Power relationships for tumbling mills. *SME/AIME*, **252** 418-423

Howat, D.D. & Vermeulen, L.A., 1988. Fineness of grind and the consumption and wear rates of metallic grinding media in tumbling mills. *Powder Technology*, **55**, 231-240

Howat, D.D. & Vermeulen, L.A., 1988. Pebbles as grinding medium: Interrelationships of some milling parameters. *Journal of South African Institute of Mining and Metallurgy*, **88**, (12) 393-400

Jang, J. W. & Iwasaki, I., 1992. Size and morphology of grinding media wear debris. *Mineral and Metallurgical Processing*, **9**, 158-160

Kavetsky, A. & Whiten, W.J., 1982. Scale-up relations for industrial ball mill. *Proc. Australas Inst. Min. Metall.,* **282** 47-55

Kawatra, K.S., 1992. Comminution –Theory and practice. *AIME-SME*

Kelsall, D. F., Stewart, P.S.B. & Weller, K. R., 1973. Continuous grinding in a small wet ball mill EM DASH 5. A study of the influence of media shape. *Powder Technology*, **8**, 77-83.

Kotake, N., Suzuki, K., Asahi, S. & Kanda, Y., 2002. Experimental study on the grinding rate constant of solid materials in a ball mill. *Powder Technology,* **122**, 101-108.

Liddell, K.S. & Moys, M.H., 1988. The effects of mill speed and filling on the behaviour of the load in a rotary grinding mill. *Journal of South African institute of mining and metallurgy,* 88, (2) 49-57.

Lynch, A.J., Whiten, W.J. & Narayanan, S.S., 1986. Ball mill models: Their evolution and present status. *Arbiter Symposium* 48-66

Mishra B.K. & Rajamani, R. K., 1992. The discrete element method for simulation of ball mills. *Applied Mathematical Modelling*, **16**, 598

Morrell, S., 1993. The prediction of power draw in wet tumbling mills*, PhD. Thesis, University of Brisbane.*

Moys, M.H., 1984. The measurement of parameters describing behaviour of the load in a grinding mill. *Mintek 50. Proceedings of International Conference on Mineral Science and Technology" Sandton, South Africa,* 205-219.

Moys, M.H. & Montini, A., 1987. The use of conductivity measurement in the control of grinding mill, *CIM Bulletin.*

Moys, M.H., 1993. A model of mill power as affected by mill speed, load volume and liner design. *Journal of South African Institute of Mining and Metallurgy*, **93**, (6) 135-141

Moys, M.H. & Skorupa, J., (1993). Measurement of the radial and tangential forces exerted by the load on a liner in a ball mill as a function of load volume and mill speed. *International Journal of Mineral Processing*, **37**, 239-256

Moys, M.H., van Nierop, M.A. & Smit, I., 1996. Progress in measuring and modelling Load behaviour in pilot industrial mills. *Minerals Engineering*, **9**, (12) 1201-1214.

Narayanan, S.S., 1987. Modelling the performance of industrial ball mill using single particle breakage data. *International Journal of Mineral Processing,* **20**, 211-228.

Powell, M. S. & Vermeulen L.A., 1994. Influence of liner design on the rate of production of fines in rotary mill. *Minerals Engineering*, **7**, 169-183.

Powell, M. S. & Nurick, G.N., 1996. A study of charge motion in rotary mills Part 1-Extension of the theories. *Minerals Engineering***, 9**, (2) 259-268.

Powell, M. S. & Nurick, G.N., 1996. A study of charge motion in rotary mills Part 2-Experimental work. *Minerals Engineering*, **9**, (3) 343-350

Powell, M. S. & Nurick, G.N., 1996. A study of charge motion in rotary mills Part 3-Analysis of results. *Minerals Engineering*, **9**, (4) 399-418

Powell, M. S. & Smit I., 2001. Startling effect of ball scats removal on SAG mill performance. *International Autogenous and Semi-Autogenous Grinding Technology*, **4** (4) 124-137.

Radziszewski, P., 1997. Predictive model for ball mill wear. *Canadian Metallurgical Quarterly*, **36**, (2), 87-93.

Radziszewski, P., 2002. Exploring total media wear. *Mineral Engineering*, **15**, 1072-1087.

Rajagopal, & Iwasaki, 1992. The properties and performance of cast iron grinding media. *Mineral Processing and Extractive Metallurgical Review*, **11,** 75-106

Rajamani, K. & Herbst J.A., 1984. Simultaneous estimation of selection and breakage functions from batch and continuous grinding data. *Transactions of Institution of Mining and Metallurgy,* **93** 74-85

Shi, F., 2004. Comparison of grinding media-cylpebs versus balls. *Mineral Engineering*, **17** 1259-1268.

Shoji, K., 1982. Further studies of ball and powder filling effects in ball milling. *Powder Technology*, **31**, 121-126

Smit, I., 2000. Effect of slurry viscosity and mill speed on the behaviour of a rotary grinding mill, *MSc. (Eng.). Dissertation, University of Witwatersrand, Johannesburg.*

Teke, E., Yekeler, M., Ulusoy, U. & Canbazoglu, M., 2002. Kinetics of dry grinding of industrial minerals: calcite and barite" *International Journal of Mineral Processing*, **67**, 29-42.

van Nierop, M.A. & Moys, M.H., 1997. Measurement of load behaviour in industrial grinding mill. *Control Eng. Practice*, 5 (2) 257-262.

van Nierop, M.A. & Moys, M.H., 1999. Discrete element method simulations: predicting grinding mill load behaviour. *Chemical Technology*, Nov.Dec.3-5

Vermeulen, L.A. & Howat, D.D., 1983 Theories of ball wear and the results of a marked-ball test in ball milling" *Journal of South African Institute of Mineral and Metallurgy,* **83,** (8) 189-197

Vermeulen, L.A. 1986. Contribution to ball wears and ball size distributions in tumbling ball mills. *Powder Technology* **46**, 281-285

Vermeulen, L.A. & Howat, D.D., 1989. A sampling procedure validated. *Journal of South African Institute of Mineral and Metallurgy,* **89** (12) 365-370

Yildirim, K., Austin, L. G. & Cho, H., 1997. Study of mill power as a function of media type and shape. *Particulate Science and Technology*, **15**, (2) 179

Yildirim, K. & Austin, L. G., 1998. The abrasive wear of cylindrical grinding media. *Wear,* **218**, 15-20

Yildirim, K., Cho, H. & Austin, L. G., 1999. The modelling of dry grinding of quartz in tumbling media mills. *Powder Technology* **105**, 210-221

Zhou, Y.C., Xu, B.H., Yu, A.B. & Zulli, P., 2002. An experimental and numerical study of the angle of repose of coarse spheres. *Powder Technology,* **125,** 45-54

Appendices

Appendix A: Ball Size Distribution
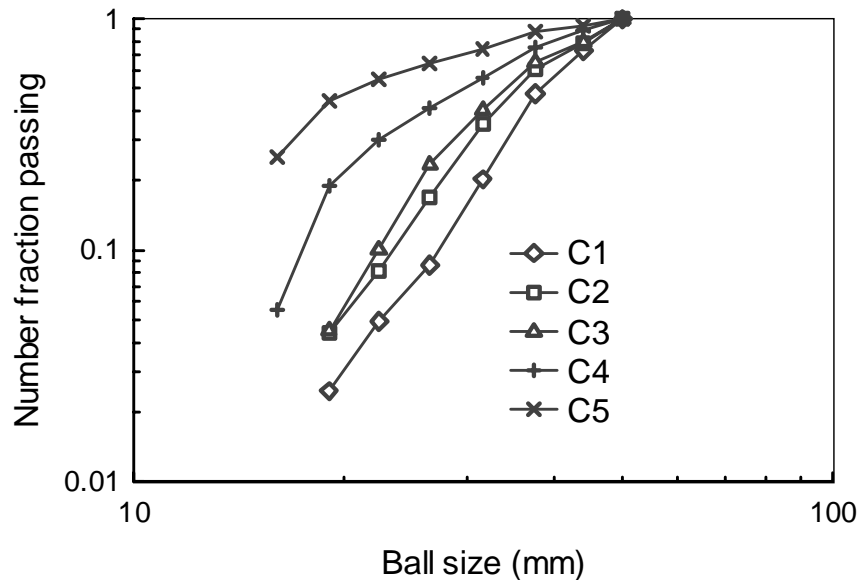
Figure A.1 Ball size distribution by number (central sample)
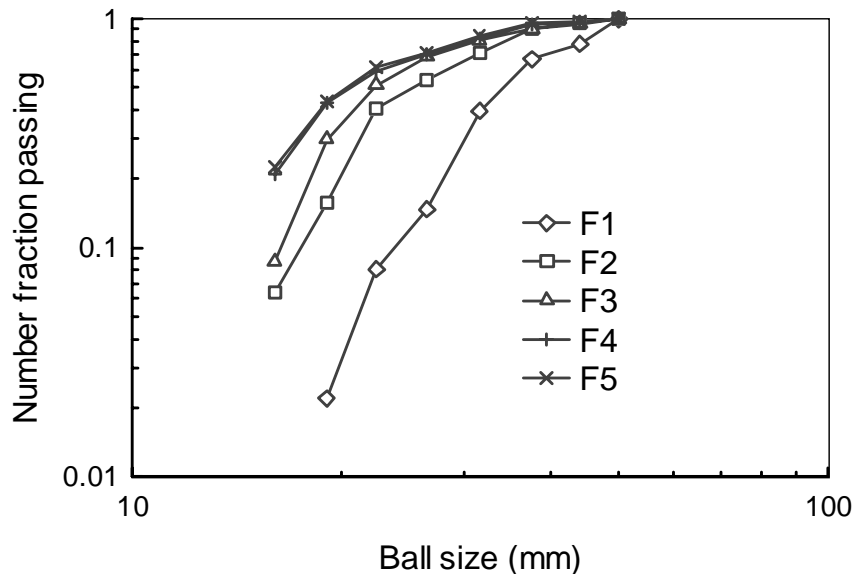

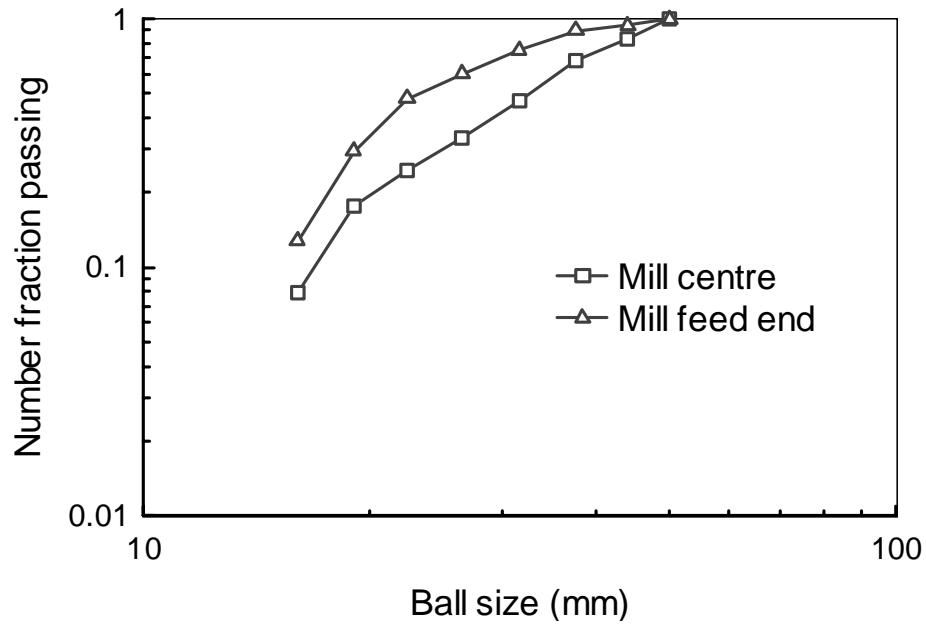
Figure A.2 Ball size distribution by number (feed end)

Figure A.3 Ball size distribution by number along the mill length
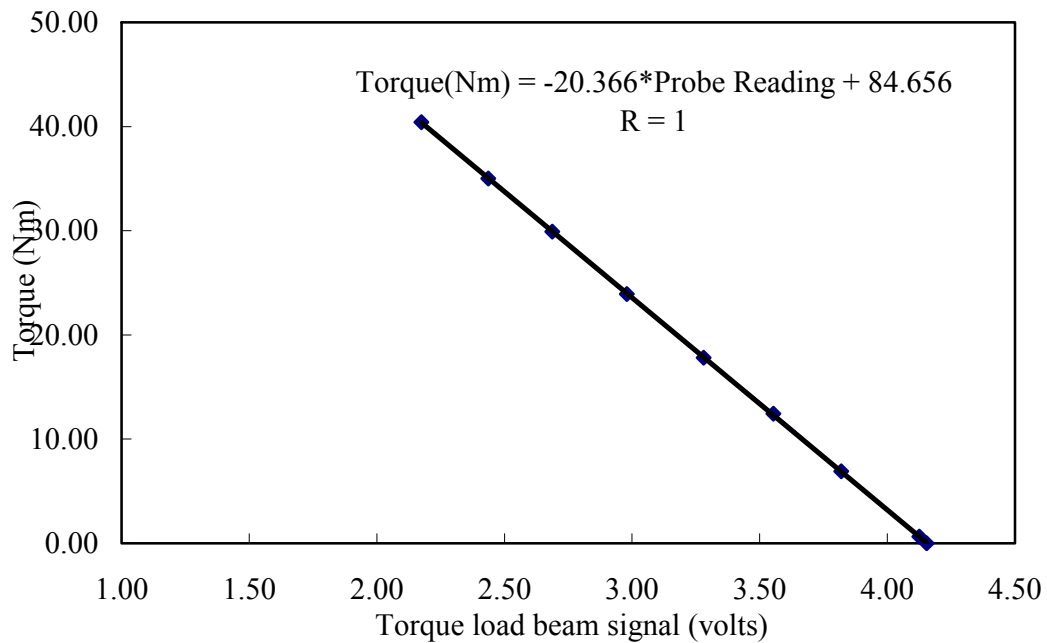
Appendix B: Power Measurements and Calibration

Torque(Nm) = -20.366*Probe Reading + 84.656
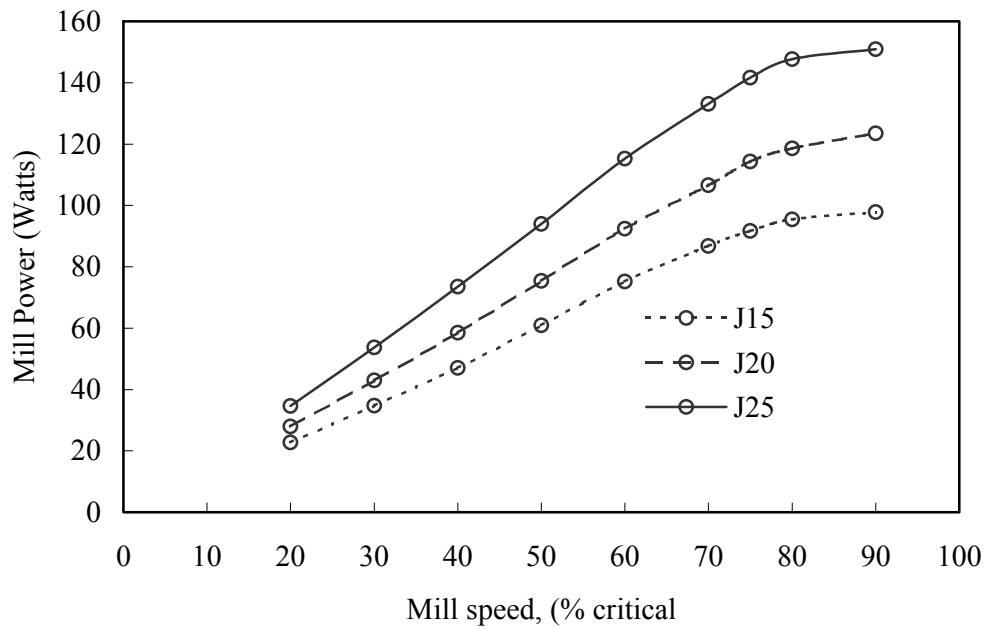
R = 1

Figure B.1 Torque calibration graph

Figure B.2 Variation of mill power with mill filling levels (spheres)
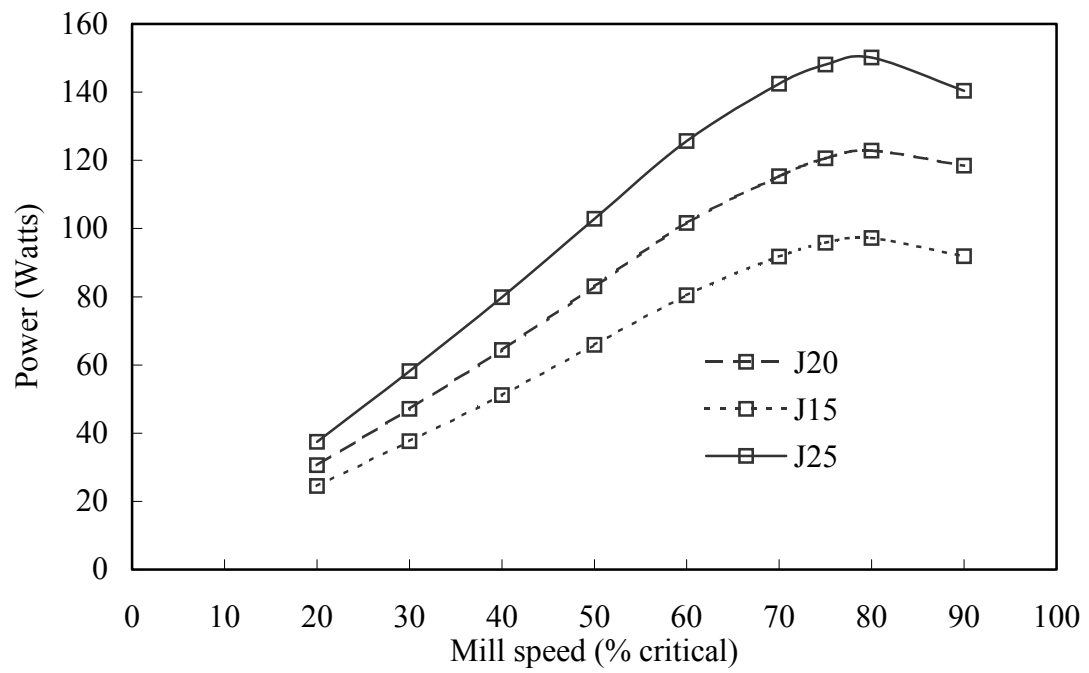
Figure B.3 Variation of mill power draw with mill filling levels, J (worn balls)

Appendix C: Experimental Mill Products Distribution

C.1   Sampling method

Obtaining a reliable representative sample is very important in order to get meaningful results. Tests were done to study particles size distribution at different points along the mill length. The aim was to establish a best and less tedious way of obtaining a sample that represent the whole content of the mill.
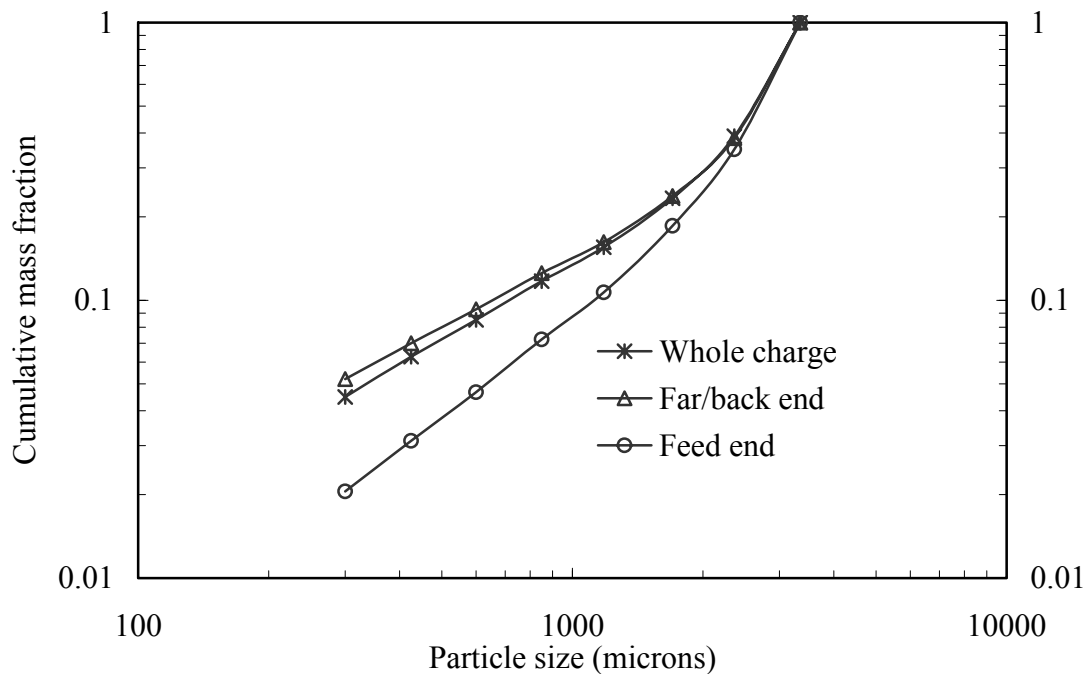
Figure C.1 Particle size distribution at different sampling points along the mill length (2360x3350μm)

Charges were withdrawn from front/feed end, back end and the rest of the charge. The materials were then separated from balls by tipping the content through a coarse screen. The fines were splinted to obtain suitable samples for screening. The particle size results obtained are shown in Figure C.1. The three samples showed marked differences in particle size distribution. There are possible explanations for this. First, it is acceptable that, there is axial and radial particle segregation inside the mill.

Secondary, the sizes of balls used were large living voids among themselves that at low (U=0.8) materials fillings, particle tended to percolate to the bottom. Thirdly, fine particles adhered to the liners. Based on such observations, it was therefore decided that, the whole charge must be withdrawn from the mill. For all the experiments, the charge was withdrawn after grinding; tipped through coarser screen size to remove balls and the content was then splinted to obtain small sample of about 50grams for particle size analysis.

C.2   Product particle size distribution
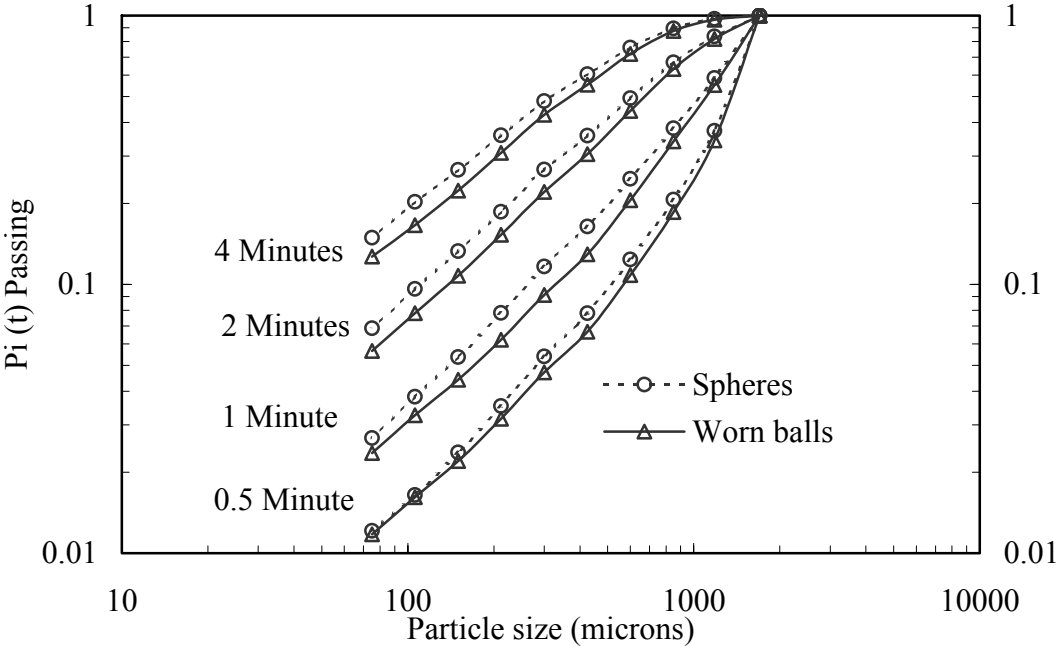
Figure C.2 Comparison of mill product particle size distribution at different grinding times (spherical and worn balls, 1180x1700μm, J=0.2, U=0.8).
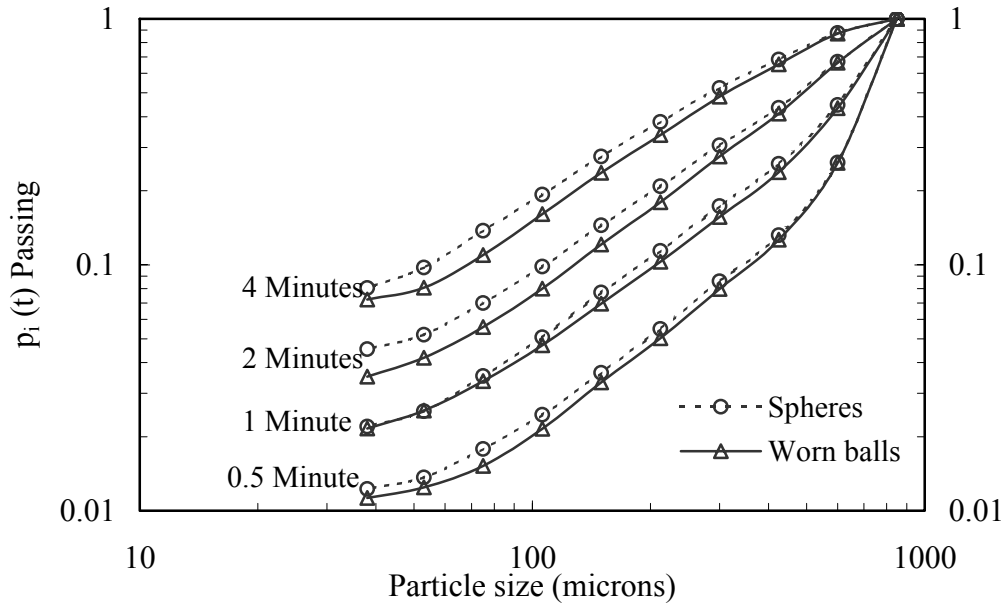
Figure C.3 Comparison of mill product particle size distribution at different grinding times (spherical and worn balls, 600x850μm quartz, J=0.2, U=0.8).
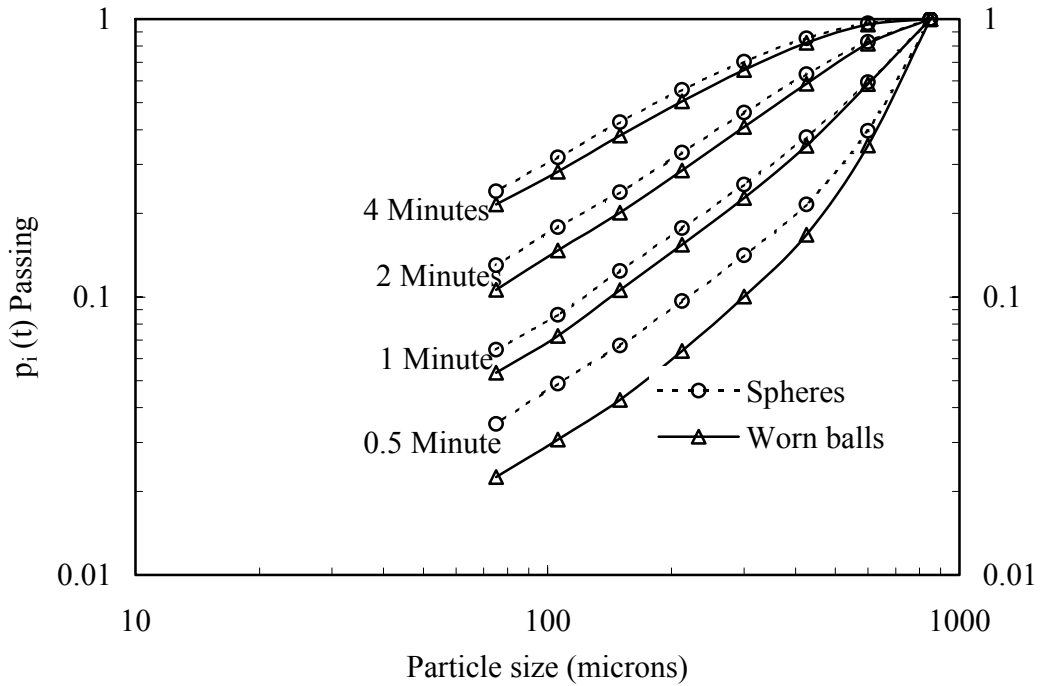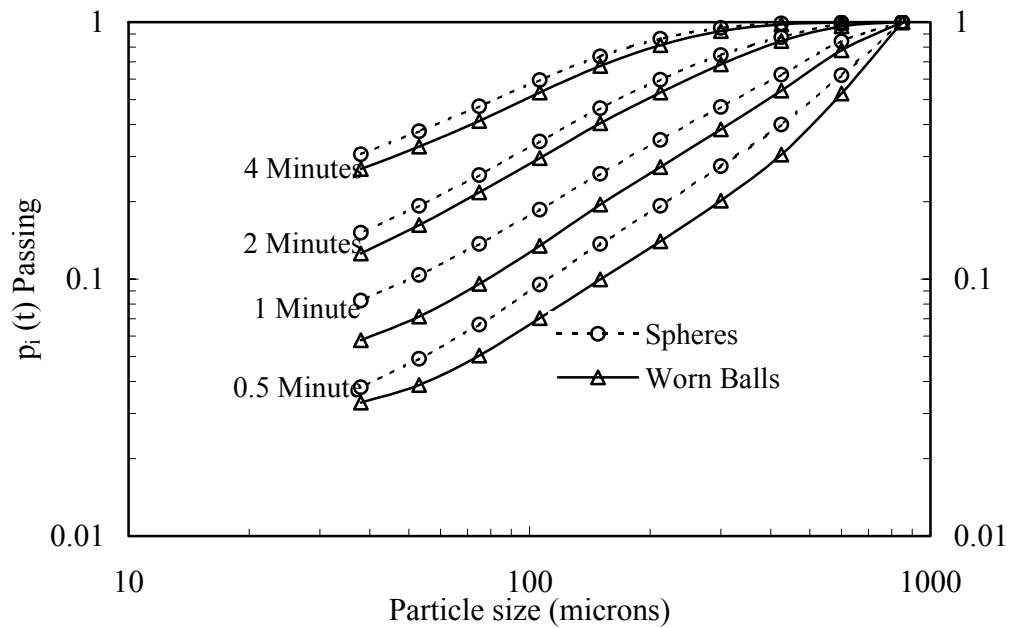

Figure C.4 Comparison of mill product particle size distribution at different grinding times (spherical and worn balls, 600x850μm quartz, J=0.2, U=0.5).

Figure C.5 Comparison of mill product particle size distribution at different grinding times (spherical and worn balls, 600x850μm, J=0.2, U=0.2).
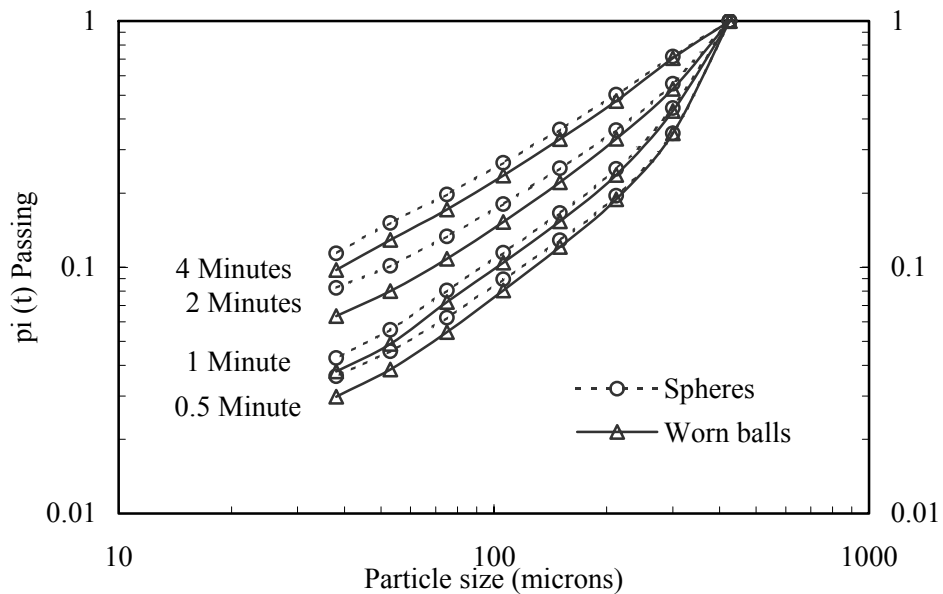

Figure C.6 Comparison of mill product particle size distribution at different grinding times (spherical and worn balls, 300x425μm, J=0.2, U=0.8).

Appendix D: Breakage Parameters Prediction

D.1   Parameter predicting program

A spreadsheet-based program was designed to estimate the breakage model parameters that characterize the grindability of materials. The model is based on Size-mass balance also known as Population Balance Model (PBM)

The spread sheet provide an effective algorithm to search for the set of parameters value that best approximate the model response to the actual experimental measurements available (obtained from batch pilot scale mills) based on a typical non-linear least square criterion.

Based on batch grinding data obtained from pilot ball mill, the spreadsheet allows the calculation of S and Bij parameters that minimizes the least square of the objective function using the excel solver subroutines.

The objective function was obtained as a summation of the square of the weighted percentage error over all grinding times:

$$Objective\ function = \sum_{T=1}^{4}\sum_{i=1}^{n}\left[\frac{w_i}{W}X\left(\frac{p_{iExpt}-p_{iModel}}{p_{iModel}}X100\right)^2\right] \qquad \text{D.1}$$

where n is the total number of size intervals p_{iexpt} represents the experimental size distribution of the mill product (as percentage retained on a screen i) and p_{imodel} represents the model response for each corresponding p_{iexpt} for a given set of model parameters.

w_i represents weighting factor that quantify the relative quality and reliability of each particular mesh value with respect to the other screens data. W is the sum total of w_i's.

Relatively high value of w_i indicates more reliable measurements.

p_{imodel} is obtained from equation 2.7 in Chapter Two which is the analytical solution of a differential equation 2.6 under the assumption that the parameters S and B are invariant with time.

Knowing that S and B parameters are different for different particle sizes and interstitial filling; their dependence on particles size and powder filling are given as:

$$S_i = a'\left(\frac{l_i}{l_o}\right)^\alpha Exp(-\lambda U), l_i << d, \qquad\qquad D.2$$

and

$$B_{i,j} = \Phi_i\left(\frac{l_{i-1}}{l_j}\right)^\gamma + (1-\Phi_j)\left(\frac{l_{i-1}}{l_j}\right)^\beta \quad , i \geq j \qquad\qquad D.3$$

and

$$b_{ij}=B_{i-1,j}-B_{ij} \qquad\qquad D.4$$

D.2   Predicted results

The approximation was carried out in an effort to establish parameters describing the manner in which selection and breakage functions relate to material properties such as particle size, x_i and material filling, U. Because of many parameters involved, only two parameters, a' and α were estimated. Other parameters were based on information available in literatures (Austin et al, 1984) for material (quartz) used.
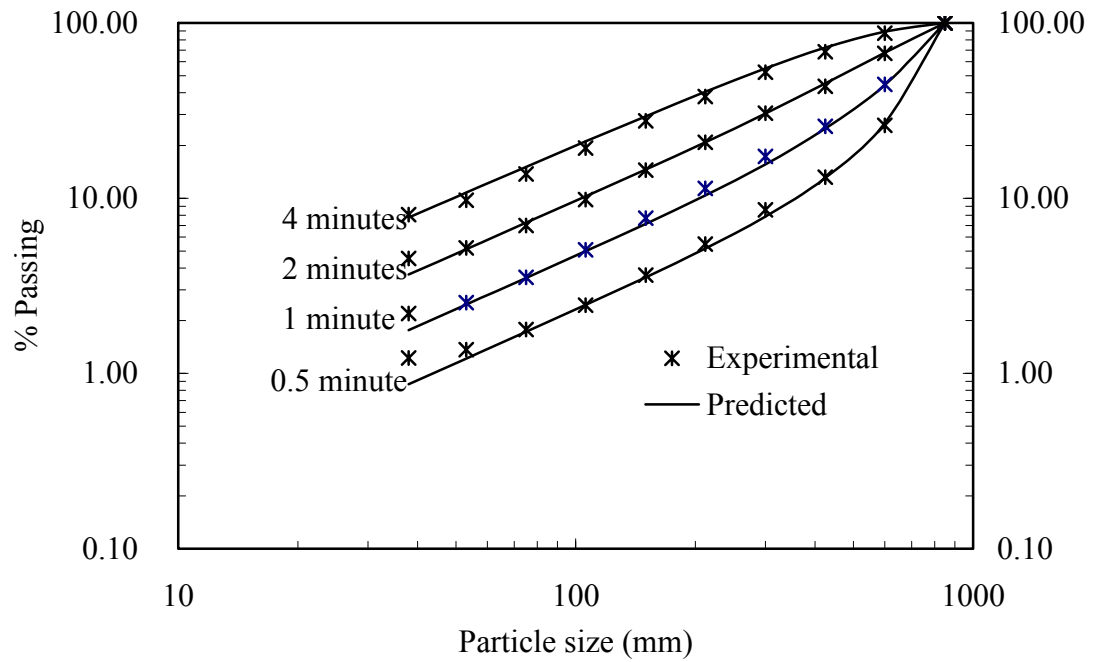
Figure D.1 Comparison of particle size distribution for spherical balls (600x850μm, U=0.8).
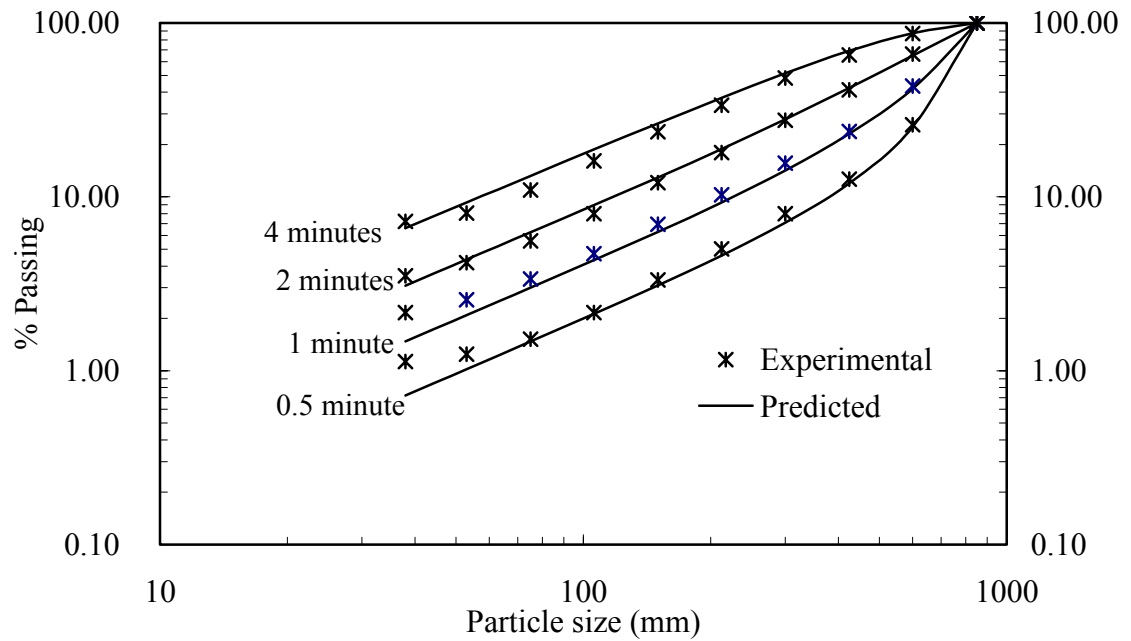

Figure D.2 Comparison of particle size distribution for worn balls (600x850μm, U=0.8).
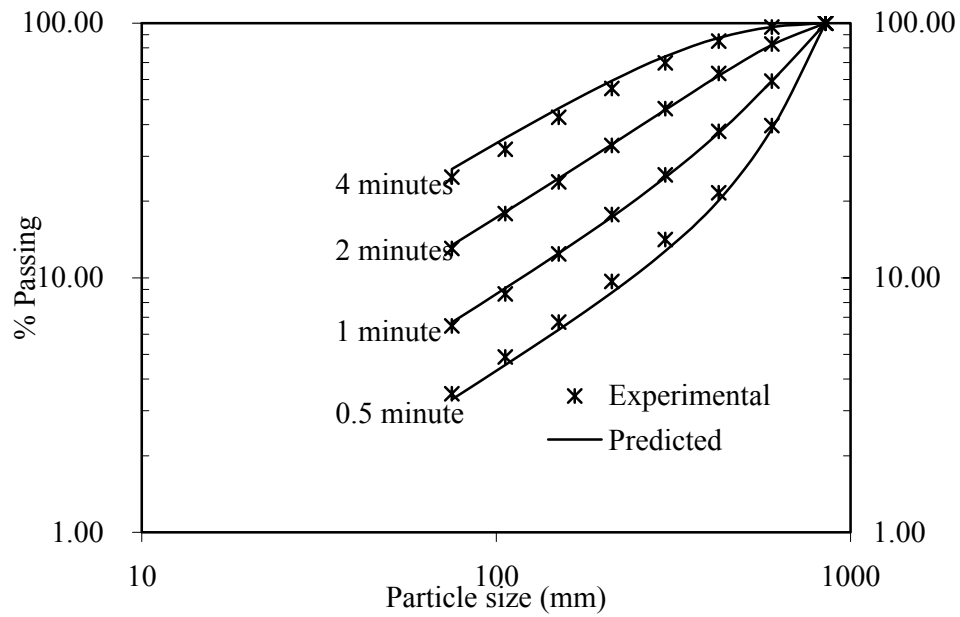
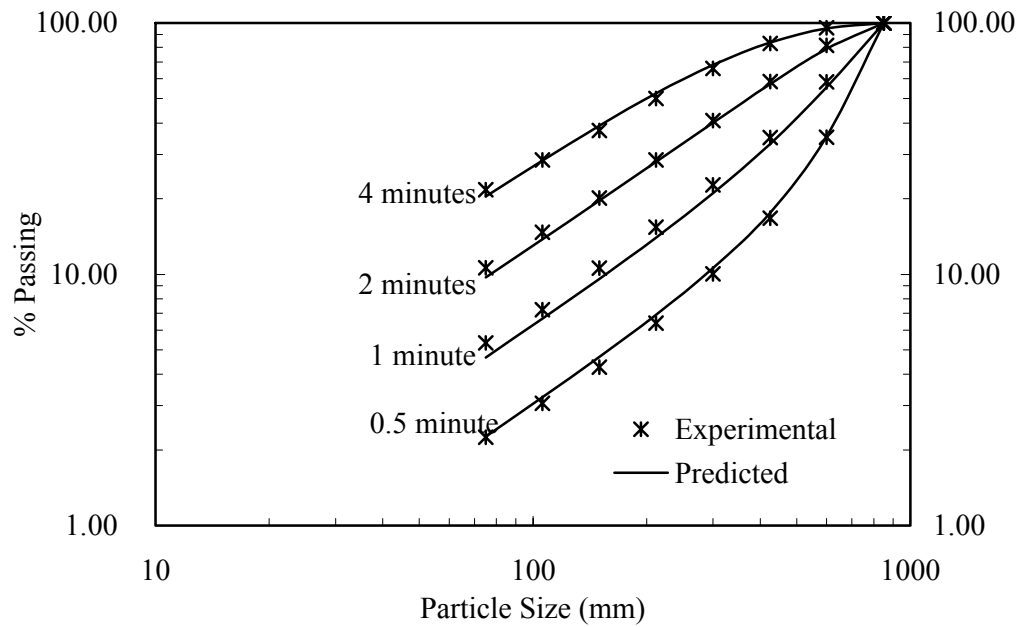**Figure D.3** Comparison of particle size distribution for spherical balls (600x850μm, U=0.5).

Figure D.4 Comparison of particle size distribution for worn balls (600x850μm, U=0.5).